

Max-Planck-Institut für Biochemie
Abteilung Strukturforschung

Cloning, Purification and Crystallization of Selenophosphate Synthetase

Cloning, Purification and Crystallization of ERp44 from *Mus musculus*

Li-Chi Chang

Vollständiger Abdruck der von der Fakultät für Chemie
der Technischen Universität München zur Erlangung des akademischen Grades eines

Doktors der Naturwissenschaften

genehmigten Dissertation.

Vorsitzender: Univ.-Prof. Dr. St. J. Glaser

Prüfer der Dissertation:

1. apl. Prof. Dr. Dr.h.c. R. Huber
2. Univ.-Prof. Dr. J. Buchner

Die Dissertation wurde am 20.02.2006 bei der Technischen Universität München eingereicht
und durch die Fakultät für Chemie am 24.03.2006 angenommen.

Summary

Selenocysteine is found as an active site of the enzymatic activity of redox proteins such as formate dehydrogenase. Selenophosphate synthetase, encoded by the gene *selD*, plays an important role regulating the incorporation of selenide into the amino acid selenocysteine through a specific pathway (reviewed by Böck *et al.*, 1991; Heider & Böck 1993; Böck & Sawers 1996). Selenophosphate synthetase produces an 'activated form of selenium, selenophosphate (Veres *et al.*, 1992), which is used for charging the serine-tRNA^{Sec} with Se by selenocysteine synthetase (*selA*), resulting the specific selenocystyl-tRNA^{Sec}. The first part of my research works is trying to solve the structure of *selD* proteins, elucidating the catalytic mechanism of selenophosphate biosynthesis.

ERp44, a novel UPR induced ER protein, was first identified from the co-immunoprecipitation and mass spectrometry. The molecular weight of matured ERp44 is about 43.9 kDa after cleavage. ERp44 was reported to form mixed disulfides with various proteins including both human Ero1 homologues, Ero1-L α and Ero1-L β , as well as with partially unfolded Ig subunits. The ERp44 was also in presence of reducing cysteine residues of InsP3R. It indicated the interaction with ERp44 is regulated by the thiol oxidation status of InsP3R. Furthermore, the interaction was sensitive to the concentration of ER luminal calcium with concentrations above 100 μ M resulting dissociation of ERp44 from the InsP3R *in vitro*. The second part of this dissertaional works is trying to solve the structure of ERp44. It can help to understand the modulation of calcium redoxing and disulfate bridges forming inside the ER lumen.

Zusammenfassung

Selenocystein wirkt als katalytische Aminosäure bei der enzymatischen Aktivität von Redoxproteinen, wie z.B. der Format-Dehydrogenase. Die Selenophosphat-Synthetase, die vom Gen *selD* kodiert wird, spielt eine wichtige Rolle bei der Regulation des Selenid-Einbaus in die Aminosäure Selenocystein, ausgeführt durch einen spezifischen Reaktionsmechanismus (beschrieben in Böck *et al.*, 1992; Heider & Böck 1993; Böck & Sawers 1996). Die Selenophosphat-Synthetase bildet eine aktivierte Form des Selens, das Selenophosphat (Veres *et al.*, 1992), welches zur Beladung der Serin-tRNA^{Sec} mit Selen durch die Selenocystein-Synthetase (*selA*) verwendet wird. Die beladene tRNA wird als Selenocystyl-tRNA^{Sec} bezeichnet. Im ersten Teil dieser Arbeit wurde versucht, die Struktur des Proteins *selD* zu lösen, um dadurch den katalytischen Mechanismus der Selenophosphat-Biosynthese aufzuklären.

ERp44, eine neues UPR-induziertes ER-Protein wurde erstmals durch Ko-Immunopräzipitation und Massenspektrometrie identifiziert. Das Molekulargewicht des durch Spaltung prozessierten ERp44 beträgt ca. 43,9 kDa. ERp44 bildet gemischte Disulfide mit verschiedenen Proteinen, unter anderen mit beiden humanen Ero1 Homologen (Ero1-L α und Ero1-L β), und mit teilweise entfalteten Ig-Untereinheiten. ERp44 wurde ebenfalls in Gegenwart reduzierender Cysteinreste von InsP3R gefunden. Dies deutet auf eine Regulation der Interaktion mit ERp44 durch den Oxidationszustand der Thiole in InsP3R hin. Darüberhinaus wurde entdeckt, daß Kalziumkonzentrationen im ER-Lumen über 100 μ M *in vitro* zur Dissoziation des ERp44 von InsP3R führen. Im zweiten Teil dieser Arbeit wurde versucht, die Struktur von ERp44 zu lösen. Dies könnte zu einem besseren Verständnis der Modulation des Kalziumtransports und der Bildung von Disulfidbrücken innerhalb des ER-Lumens führen.

CONTENTS

I. Cloning, Purification and Crystallization of Selenophosphate Synthetase

1 Introduction	1
1.1 Selenoprotein biosynthesis in Prokaryotes	2
1.2 Selenoprotein biosynthesis in Eukaryotes	5
1.3 Selenophosphate synthetase (SelD) and the role in selenoprotein biosynthesis	6
1.3.1 SelD and AIR synthase related protein Superfamily	7
1.3.1.1 Structure of monomer	8
1.3.1.2 Structure of the dimer	10
1.3.2 SelD in eukaryotic cells	11
1.4 Selenoprotein and antioxidant defense	12
1.4.1 Selenium and cancer	14
1.4.2 Selenium and immunity	15
1.4.3 Selenium and aging	16
1.4.4 Other selenium effects	16
1.5 SelD gene is essential for development and cell proliferation	17
2 Materials and Methods	18
2.1 Materials	18
2.1.1 Chemicals	18
2.1.2 Bacterial strains	19
2.1.3 Nucleotides	19
2.1.6 Vectors and plasmids	21
2.1.7 Reaction sets (Kits)	22
2.1.8 Equipments	22
2.1.9 Special materials	23
2.2 Methods	24
2.2.1 Molecular Cloning	24
2.2.1.1 PCR amplification	24
2.2.1.2 Agarose gel electrophoresis and DNA fragment isolation	25
2.2.1.3 Enzyme digestion and ligation	26
2.2.1.4 Bacterial transformation	27
2.2.1.4.1 Transformation of <i>E. coli</i> cells by electroporation	27
2.2.1.4.2 Transformation of <i>E. coli</i> cells by heat shock	28

2.2.1.5 Mini-preparation of plasmid DNA	29
2.2.1.6 DNA sequencing	29
2.3 Protein expression and purification	32
2.3.1 Small scale expression	32
2.3.2 Protein assay	33
2.3.3 Large scale expression and purification of recombinant proteins	33
2.4 Crystallization	34
2.4.1 Screening	34
2.4.2 Optimization	34
2.4.3. Cryo solutions	35
2.4.4. Heavy atom derivatives	36
2.5. X-ray data collection and processing	37
3 Results and Discussion	38
3.1 Protein expression and purification	38
3.1.1 Construction of the <i>Thermoanaerobacter tengcongensis</i> SelD expression plasmid and small scale expression	38
3.1.2 Purification of recombinant ZZ-SelDtt	39
3.1.2.1 Removing the ZZ-tag from ZZ-SelDtt	40
3.1.2.2 Thermostability examination of purified SelDtt	40
3.1.2.3 The size-exclusion chromatography of SelDtt	41
3.1.3 Expression and purification of SelDtt from pETM-10 construct	41
3.1.4 Construction and small scale expression of the <i>Drosophila melanogaster</i> SPS1 and SPS2 clones	44
3.1.5 Expression and purification of recombinant SPS1	46
3.1.6 Expression and purification of recombinant ZZ-SPS1	47
3.1.7 Expression and purification of other recombinant SelD proteins	48
3.1.8 Other recombinant AIR synthase related proteins	49
3.1.8.1 Expression and purification of <i>E. coli</i> HypE	50
3.2 Crystallization	51
3.2.1 Initial screening	51
3.2.2 Optimization of crystallization conditions	51
3.2.2.1 The SPS1 crystal	51
3.3 Data Collection of SelDaa	52
4 References	55

II. Cloning, Purification and Crystallization of Erp44 from Mus musculus

1. Introduction	68
1.1 The endoplasmic reticulum stress	68
1.1.1 Overview of the ER quality control	70
1.1.2 The ER-initial cell death (ER Stress)	73
1.2 Protein folding inside the ER lumen	73
1.2.1 The topology and chemical environment of the ER	73
1.2.2 N-linked glycosylation	74
1.2.3 Pathways for proteins disulfide bond formation	75
1.3 The characteristics of protein disulfate isomerase (PDI)	77
1.3.1 The achievement of the human PDI structure from its thioredoxin domains	78
1.3.1.2 Structural comparison between a and b thioredoxin domains of yeast PDI	79
1.3.1.3 The importance of the b' domain of PDI	81
1.3.2 Other PDI like proteins	82
1.3.3 A novel protein of PDI superfamily- ERp18	83
1.4 The structure of Ero1p	83
1.4.1 The -CXXCXXC- motif	86
1.5 The role of ERp44	87
1.5.1 Thiol-mediate retention of ERO1 in the ER	88
1.5.2 Redoxing calcium by IP3 receptor	89
1.5.3 ERp44 and type 1 InsP3R	90
2. Materials and Methods	92
2.1 Materials	92
2.1.1 Chemicals	92
2.1.2 Bacterial strains	93
2.1.3 Nucleotides	93
2.1.4 Oligonucleotide primers for PCR (Table 2.1)	93
2.1.6 Vectors and plasmids (Table 2.2)	94
2.1.7 Reaction sets (Kits)	94
2.1.8 Equipments	95
2.1.9 Special materials	96
2.2 Methods	96
2.2.1 Molecular Cloning	96

2.2.1.1 PCR amplification	97
2.2.1.2 Agarose gel electrophoresis and DNA fragment isolation	98
2.2.1.3 Enzyme digestion and ligation	99
2.2.1.4 Bacterial transformation	99
2.2.1.4.1 Transformation of <i>E. coli</i> cells by electroporation	100
2.2.1.4.2 Transformation of <i>E. coli</i> cells by heat shock	100
2.2.1.5 Mini-preparation of plasmid DNA	101
2.2.1.6 DNA sequencing	102
2.3 Protein expression and purification	104
2.3.1 Small scale expression	104
2.3.2 Protein assay	105
2.3.3 Large scale expression and purification of recombinant proteins	105
2.3.3.1 GST-ERp44	106
2.3.3.2 ZZ-ERp44	106
2.3.3.3 ZZ-ERO1A	107
2.3.3.4 ZZ-1L3V	108
2.3.3.5 ERp18	109
2.4 Crystallization	110
2.4.1 Screening	110
2.4.2 Optimization	110
2.4.3. Cryo solutions	111
2.4.4. Heavy atom derivatives	112
2.5. X-ray data collection and processing	
114	
3. Results and Discussions	115
3.1 Protein expression and purification	115
3.1.1 Construction of the GST-ERp44 expression plasmid and small scale expression	115
3.1.1.1 Purification of recombinant GST-ERp44	116
3.1.1.2 The size-exclusion chromatography of GST-ERp44	117
3.1.2 Construction of the ERp18 (6xHis) expression plasmid and small scale expression	118
3.1.3 The construction and purification of ZZ-ERp44	120
3.1.3.1 Removing the ZZ-tag from ZZ-ERp44	121
3.1.3.1 Purification of ZZ-ERp44 without removing the ZZ-tag	122
3.1.4 The construction and purification of ZZ-ERO1A	124
3.1.4.1 The co-expression and co-purification of ERp44-ERO1A complex	126
3.1.5 The construction and purification of ZZ-1L3V	127
3.1.5.1The co-expression and co-purification of ERp44-1L3V complex	128

3.2 Crystallization	129
3.2.1 Initial screening	129
3.2.2 Optimization of crystallization conditions	130
3.2.2.1 The ZZ-ERp44	130
3.2.2.2 The ERp44	132
4. References	136
Acknowledgements	166

I. Cloning, Purification and Crystallization of Selenophosphate Synthetase

1. Introduction

Selenoproteins are a group of selenocysteine-containing proteins crucial for development, metabolic homeostasis, and antioxidant defense from bacteria to metazoans (Kohrle et al. 2000, Rayman 2000). In human, 25 selenoproteins have been discovered (Kryukov et al. 2003) including deiodinases, which govern mammalian thyroxin metabolism, the glutathione peroxidases (GPx), and the thioredoxin reductases (TrxR), key regulators of cellular redox state (Kohrle et al. 2000). The unusual amino acid selenocysteine (Se-cys), so-called the 21st amino acid, is encoded by the UGA stop codon (Fig. 1.1) which has to be differentially recognized by a specialized tRNA molecule, selenocysteine tRNA^{[Ser]Sec} (Sec- tRNA) (Hatfield and Gladyshev 2002).

Middle Base 5' Base	U	C	A	*G	Middle Base 3' Base
*U	Phe Phe Leu Leu	Ser Ser Ser Ser	Tyr Tyr <i>Stop</i> <i>Stop</i>	Cys Cys *Sec <i>Stop</i> } Trp	U C *A G
C	Leu Leu Leu Leu	Pro Pro Pro Pro	His His Gln Gln	Arg Arg Arg Arg	U C A G
A	Ile Ile Ile ▲ Met <i>Initiator</i> }	Thr Thr Thr Thr	Asn Asn Lys Lys	Ser Ser Arg Arg	U C A G
G	Val Val Val Val	Ala Ala Ala Ala	Asp Asp Glu Glu	Gly Gly Gly Gly	U C A G

Figure 1.1 Genetic code showing that the 21st amino acid, Sec is coded by UGA.

The post-transcriptional modification of the primary transcript of the Sec-tRNA was found to be essential for the tRNA to be functional as well as the other regular tRNAs. Even though selenoproteins play an important metabolic role in many aspects from bacteria to human, the proteomes of both prokaryotes and eukaryotes, with the exception of yeast, contain only few selenoproteins. This can be explained why the cell under aerobic condition is needed to conserve selenoenzymes that control redox homeostasis after the introduction of oxygen into the atmosphere. It is also reported that insufficient expression of selenoprotein in *Drosophila* and vertebrate, for example, impairs the oxidative stress defense and causes lethality (Morey et al., 2003).

1.1 Selenoprotein biosynthesis in Prokaryotes

In the earlier year, it was reported that the addition of the inorganic compounds to a medium used for anaerobic growth of bacteria *Escherichia coli* could supported synthesis of the enzyme formate dehydrogenase (Lester & DeMoss, 1971). It was also shown that radioactive selenium (^{75}Se) was incorporated into other proteins during in vivo synthesis when provided.

After spending lots effort in learning how to handle oxygen-sensitive selenium compounds, people finally could identify the selenium compound in glycine reductase as selenocysteine, an analog of the sulfur-containing amino acid cysteine (Cone *et al.*, 1976). Surprisingly, a selenocysteine is not a result of post-translational modification of a cysteine but is encoded by its own codon. As it turned out, a sequence in the mRNA that normally told the translation machinery to terminate the process—the stop codon UGA—now can specify a different set of instructions to conduct selenocysteine addition at the UGA codon.

A special selenocysteine-specific tRNA (tRNA^{Sec}), which is encoded by *selC* gene in *E. coli* (Leinfelder *et al.*, 1988), was found to be the key factor that recognizes the specific UGA codon on mRNA for selenocysteine insertion. After being transcribed from DNA, tRNA^{Sec} is first aminoacylated with L-serine by seryl-tRNA synthetase (SerS) and forms Seryl-tRNA^{Sec} (see Fig. 1.2).

Because of its unusual structural features, this aminoacylation process of tRNA^{Sec} is conducted with very low efficiency compare to the charging efficiency of cognate serine isoacceptors (Baron & Böck, 1991). Next, seryl- tRNA^{Sec} is converted to selenocysteyl- tRNA^{Sec} facilitated by selenocysteine synthase (sela) (Forchhammer *et al.*, 1991).

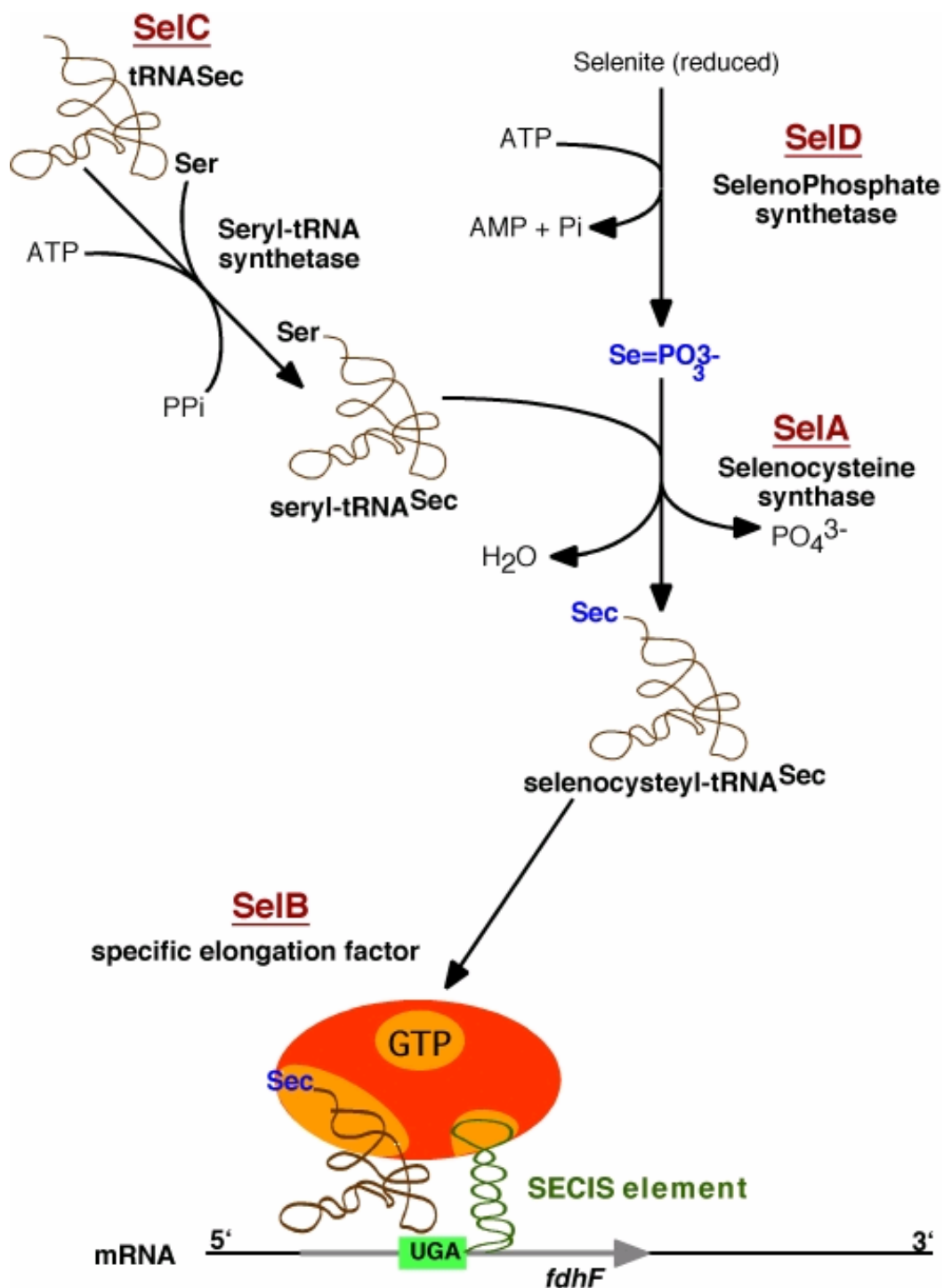


Figure 1.2 Selenocysteine biosynthesis and incorporation pathway in *E. coli*

In this reaction, the amino group of the seryl residue of seryl-tRNA^{sec} forms a Schiff base with the carbonyl of the pyridoxal 5-phosphate cofactor of selA. After dehydration, an aminoacrylyl intermediate forms and selenide is introduced into the molecule followed by the releasing of selenocysteyl-tRNA^{sec} (Forchhammer & Böck, 1991). The selenium donor for this reaction is selenophosphate (Glass *et al.*, 1993), which is synthesized by selenophosphate synthetase (SelD) from selenide and ATP (Ehrenreich *et al.*, 1993; Veres *et al.*, 1994). During translation, Sec-tRNA^{sec} is not bound by the regular elongation factors but bound by the specialized elongation factor (EF) SelB (Forchhammer *et al.*, 1989), which has partial homolog to EF-Tu, but differs from it in having a carboxyl-terminal extension of 272 amino acids containing an mRNA-binding domain (Kromayer *et al.*, 1996). The mRNA which contains UGA triplet coding for selenocysteine forms a secondary structure (SECIS element; see Fig. 1.3) and the SelB-GTP-Sec-tRNA^{sec} ternary complex is tethered to it and positioned immediately downstream of the UGA triplet (Zinoni *et al.*, 1990; Huenttenhoffer *et al.*, 1996).

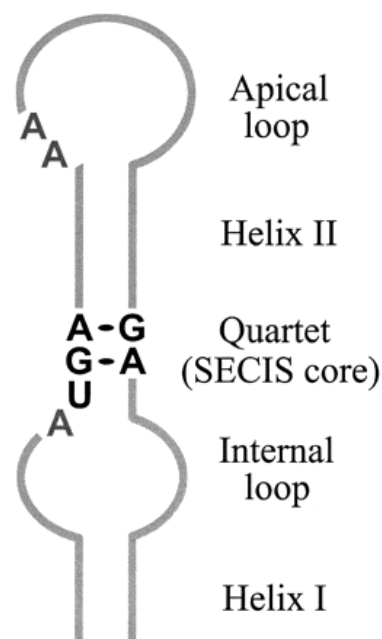


Figure 1.3 SECIS element consensus structure. Condon UGA which encodes for selenocysteine forms a special secondary structure, SECIS element, including helix I, internal loop, quartet (SECIS core), helix II and apical loop. The conserved nucleotides in the SECIS core (Quartet) are shown in boldface.

After formation of this quaternary complex, the conformation of SelB changes and hence the approaching ribosome is able to interact with SelB. Finally, SelB delivers Sec-tRNA^{sec} to the ribosomal A site containing the UGA codon, which in turn triggers GTP hydrolysis and release of SelB·GDP.

1.2 Selenoprotein biosynthesis in Eukaryotes

In contrast to the relatively few selenoproteins in prokaryotes, there are several dozen selenoproteins in archaea and eukaryotes. A comprehensive computational analysis identified 25 selenoproteins in human genome (Kryukov *et al.*, 2003). In spite of the well-characterized biosynthesis of Sec from serine to Sec tRNA^{[Ser]Sec} in *E. coli* (Böck *et al.*, 1991), the specific steps in this process in eukaryotes are not yet clear. In *E. coli*, an aminoacyl intermediate is formed by the action of a pyridoxal phosphate-dependent Sec synthase to remove the hydroxyl group from serine. This intermediate serves as the acceptor for activated selenium and is then converted to selenocysteyl tRNA^{[Ser]Sec} (Böck *et al.*, 1991).

In eukaryotes, a minor seryl tRNA which was found to be able to decode UGA (Hatfield & Portugal, 1970) and form phosphoseryl tRNA (Hatfield *et al.*, 1982) was identified as Sec tRNA^{[Ser]Sec} subsequently (Lee *et al.*, 1989). The roles of the kinase and phosphoseryl tRNA^{[Ser]Ser} in the biosynthesis of Sec are not well characterized yet. However, the formation of phosphoserine agrees with a Sec synthase-catalyzed reaction, since phosphorylated serine would have a better leaving group than serine in the Sec biosynthetic pathway.

In archaea and eukaryotes, additional SECIS-binding proteins (SBP2) were reported to mediate the SelB-SECIS interaction.

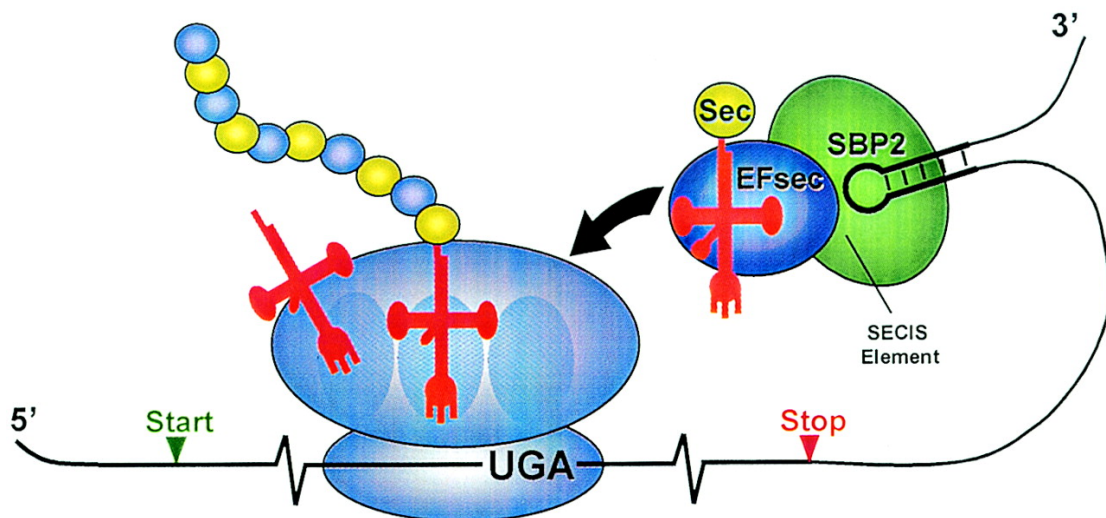


Figure 1.4 Mechanism of Sec insertion in eukaryotes. Selenocysteyl-tRNA (in orange with Sec in yellow) is shown in a complex with EFsec (in blue) and SBP2 (in green) and the SECIS element (shown as a hairpin loop in black) that is ready for donation to the ribosomal A site to be decoded by UGA (shown in the selenoprotein mRNA in black). Once the Sec-tRNA^{[Ser]Sec} complex is donated to the A site, Sec-tRNA^{[Ser]Sec} is transferred to the peptidyl site and Sec is incorporated into the nascent selenopeptide. The growing selenopeptide is shown as alternating gold and blue balls attached to the tRNA in the peptidyl site. The mRNA (shown in black with its start and stop codons indicated) is attached to the smaller of the two ribosomal subunits, and the unacylated tRNA is shown leaving the ribosomal exit site. (Adapted from Hatfield & Gladyshev, 2002)

1.3 Selenophosphate synthetase (SeID) and the role in selenoprotein biosynthesis

Selenocysteine is found residues at the active site and is crucial for the enzymatic activity of redox proteins such as formate dehydrogenase. Selenophosphate synthetase, encoded by the gene *seID*, plays an important role regulating the incorporation of selenide into the amino acid selenocysteine through a specific pathway (reviewed by Böck *et al.*, 1991; Heider & Böck 1993; Böck & Sawers 1996). Selenophosphate synthetase produces an 'activated form of selenium, selenophosphate (Veres *et al.*, 1992), which is used for charging the serine-tRNA^{Sec} with Se by selenocysteine synthetase (*seIA*), resulting the specific selenocystyl-tRNA^{Sec} (See Fig. 1.5).

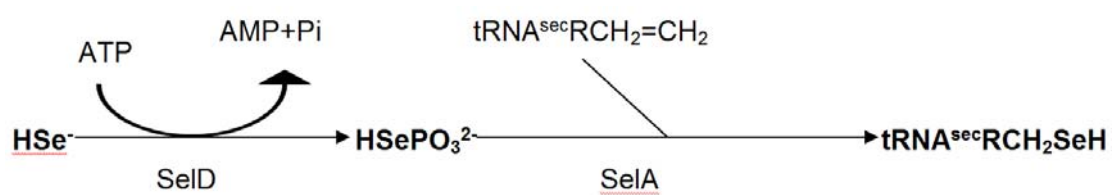


Figure 1.5 Mechanism of selenide incorporation into selenocystyl-tRNA^{Sec}.



Figure 1.6 Structure of the PurM (homo-tetrameric; from PDB 1cli).

1.3.1 SelD and AIR synthase related protein Superfamily

Selenophosphate synthetase (SelD) (Veres *et al.*, 1994) was recently proposed to be grouped to a new PurM structural superfamily (Li *et al.*, 1999) based on the iterative BLAST searches on the similarity in the functions and catalytic mechanisms of aminoimidazole ribonucleotide (AIR) synthetase (PurM) (Fig. 1.6) which catalyzes the conversion of formylglycinamide ribonucleotide (FGAR) and ATP to AIR, ADP, and Pi in the purine biosynthetic pathway. This super family also includes the ATP-dependent enzymes HypE (a NiFe hydrogenase maturation protein) (Reissmann *et al.*, 2003), and thiamine phosphate kinase (ThiL) (Begley *et al.*, 1999).

To determine the structure of PurM, multiwave-length anomalous diffraction (MAD) phasing techniques using SeMet-incorporated protein (Li *et al.*, 1999) have been employed and the results suggested that PurM forms a homo tetramer (Fig 1.6).

1.3.1.1 Structure of monomer

The PurM monomer contains 345 amino acid residues in a single polypeptide that can be divided into two clear structural domains of similar sizes. The N-terminal domain A includes amino acid residues 16–166 and the C-terminal domain B includes amino acid residues 178–345. Both domains have an α/β -type fold. The N-terminal domain A consists of 47% α helix, 28% β sheet and 25% loops. The first 16 residues of domain A and the polyhistidine tag which was used for purification purposes are disordered.

Domain A includes an four-stranded mixed β sheet with order $\beta 1\beta 4\beta 2\beta 3$. Each β strand, which is unusually long, has 10-11 residues. Strands $\beta 1$, $\beta 2$ and $\beta 3$ are parallel to each other and strand $\beta 4$ is antiparallel to the other three. This β is flanked on one side by four α helices and the other side of the β sheet forms the PurM dimer interface. Three of the α helices consist of around 20 residues, and the $\alpha 2$ consists of 10 residues. A long and poorly ordered glycine-rich loop was determined between helix $\alpha 1$

and strand $\beta 1$ in domain A. This loop includes residues 40–46 (GGLGGFG), which have comparatively high temperature factors.

The C-terminal domain B is consists of 36% α helix, 28% β sheet, and 46% loops. Both the α helices and the β strands in domain B are found shorter than those in domain A. Domain B includes a six-stranded mixed β sheet with order $\beta 6\beta 8\beta 5\beta 9\beta 7\beta 10$. All six β strands have about seven to nine residues.

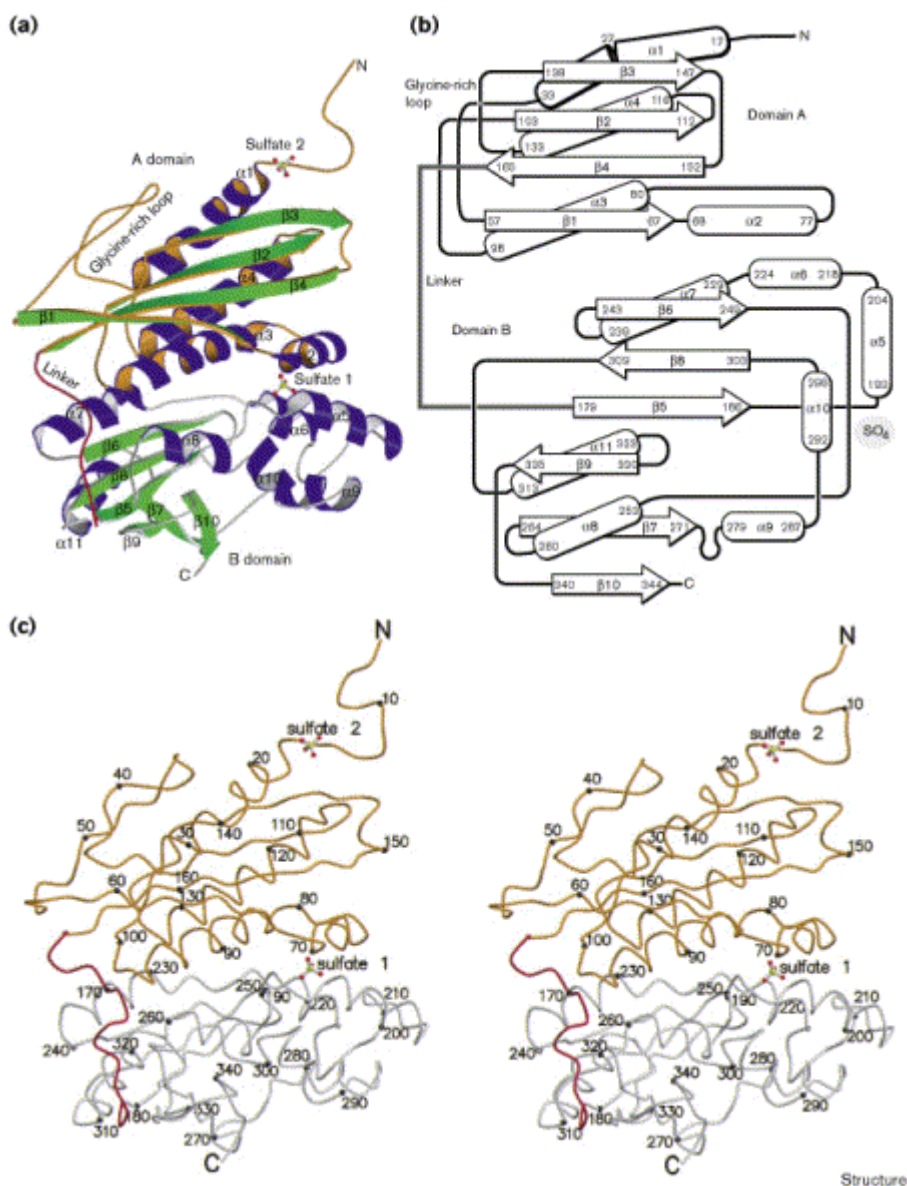


Figure 1.7 Structure of the PurM monomer. (a) Ribbon diagram showing key structural features. Helices are shown in blue and strands in green. Domain A is outlined in gold and domain B is outlined in silver. (b) Topology diagram. Secondary structural elements are

labeled with the first and last amino acid sequence number. (c) Stereoview of the C α backbone. Every tenth C α position is labeled. Domain A is shown in gold and domain B is shown in silver (Adapted from Li *et. al.*, 1999).

Inside the β sheet, the first five strands form an antiparallel sheet with the final strand, β 10, parallel to β 7. The β sheet is flanked on one side by two α helices α 7 and α 11, and on the other side by α 8. Four helices α 5, α 6, α 9 and α 10 were found clustered along one edge of the β sheet. Helices α 5– α 10 has 9–11 residues while longer α 11 has 13 residues. The two domains are linked by a well-ordered hinge-like loop that consists of 11 residues (S167EIIDGSKVSD177) (red trace in Figure 1.7a). In addition, the strong interaction between helix α 3 of domain A and helices α 6 and α 7 of domain B as well as helix α 2 of domain A and helices α 5 and α 6 of domain B also favor PurM dimer formation.

1.3.1.2 Structure of the dimer

The PurM dimer is formed from identical monomers related by a noncrystallographic twofold axis with the N and C termini of different subunits about 20–25 Å apart.

The size of the PurM monomeric subunit is about 55 Å long, 30 Å wide and 15 Å thick on the domain-A side and around 25 Å thick on the domain-B side. The dimer forms a prolate ellipsoid with 85 × 45 × 60 Å in dimensions. Two obvious clefts are on opposite sides (Figure 1.8). The dimer is linked by combining two four-stranded β sheets from each subunit face to face, resulting in an eight-stranded β -barrel-like structure flanked by eight α helices (Figure 1.8). The distances of most backbone between the two sheets are in the range of 6–7 Å and hydrophobic interaction contributes the most intersubunit interactions. Basically all the critical dimer interactions occur between domain A of each subunit. Therefore, PurM dimer shows a four-layer $\alpha\beta\beta\alpha$ sandwich core made from two copies of domain A. The dimensions of the core structure are about 50 Å in length along the barrel axis and about 35 Å in the direction perpendicular to the barrel axis. Two copies of

domain B are connected to opposite ends of the core structure by a single connecting loop (Figure 1.8).

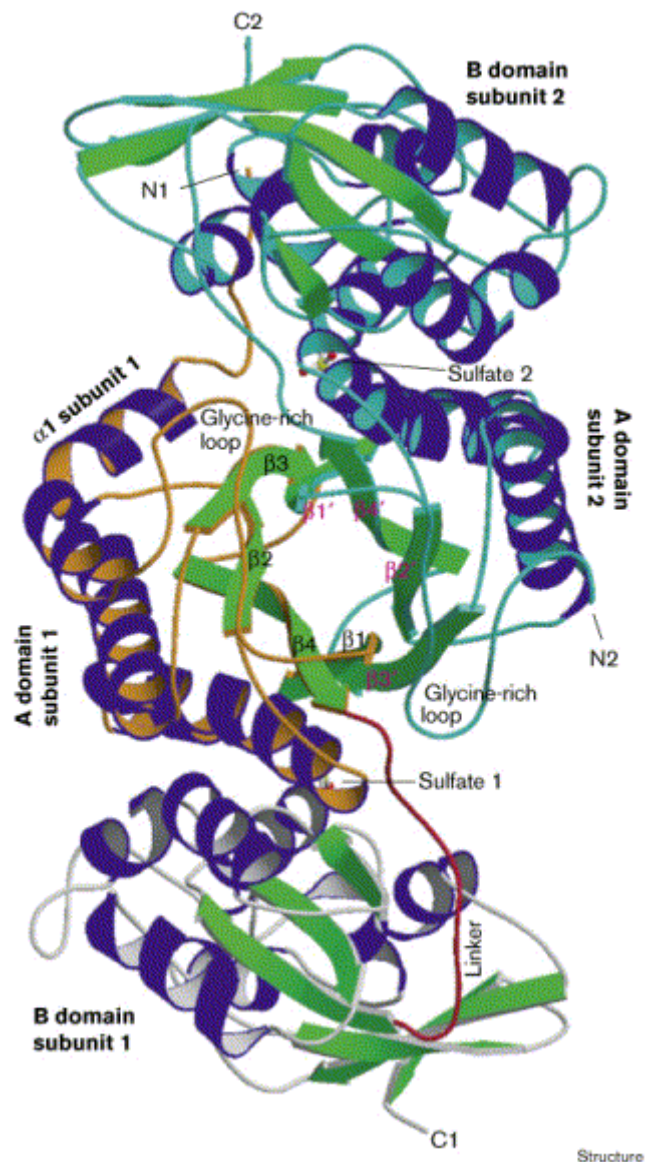


Figure 1.8 Structure of the PurM dimer showed by Ribbon diagram viewed down the twofold axis. Structural features and the strands of the central β barrel, which form most of the dimer interface, are labeled. For subunit 1, the domain-A ribbon is marked in gold, the domain-B ribbon is marked in silver and the linker is displayed in red. For subunit 2, the ribbon is marked in light blue (Adapted from Li *et al.*, 1999).

1.3.2 SelD in eukaryotic cells

SelD gene products, selenophosphate synthetase (SPS), from organisms including *E. coli*, *Drosophila* and mammals can be grouped into two major categories based on the presence of a cysteine or SeCys residue

at the site corresponding to Cys-17 in *E.coli* SELD. The first group of SPS enzymes, which have a Cys-17 or SeCys-17 residue can catalyze the selenide-dependent monoselenophosphate formation of *in vitro*. Studies found that replacement of Cys-17 with serine causes SPS unable to neither hydrolyze-ATP nor utilize selenide as substrates (Kim *et al.*, 1992). Analysis of the genome sequences of *Methanococcus jannaschii* (Bult *et al.*, 1996) and *Haemophilus influenzae* (Fleishmann *et al.*, 1995) showed that the *selD* gene in these organisms has a TGA codon at the position of the *E. coli* Cys-17, suggesting the presence of a SeCys residue. Moreover, SeCys-containing SPS variants were also discovered in mouse and human (Guimaraes *et al.*, 1996). Substitution of the SeCys residue of the mouse enzyme with cysteine lowered but did not eliminate enzymatic activity, however, changing Cys-17 of SELD to Ser abolished catalytic activity (Kim *et al.*, 1992).

The second group of SELD homologs which were identified from eukaryotic organisms including human (Low *et al.*, 1995), mouse (Guimaraes *et al.*, 1996), and *Drosophila* (Persson *et al.*, 1997) share high sequence similarity with the *E. coli* SPS but lack a cysteine or SeCys residue in the position that corresponds to Cys-17 of the *E. coli* enzyme. At this position, the human SPS homolog has a threonine substitution (Low *et al.*, 1995), and a homolog from *Drosophila melanogaster* harbors an arginine (Persson *et al.*, 1997). The overproduced threonine-containing human SPS homolog weakly complemented a *selD* mutation in *E. coli*, and overexpression of this gene in mammalian cells caused an increased ⁷⁵Se labeling of mammalian selenium-dependent deiodinase.

Prokaryotes, such as bacteria and archaea, have only group 1 SPS gene while eukaryotic organisms including *D. melanogaster*, mouse, and human contain a copy of both group 1 and group 2 SPS genes. Based on this evident substrate specificity of the *Sps1* and *Sps2* gene products, it is speculated that the *Sps1*-encoded enzyme depends on a selenium salvage system that recycles L-selenocysteine, whereas the *Sps2*-encoded enzyme functions with a selenide assimilation system (Tamura *et al.*, 2004).

1.4 Selenoprotein and antioxidant defense

Sodium selenide is the major inorganic form of selenium. Selenomethionine and selenocysteine, the organic form of selenium, carry a selenium atom in the position corresponding to a sulfur atom in the amino acids methionine and cysteine. Se-methylselenocysteine is also observed while the hydrogen atom was replaced with a methyl group on the selenium atom of selenocysteine. In mammals, 25 selenoproteins containing selenocysteine were identified so far. In most cases, selenocysteine plays an important role in regulating the enzymatic activity of the selenoprotein. For examples, antioxidant enzymes glutathione peroxidase and thioredoxin reductase both have a selenocysteine at the active site. Thioredoxin reductase functions at providing the deoxyribonucleases required for DNA synthesis (Holmgren, 1989) as well as maintaining cellular proteins in a reduced state. While thiol (-SH) compounds are considered as antioxidant reducing agents (by hydrogen atom donation), selenium is more nucleophilic (electron-rich) and therefore releases the hydrogen more easily hence a more efficient antioxidant reducing agent. It is speculated that a 15% longer (than sulfur) bond-length of selenium facilitates the formation of selenium-sulfur bonds at the catalytic sites (Gromer *et al.*, 2003). It is also reported that the presence of selenocysteine rather than cysteine in thioredoxin reductase not only increases catalytic activity 100-fold, but also optimizes the activity at physiological pH (Zhong & Holmgren, 2000).

Antioxidants such as Vitamin E, Vitamin C and Co-Enzyme Q10 function at neutralizing free radicals and becoming free radicals that are less harmful than those they neutralize. However, the free radical forms of antioxidants must then be regenerated otherwise they cannot continue to work as effective antioxidants, and may even cause damage to cells. To regenerate antioxidants, the glutathione and thioredoxin antioxidant systems are relied to provide the primary antioxidant defense in the water phase. Both glutathione peroxidase and thioredoxin reductase, two natural antioxidant enzymes, contain selenium which is essential for their antioxidant activity. To increase the antioxidant activity, both glutathione and thioredoxin systems

facilitate to induction of other natural antioxidant enzymes (Hansen *et al.*, 2004) such as superoxide dismutase (Das *et al.*, 1997). In addition to these antioxidant systems, both selenite and selenomethionine supplementation have been reported to dramatically decrease oxidative DNA damage (8-OHdG formation) caused by ultraviolet radiation (Rafferty *et al.*, 2003).

1.4.1 Selenium and cancer

Selenium was reported to affect in various cellular aspects including oxidative stress, DNA methylation, DNA repair, inflammation, apoptosis, cell proliferation, carcinogen metabolism, hormone production, angiogenesis and immune function (Taylor *et al.*, 2004). Among those, cancer seems to be a combination of many irregularities which could be affected by Selenium. Cancer usually starts with DNA mutation, aberrant DNA methylation or faulty cell-cycle control. DNA is usually protected from carcinogen, cancer-causing substances, by methyl groups. However, selenium deficiency (like folic acid deficiency) was reported to result in DNA methylation drop and hence increased DNA damage (Davis & Uthus, 2003). Selenium also raises the activity of p53 protein, the most important tumor suppresser gene. More than half of all cancers have p53 protein deficiency. p53 functions at inducing DNA repair system while DNA is damaged or promoting cells to commit suicide (apoptosis) if the DNA damage is impossible to repair. The thioredoxin reductase system was found to increase the expression of p53 hence DNA repair enzymes (Seo *et al.*, 2002). Cells exposed to selenomethionie have been observed to reveal a 3-fold increase in p53 activity (Longtin, 2003). Selenium compounds have also been shown to inhibit DNA transcription factors that would exacerbate the inflammatory response (Jozsef & Filep, 2003). In addition, selenium compounds were found very effective at protecting endothelial cells from peroxynitrite-induced DNA damage (Roussyn *et al.*, 1996). Glutathione peroxidase and possibly other selenoproteins can directly work on reduction of peroxynitrite to nitrite (Sies *et al.*, 1997).

1.4.2 Selenium and immunity

Selenium deficiency causes more pro-inflammatory immune response (Beck *et al.*, 2003) and increases the virulence of viral infection by boosting T-cell production (Broome *et al.*, 2004). Therefore, AIDS patients who are selenium-deficient were found around 20 times more likely to die from HIV-related symptoms than patients with sufficient selenium. Neutrophils with less glutathione peroxidase due to selenium deficiency are less able to protect themselves from the free radicals they release onto pathogens (Davis & Uthus, 2003). An study by oberseving aged mice indicated that sodium selenite supplementation above the normal levels of selenium could restore lymphocyte proliferation due to antigens to the similar levels of young adult mice (Roy *et al.*, 1995). Also, the same group also showed that increasing selenium above normal levels in young adult mice increased the bacteria-killing activity of spleen lymphocytes by 22.3%.

The selenium-containing iodothyronine deiodinase enzyme catalyzes the conversion of thyroid hormone from inactive (T4) to active (T3) form. Thyroid problems are also linked to selenium deficiency (Olivieri *et al.*, 1996). T3 is usually responsible for controlling the rate of metabolism and the activity of many other hormones. Although most T3 is expressed in liver cells, the thymus gland (which produces T-cells) has a local form of iodothyronine deiodinase, which shows the importance of selenium for the development and function of thymic cells. Selenium is found not boost the immune system to protect against sepsis, but also works directly blocking bacterial lipopolysaccharide (LPS), a large molecule that contributes significantly to endotoxic shock (death due to bacterial toxins) (Kim *et al.*, 2004). Since multiple organ failure, the leading cause of death in intensive care units, is often caused by systemic sepsis, elderly people worried about the risk of hospital infections should also consider selenium supplementation as part of their protection.

1.4.3 Selenium and aging

The natural selenium-containing antioxidant enzymes such as glutathione peroxidase and thioredoxing reductase can reduce the effect of free radicals and were speculated to be a potential factor that can inhibit the aging process. Disulfide bonds can cross-link proteins, decreasing enzyme activity and increasing the sinew associated with aging collagen. Thioredoxin reductase is especially effective in reducing disulfide bonds (Stewart *et al.*, 1998). One form of methionine sulfoxide reductases, which directly repairs oxidative damage to the methionine residues in proteins, contains selenium at its active site. Both forms depend upon the thioredoxin system for regeneration. Interestingly, selenium deficiency has been shown to increase protein oxidation, which causes aging, in mice (Moskovitz & Stadtman, 2003). Surprisingly, transgenic fruit flies that overexpress the non-selenium-containing methionine sulfoxide reductase have shown a 70% increase in lifespan (Ruan *et al.*, 2002). Since so-called accelerated aging diseases are generally due to defective DNA repair, DNA damage has been associated with aging. In addition, an epidemiological study has shown a statistically significant relationship between low selenium blood levels and high levels of DNA damage. All these findings suggest that selenium is an interesting target for studying anti-aging.

1.4.4 Other selenium effects

AP-1 (Activator Protein-1), like NF- κ B, is a transcription factor that stimulates inflammatory response, immune function, cell adhesion and cell growth. The phosphorylation of the proteins Fos and Jun, which is necessary for AP-1 activation, is mediated by two MAPK (Mitogen-Activated Protein Kinase) growth factor pathways: ERK and JNK, respectively. Selenium compounds were found inhibit the JNK & p38 MAPK growth factor pathways and hydrogen peroxide-induced DNA-binding of AP-1 (Yoshizumi *et al.*, 2002), but not the ERK MAPK (Zhong *et al.*, 2000). The p38 MAPK play an essential role in induction of NF- κ B-dependent gene transcription of pro-inflammatory cytokines (like IL-1 and TNF- α) in monocytes & macrophages.

Oxidative stress quickly induces translocation of the redox protein thioredoxin from the cytoplasm to the nucleus where it can create the reduced environment required for the AP-1, NF- κ B and NF-E2-related factor 2 (Nrf2) to bind to DNA. Nrf2 is a transcription factor of the regulatory genes for producing antioxidant enzymes, the Antioxidant Response Element (ARE). Selenium deficiency is also reported to be associated with increased cardiovascular disease, osteoarthritis and infertility (Ursini *et al.*, 1999).

1.5 SelD is essential for development and cell proliferation

Current investigations of physiological roles of *Sps1* and *Sps2* started from their functions in selenium homeostasis in mammals. It has been shown that *Sps2* is specifically expressed at very early stages of development in mouse embryonic sites of hematopoiesis (Guimaraes *et al.*, 1996). Since *Sps2* is a T cell activation gene, the up-regulated *Sps2* in T cells is speculated to play a role in managing the production of selenophosphate for synthesizing selenoproteins which are involved in the immune response rather than in cell growth and division.

In *Drosophila melanogaster*, a null mutation in the *Drosophila melanogaster selenophosphate synthetase 1 (sps1)* gene impacts on the Ras/MAPK signaling pathway. The *selD^{otuf}* mutation was observed dominantly suppresses the phenotypes in the eye and the wing caused by hyperactivation of the Ras/MAPK cassette and the activated forms of the *Drosophila* EGF receptor (DER) and Sevenless (Sev) receptor tyrosine kinases (RTKs), which signal in the eye and wing, respectively (Morey *et al.*, 2001).

2. Materials and Methods

2.1 Materials

2.1.1 Chemicals

Acrylamide solution	Roth, Karlsruhe
Acetic Acid	Merck, Darmstadt
Agarose	Invitrogen, USA
Amonium persulfate (APS)	Merck, Darmstadt
Ampicilin	Sigma, Deisenhofen
Bradford solution	Biorad, Muenchen
Bromophenol blue	Merck, Darmstadt
Choloramphenicol	Boehringer, Mannheim
Coomassie Brillant Blau R250	Serva, Heidelberg
Dimethyl sulfoxide (DMSO)	Sigma, Deisenhofen
Dithiothreitol (DTT)	Roth, Karlsruhe
Ethanol	Merck, Darmstadt
Ethidium bromide solution	Roth, Karlsruhe
Glutathion (reduced)	Sigma, Deisenhofen
Glycerol	Merck, Darmstadt
Guanidinium hydrochloride	Fluka, Schweiz
HEPES	Calbiochem, USA
Imidazole	Merck, Darmstadt
Isopropyl- β -D-thiogalactoside (IPTG)	Sigma, Deisenhofen
Kanamycin	Boehringer, Mannheim
Lysozyme	Boehringer, Mannheim
1 kb DNA ladder	Invitrogen, USA
Polyethleneglycol 3350	Fluka, Schweiz
Polyethleneglycol 4000	Fluka, Schweiz
Polyethleneglycol 8000	Fluka, Schweiz
Potassium chloride	Merck, Darmstadt
Precision protein standard marker	Biorad, Muenchen
Sodium Chloride	Merck, Darmstadt
Sodium dodecyl sulfat (SDS)	Merck, Darmstadt

N, N, N', N'-tetramethylethylenediamin (TEMED)	Sigma, Deisenhofen
Tris-(hydroxymethylen) aminomethan (TRIS)	Roth, Karlsruhe

2.1.2 Bacterial strains

<i>E. coli</i> BL21(DE3)	Novagen, Darmstadt
<i>E. coli</i> DH5 α	Invitrogen, USA
<i>E. coli</i> Rossetta (DE3)	Novagen, Darmstadt
<i>E. coli</i> BL21(DE3)-RIL	Stratagene, Heidelberg
<i>E. coli</i> B834(DE3)	Stratagene, Heidelberg

2.1.3 Nucleotides

Deoxynucleoside-5'-Triphosphate, 100 mM (dATP, dCTP, dGTP, dTTP)

Nucleoside-5'-Triphosphate, 100 mM (ATP, CTP, GTP, UTP)

2.1.4 Oligonucleotide primers for PCR (Table 2.1)

Protein	Oligo	Description	Sequence (5'→3')
SelDtt	SelDtt/BsmB1/fw	SelDtt; <i>Thermoanaerobacter tengcongensis</i>	ACGTACCCATGGC AAGTCTTGATTCAG AGAATATAGATG
	SelDtt/KpnI/rv		ACGTACGGTACCT TACAGCTCATCTC GATCCCTCAATAAA G
SPS1	SPS1/BsmB1/fw	SPS1; <i>Drosophila melanogaster</i>	ACGTACCGTCTCC CATGAGCTACGCC GCTGATGTGCTGA ACTCGG
	SPS1/KpnI/rv		ACGTACGGTACCC TAGTCCTTGGCGG GCACCTCAATGAC

			GC
	SPS1/NdeI/fw		ACGTACCCTT <u>CATA</u> TGAGCTACGCCGC TGATGTGCTGAAC TCGG
	SPS1/XhoI/rv		ACGTACGGT <u>CTCG</u> AGGTCCTTGGCGG GCACCTCAATGAC GC
SPS2 (370)	SPS2/BsmB1/fw	SPS2 (370); <i>Drosophila melanogaster</i>	ACGTACCGTCTCC CATGTTTCAACCC GAAAACATGGGC
	SPS2_370/KpnI/r v		ACGTACGGTACCC TAAAGGCTAACTTC GATAAACTCTACAT CTTCGC
	SPS2/NdeI/fw		ACGTACCCTT <u>CATA</u> TGTTTCAACCCGAA AAACATGGGC
	SPS2/XhoI/rv		ACGTACGGT <u>CTCG</u> AGAAGGCTAACTT CGATAAACTCTACA TCTTCGC
SPS2 (305)	SPS2/BsmB1/fw	SPS2 (305); <i>Drosophila melanogaster</i>	ACGTACCGTCTCC CATGTTTCAACCC GAAAACATGGGC
	SPS2_305/KpnI/r v		ACGTACGGTACCT CAGCAGGAAGGCA TATTAAGGC
	SPS2/NdeI/fw		ACGTACCCTT <u>CATA</u> TGTTTCAACCCGAA AAACATGGGC

	SPS2/XhoI/rv		ACGTACGGTCTCG <u>AGGCAGGAAGGCA</u> TATTAAGGC
SelDec	SelDec/BsmB1/fw	SelDec; <i>E. coli</i>	ACGTACCGTCTCC CATGAGCGAGAAC TCGATTCGTTTGAC C
	SelDec/KpnI/rv		ACGTACGGTACCT TAACGAATCTCAAC CATGGCACGACCG
SelDhi	SelDhi/BsmB1/fw	SelDhi; <i>Haemophilus influenzae</i>	ACGTACCGTCTCC CATGGAAGAAAA ATTCGGCTGAC
	SelDhi/NotI/rv		ACGTAC <u>CGCGCCG</u> <u>CTTTACTTCAACA</u> ACG
HypE	HYPE/NcoI/fw	HypE; <i>E. coli</i>	ACGTAC <u>CC</u> <u>ATGGAGCAATTAAT</u> CAACAGCCTGTTT
	HYPE/Acc65I/rv		ACGTACGGTACC TTAGCATATACGC GGAAGCGGTTCCGG CGTG
pur2p	PUR2/NdeI/fw	pur2p; <i>Saccharomyces cerevisiae</i>	ACGTACCCTT <u>CATA</u> <u>TGCTCAACATTCTC</u> GTTTTAGGAAACG
	PUR2/XhoI/rv		ACGTACGGTCTCG <u>AGGTAAAGCTTAG</u> TTCCGTTTTCAATC ACACA
pur4p	Pur4/NdeI/fw	pur4p; <i>Saccharomyces cerevisiae</i>	ACGTACCCTT <u>CATA</u> <u>TGACTGATTATATT</u> TTGCCGGGTCCCA

			AG
	Pur4/XhoI/rv		ACGTACGGT <u>CTCG</u> AGACCGACCCATC TTCTGGCAGATCT GAATAA

2.1.6 Vectors and plasmids (Table 2.2)

Plasmid	Description	Source
pETM-ZZ	zz-domain of protein A fusion expression vector, T7 promoter, Kan ^r	Dr. Guenter Stier
pETM-10	n-terminus 6xHis-fusion expression vector, T7 promoter, kan ^r	Dr. Guenter Stier
pETM-11	n-terminus 6xHis-fusion expression vector, T7 promoter, kan ^r	Dr. Guenter Stier
pETM-13	c-terminus 6xHis-fusion expression vector, T7 promoter, kan ^r	Dr. Guenter Stier
pET22b(+)	C-terminus 6xHis expression vector, Amp ^r	Novagen

2.1.7 Reaction sets (Kits)

ABI PRISM™ Dye Deoxy Cycle Sequencing Kit	Applied Biosys., Weiterstadt
Amicon Centriplus Concentrator	Millipore, France
ECL Western Blot Detection Kit	Amersham Biosciences,
Freiburg	
GFX Purification Kit	Amersham Biosciences,
Freiburg	
Mouse 18-day embryonic cDNA Library	Clontech, Heidelberg
QIAprep Spin Miniprep Kit	Qiagen, Hilden
QIAquick Gel Extraction Kit	Qiagen, Hilden

QIAquick PCR Purification Kit	Qiagen, Hilden
TNT [®] T7 Coupled Reticulocyte Lysate System	Promega, USA

2.1.8 Equipments

ABI PRISM™ 310 Genetic Analyzer	Applied Biosys., Weiterstadt
Biofuge (pico/fresco)	Heraeus, Hanau
Electrophorese apparaturen	BiorRad, München
Gel documentation system	Biorad, München
Gradient Master Modell 106	BioComp., Canada
Heating block Hybaid	Biometra, UK
Head over tail Rotor 7637-01	Cole-Parmer, USA
Hybridisation oven	Hybaid, Biometra
Incubator BK-600	Heraeus, Hanau
Incubation shaker	Multitron Infors, Switzerland
pH Meter	Molecular Dynamics
Replica plater	Qbiogene, Eschwege
SMART System	Pharmacia Biotech
Sonifier	Heinemann Labortechnik
Sorvall Rotor	Kendro, USA
Speed Vac Concentrator 5301	Eppendorf, Hamburg
Spectrophotometer Ultropsec 300 pro	Amersham Biosciences, Freiburg
SW60 Rotor	Beckman, USA
Ultra centrifuge	Sorvall/Beckman, USA
UV Lamp 254nm	Bachofer, Reutlingen
Thermal Cycler Hybaid	Omni Gene, UK

2.1.9 Special materials

Cuvettes for Monolight 3010	Pharmingen, USA
Collodium Bags	Sartorius GmbH, Göttingen
Dialysis cassettes	Pierce, USA
Falcon tubes (5, 15, 50 ml)	Greiner, Kremsmünster

Glass Beads (425-600 microns)	Sigma, Deisenhofen
Glutathione Sepharose 4B	Amersham Biosciences, Freiburg
N ⁺ -NTA Agar	Qiagen, Hilden
Pipettes	Eppendorf, Hamburg
Protein A Sepharose	Amersham Biosciences, Freiburg
Protran Nitrocellulose Membrane	Schleicher & Schuell, Dassel
Reaction tubes (0.5; 1.5; 2 ml)	Eppendorf, Hamburg
Sterile filter (0.22 & 0.45 µm)	Millipore, France
Vivaspin concentrators	Vivascience, Sartorius

2.2 Methods

2.2.1 Molecular Cloning

DNA fragments used for the plasmids construction were amplified with the desired restriction enzyme sites introduced at the 5' end by PCR (section 3.2.1.1). The PCR products were first purified from the agarose gel (section 3.2.1.2); the purified DNA was then digested by appropriate enzymes and ligated with target vectors after purification (section 3.2.1.3). 1-2 µl ligation reaction was used for transformation (section 3.2.1.4). The positive colonies were inoculated in LB medium and the plasmid DNA was prepared (section 3.2.1.5). 2 µl DNA sample from mini-preparation was digested with appropriate enzymes and examined on the agarose gel. The clones which have right-sized insert DNA fragment were verified by sequencing (3.2.1.6).

2.2.1.1 PCR amplification

Polymerase chain reaction (PCR) was mostly used as a tool for cDNA cloning and plasmid construction in this work. For this purpose, forward and reverse primers were designed to introduce compatible restriction enzyme sites and 3-6 additional bases were added at the 5' ends to allow efficient digestion by restriction enzymes (table 3.1). The following text describes a typical PCR reaction and a PCR cycling programme. The annealing

temperature can be chosen on the basis of the melting temperature of the primers. This may work, but sometimes the results may not match up to expectations. Therefore, a simple procedure used many times in this work was to use an initial annealing temperature of 55°C (usually good for most primers with a length around 20 bp or more). If non-specific products resulted, this temperature was increased. If there were no products, the temperature was decreased.

PCR reaction mixture (50 µl)

2.0 µl DNA sample (~20ng)

1.0 µl 5' oligo (100 pmol/µl)

1.0 µl 3' oligo (100 pmol/µl)

5.0 µl 10x cloned *Pfu* buffer

5.0 µl DMSO

5.0 µl dNTP (2.5 mM)

1.0 µl *Pfu* polymerase

30.0 µl H₂O

PCR cycling programme

92°C 3 min,

55°C 4 min,

68°C 1 min/kb,

25 cycles of [92°C 30 sec, 60°C 30 sec/kb, 68°C 1 min/kb],

92°C 30 sec,

60°C 30 sec/kb,

68°C 10 min,

hold temperature at 4°C

2.2.1.2 Agarose gel electrophoresis and DNA fragment isolation

For analysis of plasmid DNA, a 0.8% agarose gel was usually used in this study. A 1-kb DNA ladder at a concentration of 0.05 mg/ml was loaded in one lane as a marker. Gel was run in 1 x TBE buffer and stained in 0.5 µg/ml ethidium bromide (EtBr). DNA was visualized under UV light.

10x TBE buffer (pH 8.3)

1 M Tris base

0.83 M Boric acid

10 mM EDTA

5x DNA loading buffer

30% glycerol (v/v)

0.25% bromophenol blue (w/v)

0.25% xylene cyanol FF (w/v)

A QIAquick gel extraction kit (Qiagen, Hilden, Germany) was used for isolation of DNA fragments from agarose gel. The samples (PCR products or enzyme-digested DNA samples) were electrophoresed through 0.8% agarose gel and stained with EtBr. The band of interest was identified using a UV-illuminator and cut out of the gel. The gel slice containing the DNA fragment was placed in the prepared tube and weighed. Every 100 mg of gel was dissolved in 300 μ l buffer QG at 50°C for 10 minutes. After the gel slice has dissolved completely, it was applied to a QIAquick column and spun down for 1 minute. The column was washed once with 0.75 ml wash buffer PE and the DNA sample was eluted with 30 μ l elution buffer EB(10 mM Tris-HCl, pH 8.5).

2.2.1.3 Enzyme digestion and ligation

For the ligation reaction, the vector DNA and the insert DNA have to be prepared by digesting with appropriate restriction enzymes and then purified with either a GFX purification kit (Amersham Biosciences) or a QIAquick PCR purification kit (Qiagen) according to the manufacture's protocol. The ligation reaction was established as follows. For the optimal ligation efficiency, two DNA molecules were added in the reaction in the range of 3:1 to 5:1 molar ratio of insert to vector. The reaction mixture was incubated at 16°C for 3 hours or more and was then incubated at 65°C for 15 minutes to inactivate the enzyme. The sample was spun down briefly and 2 μ l was used for transformation.

20 µl ligation reaction mixture

2.0 µl 10x buffer for T4 DNA ligase

2.0 µl linearised vector DNA

8.0 µl insert DNA

7.5 µl H₂O

0.5 µl T4 DNA ligase (400 U/µl)

2.2.1.4 Bacterial transformation

Two methods were used for the bacterial transformation in this work.

2.2.1.4.1 Transformation of *E. coli* cells by electroporation

• Preparation of competent cells

One liter of culture was incubated until an OD₆₀₀ of 0.4-0.6 was reached. The culture was centrifuged at 4000 x g for 15 minutes. The pellet was washed twice with 500 ml ice-cooled, sterile water, once with 200 ml ice-cooled, sterile 10% glycerol and once with 50 ml ice-cooled, sterile 10% glycerol. The last pellet was resuspended in 4 ml of ice-cooled sterile 10% glycerol. 50 µl aliquots were prepared and were shock-frozen in liquid nitrogen and placed in the -70°C freezer for storage.

• Transformation

Before transformation, a 50 µl aliquot of competent cells was thawed on ice. The DNA to be transformed was then added to competent cells and the cell mixture was transferred to a pre-chilled electroporation cuvette (BioRad). After a brief incubation on ice, the cells were exposed to a voltage of 1.8 kV (for cuvettes with 0.1 mm width) using the *E. coli* Pulser (BioRad). 950 µl of LB medium was added to the cuvette after electroporation. The cells were transferred to a 1.5-ml microcentrifuge tube, incubated at 37°C for 40-60 minutes, spread on LB plates containing appropriate antibiotics and incubated at 37°C overnight.

2.2.1.4.2 Transformation of *E. coli* cells by heat shock

• Preparation of competent cells (rubidium chloride method)

250 ml culture was incubated until an OD600 of 0.4-0.6 was reached. To collect cells, the culture was centrifuged at 4000 x g for 15 minutes at 4°C. Next, the cell pellet was resuspended in 100 ml ice-cooled TFBI buffer and incubated on ice for 10 minutes. The resuspension was then centrifuged at 4000 x g for 5 minutes at 4°C, and the pellet was resuspended in 10 ml ice-cooled TFBII buffer and incubated on ice for at least 15 minutes. 100 µl aliquots were prepared and were shock-frozen in liquid nitrogen and placed in the -70°C freezer for storage.

TFBI

30 mM potassium acetate

100 mM rubidium chloride

10 mM calcium chloride

50 mM manganese chloride

15% v/v glycerol

Adjust to pH 5.8 with acetic acid and filter (0.20 µm, Millipore) to sterilize.

TFBII

10 mM MOPS

75 mM calcium chloride

10 mM rubidium chloride

15% v/v glycerol

Adjust pH to 6.5 with KOH and filter to sterilize.

• Transformation

Before transformation, a 100 µl aliquot of competent cells was thawed on ice. The DNA or ligation reaction to be transformed was then added to the competent cells and the cell mixture was incubated on ice for 20-30 minutes and then at 42°C for 90 seconds for heat shock. 900 µl of LB medium was added and incubated at 37°C for 45 minutes and then spread on the LB plates containing appropriate antibiotic and incubated at 37°C overnight.

2.2.1.5 Mini-preparation of plasmid DNA

QIAprep spin miniprep kit (Qiagen, Hilden, Germany) was used for this purpose. The purification of plasmid DNA was performed following the methods described by the manufacturer. A single colony was inoculated into 5 ml of LB liquid medium containing appropriate antibiotic and grown overnight at 37°C with shaking. 2 ml of overnight culture was transferred to a 2-ml microcentrifuge tube and centrifuged at 13,000 rpm at 4°C for 10 minutes. The cell pellet was resuspended in 250 µl buffer P1, and then 250 µl buffer P2 was added and mixed gently by inverting the tube 4-6 times. After 5 minutes incubation at room temperature, 350 µl buffer P3 was added and mixed immediately but gently by inverting the tube 4-6 times. The tube was centrifuged at 13,000 rpm for 10 minutes. The supernatant was applied to a QIAprep spin column by decanting. The column was spun down for 1 minute to remove the liquid and washed once with 0.75 ml buffer PB and subsequently with 0.75 ml buffer PE. The residual wash buffer was removed by additional centrifugation for 1 minute and air-dried for 1 minute. To elute DNA, 50 µl of elution buffer EB was added to the center of each column and the column was allowed to stand for 1 minute at room temperature and centrifuged for 1 minute to collect the DNA sample. For checking the desired insert DNA fragment, 2 µl DNA sample was used for enzyme digestion and run on a 0.8 % agarose gel.

2.2.1.6 DNA sequencing

To minimize potential misincorporation during PCR, I used high-fidelity *Pfu* DNA polymerase to perform DNA amplification. In addition, the sequence accuracy of PCR products for each construct and cDNA was confirmed by DNA sequencing. The sequencing reaction and the PCR cycling program were established as follows:

20 µl sequencing reaction

10.0 µl H₂O

6.0 µl BigDye(Applied Biosystems, Weiterstadt, Germany)

3.0 µl DNA sample(~250 ng)

1.0 µl sequencing oligo(10 pmol/µl)

PCR cycling program

96°C 1 min

25 cycles of [96°C 30 sec, 55°C 30 sec, 60°C 4 min],

hold temperature at 4°C

Following the temperature cycling, the reaction was spun down briefly. To precipitate the sample, 15 µl of 3 M NaAc pH 5.3, 65 µl of H₂O and 300 µl of 100% ethanol were added and mixed. The tube was centrifuged at 13,000 rpm at 15°C for 20 minutes. The pellet was washed once with 750 µl 70% ethanol, dried in air and resuspended in 25 µl of template suppression reagent (Applied Biosystems, Weiterstadt, Germany). The DNA sample was sequenced by ABI PRISM™ 310 Genetic Analyzer (Applied Biosystems).

Table 2.3 List of the original constructs used in this study

protein	Construction	Description
SeIDtt-ZZ	pETMZZ/NcoI-KpnI	With n-terminus His-tag; the ZZ fusion with the target protein could be cleaved by TEV protease.
HypE-ZZ	pETMZZ/NcoI-KpnI	With n-terminus His-tag; the ZZ fusion with the target protein could be cleaved by TEV protease.
SPS1-ZZ	pETMZZ/NcoI-KpnI	With n-terminus His-tag; the ZZ fusion with the target protein could be cleaved by TEV protease.
SPS2(370)-ZZ	pETMZZ/NcoI-KpnI	With n-terminus His-tag; the ZZ fusion with the target

		protein could be cleaved by TEV protease.
SPS2(305)-ZZ	pETMZZ/NcoI-KpnI	With n-terminus His-tag; the ZZ fusion with the target protein could be cleaved by TEV protease.
SeIDtt-(6xHis)	pETM-11/NcoI-KpnI	With n-terminus His-tag; the 6 x His with the target protein could be cleaved by TEV protease.
SeIDec-(6xHis)	pETM-11/NcoI-KpnI	With n-terminus His-tag; the 6 x His with the target protein could be cleaved by TEV protease.
SeIDhi-(6xHis)	pETM-11/NcoI-KpnI	With n-terminus His-tag; the 6 x His with the target protein could be cleaved by TEV protease.
SeIDtt-(6xHis)	pETM-10/NcoI-KpnI	With n-terminus His-tag; the 6 x His with the target protein could not be cleaved by TEV protease.
SeIDhi-(C6xHis)	pETM-13/NcoI-NotI	With c-terminus His-tag; the 6 x His with the target protein could not be cleaved by TEV protease.
SPS1-(C6xHis)	pET22b(+)/NdeI-XhoI	With c-terminus His-tag; the 6 x His with the target protein could not be cleaved by TEV protease.
SPS2(370)-(C6xHis)	pET22b(+)/NdeI-XhoI	With c-terminus His-tag; the 6 x His with the target protein could not be cleaved by

		TEV protease.
SPS2(305)- (C6xHis)	pET22b(+)/NdeI-XhoI	With c-terminus His-tag; the 6 x His with the target protein could not be cleaved by TEV protease.
pur2p-(C6xHis)	pET22b(+)/NdeI-XhoI	With c-terminus His-tag; the 6 x His with the target protein could not be cleaved by TEV protease.
pur4p-(C6xHis)	pET22b(+)/NdeI-XhoI	With c-terminus His-tag; the 6 x His with the target protein could not be cleaved by TEV protease.

2.3 Protein expression and purification

2.3.1 Small scale expression

The *E. coli* host strains Rosetta (DE3) and BL21 (DE3) were transformed with different expression plasmids. Transformants of both strains were selected on Luria–Bertani (LB) plates supplemented with either ampicillin (100 µg /mL) or kanamycin (35 µg /mL). Well-grown single colonies from the selection plate were inoculated into 100 mL of LB medium containing either 100 µg /mL of ampicillin or 35 µg /mL kanamycin and the culture was incubated overnight at 37°C in an INNOVA 4330 shaker (New Brunswick Scientific, Edison, NJ) (180 rpm). Twenty milliliters of this culture was then added into 1 liter of fresh culture medium and the culture was grown in the shaker (180 rpm) at 37°C. When the absorbance at 600 nm reached around 0.7, expression of recombinant protein was induced by adding isopropyl b-D-thiogalactopyranoside (IPTG) to a concentration of 0.1 mM and incubation was continued at 18°C for various time periods. Ten milliliters of the culture medium was sampled after different culture times and the cell pellets were

collected by centrifugation. The cell pellets were resuspended in 1 ml of 1 x PBS buffer. Each suspension was sonicated 10 times for 10 second on ice with a Branson Sonifier 250 (Branson Ultrasonics, Danbury, CT), and was then centrifuged at 19,000 x g for 10 min at 4°C to separate the soluble and insoluble fractions. Both fractions were finally analyzed by using different concentrations of Sodium Dodecyl Sulphate-PolyAcrylamide Gel Electrophoresis (SDS–PAGE) followed by Coomassie Blue staining.

2.3.2 Protein assay

Protein concentration was determined in accordance with Lowry et al. using a Bovine Serum Albumin (BSA) standard. SDS-PAGE and Western Blotting SDS-PAGE was performed by the method of Laemmli. Proteins separated in the polyacrylamide gels were stained with the GelCode Blue Stain Reagent (Pierce Biotechnology), which is based on Coomassie Brilliant Blue G250 staining. The molecular weight markers were obtained from Bio-Rad.

2.3.3 Large scale expression and purification of recombinant proteins

Escherichia coli Rosetta (DE3) transformants which carry the desired protein-expression plasmids were cultured in 6 liter of LB broth containing either 100 µg /mL ampicillin or 35 µg /mL Kanamycin at 37°C. When the absorbance at 600 nm reached 0.7, 1 mM IPTG was added to induce the inducible promoter. For the production of recombinant proteins, the culture was incubated for another 24 hours at 20°C. After centrifugation, the bacterial pellets were stored at -80°C. The bacterial pellets were resuspended in 50 ml of 1 x PBS buffer. The suspension was sonicated for 30 sec 10 times on ice with a Branson Sonifier 250, and was centrifuged at 20,000 x g for 30 min at 4°C. The supernatant was dialyzed against 20 mM phosphate buffer (pH 6.2) and then applied to an open-column (Bio-rad, 20 ml) with affinity resin pre-equilibrated with the same buffer. The recombinant protein was purified by a standard procedure of affinity chromatography.

2.4 Crystallization

2.4.1 Screening

The initial screening was performed with vapor diffusion method by using Hampton Crystal Screens 1 & 2, Hampton PEG/ION screen, Emerald Wizard I & II, Emerald Cryol & II, and Nextal Screening Suites at both 4°C and 20°C. All of the above products used the sparse matrix method which is based on the successful conditions reported in the literatures. The initial protein solution was 10 mg/ml in 10 mM Tris pH8.0, 100 mM sodium chloride, and 2 mM DTT. Each drop of solution for crystallized trial was mixed with 100 nl of protein and 100 nl of crystallization screening solution by using Robot peptting.

2.4.2 Optimization

All of the initial conditions were optimized and the initial conditions gave the good crystal (Fig. 2-2b). Several parameters were tuned to grow better crystals for diffraction.

(1) Protein concentration: finding an appropriate protein concentration is important for crystallization. The protein concentration (i.e. 10 mg/ml) in the screening worked fine. Very little was changed on this parameter.

(2) Temperature: crystals can grow under several temperatures such as 4°C, 15°C, 20°C and 25°C. In general, the lower the temperature the crystallization was conducted, the more crystal nuclei and hence the smaller final size one would observe. However, the nucleation process is very difficult to control under low temperature even by adjusting other parameters. The crystallization seems to be sensitive to temperature variations and no crystals were observed in a quiet and temperature-uncontrolled room.

(3) pH and buffer: crystals were also reported appeared in buffers such as imidazol, ADA and cacodylate...etc. However, the crystals I observed looked much worse in the buffer systems other than what I documented here.

(4) Precipitant: adjusting either the concentration or the usage of different molecular weighted PEGs, e.g. PEG600, PEG400, PEG300...etc also helped to optimize the environment for crystallization.

(5) Salts: salts can be used as additives even though the crystallization is sensitive to the salt concentration which should be lower than 0.2M.

(6) Other factors: crystals prefer to grow from a material surface, e.g. the slide surface. Smearing a thin layer of silicon grease on the slide surface helped to grow better crystals and diminish mechanical damages to the crystals when mounting.

2.4.3. Cryo solutions

Several cryo-protectants were optimized for best results (table 2-1) (Rodgers, 2001). Finally, the buffer containing either [0.1M MES pH 6.1, 0.1M CsCl, 20% PEG300, 10% Glycerol] or [0.1M MES pH6.1, 0.1M sodium chloride, 20% PEG300, 10% Glycerol] was used as the cryo-solution.

Cryo-protectant	Suggested Concentration
DMSO	2-20%
Erythritol	>50%(w/v)
Ethylene glycol	15-45%
Glycerol	15-45%
Inositol	20-50%
MPD	25-40%
PEG 200-600	30-50%
Raffinose	>50%(w/v)
Sucrose	>50%(w/v)
(NH ₄) ₂ SO ₄	50% saturation
2-propanol	>70%
Xylitol	20-50%

Table 2.4 Commonly used cryo-protectants.

2.4.4. Heavy atom derivatives

Since the thioredoxin domain contains 3 cysteines and Hg^{2+} ions have a good affinity to sulfur atoms, Hg compounds are good candidates for heavy atom derivatization. In summary, several commonly used heavy atom compounds such as K_2PtCl_4 , HgCl_2 , PbAc , ZnI_2 and some lanthanide compounds etc. had been tried (table 3.5). The long soaking time is not necessary and could be shortened to 3 days. However, the very low concentration (0.05mM) of HgCl_2 is critical for successful crystallization since the derived crystals were somewhat crashed and diffracted badly when higher concentration was used.

Used times	Compound
287	Potassium tetrachloroplatinate(II)
111	Potassium dicyanoaurate(I)
103	Uranyl acetate
101	Mercury(II) acetate
98	Mercury(II) chloride
85	Ethylmercurythiosalicylate (EMTS)
82	Potassium tetraiodomercurate(II)
81	para-Chloromercuribenzenesulfonate(PCMBS)
75	Trimethyllead(IV) acetate
73	Potassium pentafluorooxyuranate(VI)
73	Phosphatotris(ethylmercury)
61	Potassium tetranitritoplatinum(II)
60	Uranyl nitrate
58	Potassium tetracyanoplatinate(II)
57	Dichlorodiammineplatinum(II)
51	Potassium hexachloroplatinate(IV)
51	Methylmercury chloride
44	Potassium tetrachloroaurate(III)
42	para-Chloromercurybenzoate(PCMB)
39	Lead(II) acetate

Table 2.5 The 23 most commonly used heavy-atom compounds reagents. The first column gives the number of times the reagent has appeared in the heavy-atom data bank. (Carvin et al.,2001)

2.5. X-ray data collection and processing

All the diffraction experiments were carried out at low temperature (100K). The crystals were soaked in the cryo solution for a short time (seconds or minutes), then plunged directly into liquid nitrogen (rather than flash cooling in the nitrogen gas).

The native data were collected on a Mar CCD detector at the synchrotron beamline X11 at the EMBL Hamburg outstation/DESY. The dose mode was used in collection. High resolution data were collected first with a high dose and fine oscillation angle, while subsequently the low resolution data were collected with low dose and wide oscillation angle. The radiation damage became apparent in the latter stage of the high resolution data collection, judged by the resolution decreasing. Hg derivative data were collected on Mar345 image plate in house. In order to overcome the non-isomorphism problem between the synchrotron and the in house data, one native dataset was also collected in house. The X-ray data were indexed & integrated with DENZO, and scaled with SCALEPACK (Otwinowski and Minor, 1997).

3. Results and Discussions

3.1 Protein expression and purification

3.1.1 Construction of the *Thermoanaerobacter tengcongensis* SelD expression plasmid and small scale expression

In *T. tengcongensis*, SelD is initially expressed as a selenoprotein consisting of 344 amino acid residues, and the codon of the 16th amino acid residue is selenocysteine (Sec or U), encoded as TGA. The primers for amplifying the cDNA fragment of the *T. tengcongensis* SelD (SelDtt) was designed to mutate the selenocysteine residues to cysteine, and cloned into a pETM-series vector, which provides a fusion tag at the N-terminus of the recombinant protein, for expressing the *T. tengcongensis* SelD (U16C) protein in *E. coli*.

Rosetta (DE3) strain is one of BL21 derivatives and is designed for enhancing the expression of eukaryotic proteins containing codons which are rarely used in *E. coli*. Rosetta (DE3) strain contains a compatible chloramphenicol-resistant plasmid which carries six tRNA genes for the rare codons AUA, AGG, AGA, CUA, CCC and GGA to achieve this purpose. A parallel protein-overexpression experiment in BL21 (DE3) cells was also conducted for comparison of the yield of the recombinant protein. After introducing the ZZ-SelDtt plasmid into Rosetta (DE3) and BL21 (DE3), transformants of both hosts were cultured at 16°C after induction with 0.1 mM IPTG. The expression level was analyzed by examining the total cell extract taken at different time points after IPTG induction by SDS-PAGE. In Rosetta (DE3) cells, the expression increased gradually and reached OD₆₀₀ ~ 1.8 twenty-four hours after induction. Indeed, Rosetta (DE3) produced more recombinant protein than BL21 (DE3), and therefore Rosetta (DE3) was chosen for the following large scale expression of ZZ-SelDtt.

3.1.2 Purification of recombinant ZZ-SelDtt

The pETM-ZZ T7 expression vector is inserted with a leading peptide, the ZZ domain of protein A for better productivity and solubility of recombinant protein. A specific proteolytic site which can be easily recognized and digested by TEV protease between the ZZ domain and the target protein, SelDtt, was inserted. As described above, Rosetta (DE3) was used for the large-scale expression of recombinant ZZ-SelDtt. The crude cell extract of Rosetta (DE3) cells expressing ZZ-SelDtt was applied to the Ni-NTA column. The recombinant ZZ-SelDtt was then eluted by a step-gradient of 0.35 M imidazole (pH8.0). As shown in Fig. 3.1, the collected fraction (Elu) shows a single band on the gel, suggesting that the recombinant ZZ-SelDtt could be purified by one step purification. The concentration of purified ZZ-SelDtt was then estimated by Bradford method. The yielding of purified recombinant ZZ-SelDtt was about 10 mg per 1 liter of LB culture (see Fig 3.1).

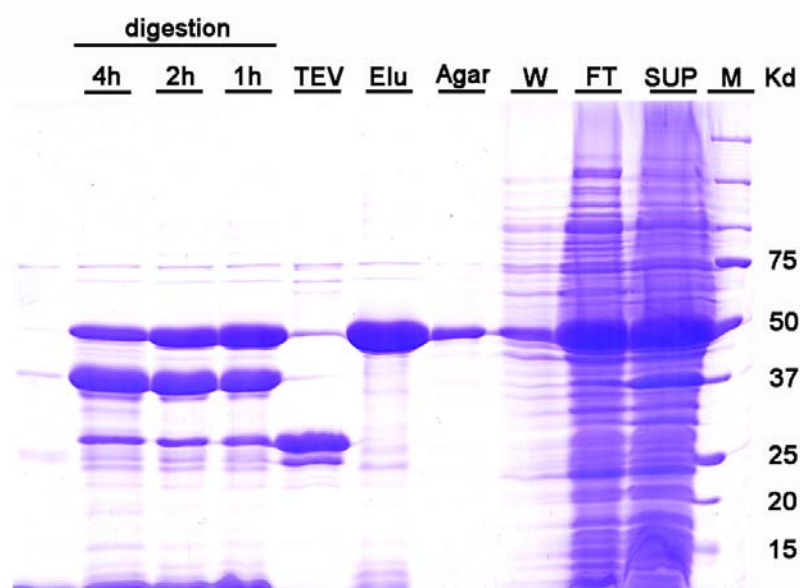


Figure 3.1 SDS-PAGE analysis of the recombinant ZZ-SelDtt purification. Proteins were visualized by Coomassie blue staining. SUP: supernatant of cell extract. FT: flow-through. W: washed through the affinity column. Agar: Ni-NTA beads after elution. Elu: recombinant protein purified from the Ni-NTA affinity column. TEV: TEV protease treated beads. Digestion: TEV digestion for 1h, 2h, and 4h.

3.1.2.1 Removing the ZZ-tag from ZZ-SeIDtt

Different incubation periods of the eluted ZZ-SeIDtt and TEV protease have been tested and the results were shown in Fig 3.1. More than 4 hr are needed for TEV protease to remove the ZZ tag from the eluted recombinant protein at 4°C.

Since the ZZ-tag, uncut fusion protein and TEV protease all contain the 6 x His-tag, they can be eliminated from the SeIDtt after a step of buffer exchange (10 mM Tris pH8.0, 100 mM NaCl, 2 mM DTT) on the PD-10 column (Bio-Rad) followed by a Ni-NTA column.

3.1.2.2 Thermostability examination of purified SeIDtt

Thermoanaerobacter tengcongensis is a thermophilic bacterium. It was first identified at the hot spring in China, and the optimal temperature for culturing it is at about 70°C. To check if the purified SeIDtt is properly folded, I have conducted a thermostability test of SeIDtt protein folded. The result showed that the purified SeIDtt is stable at 70°C (Fig. 3.2).

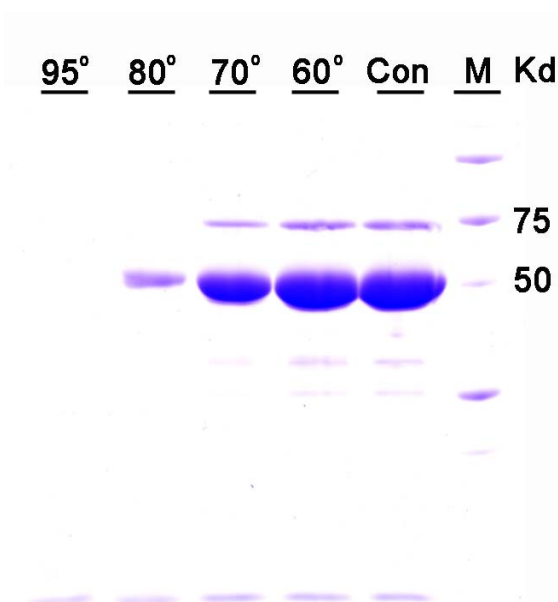


Figure 3.2 SDS-PAGE analysis of the thermostability of SeIDtt. The protein sample was heated at different temperature, namely 60°C, 70°C, 80°C, and 95°C, for 15 min, and then the pellet was removed after centrifugation. The supernatant was applied onto the gel and

proteins were visualized by Coomassie blue staining. Con: an unheated SelDtt serves as the control.

3.1.2.3 The size-exclusion chromatography of SelDtt

To seek the homogeneity of the partially purified SelDtt for crystallization, the recombinant SelDtt protein from the elution fraction described above was subjected to another purification procedure. The TEV-digested SelDtt was first applied onto a size-exclusion column, Superdex-75 26/60, and then eluted by the elution buffer. The elution profile revealed a significant peak around fraction #23 and #24 (Fig. 3.3). Fractions #21 to #28 were then collected and concentrated for further crystallization trials.

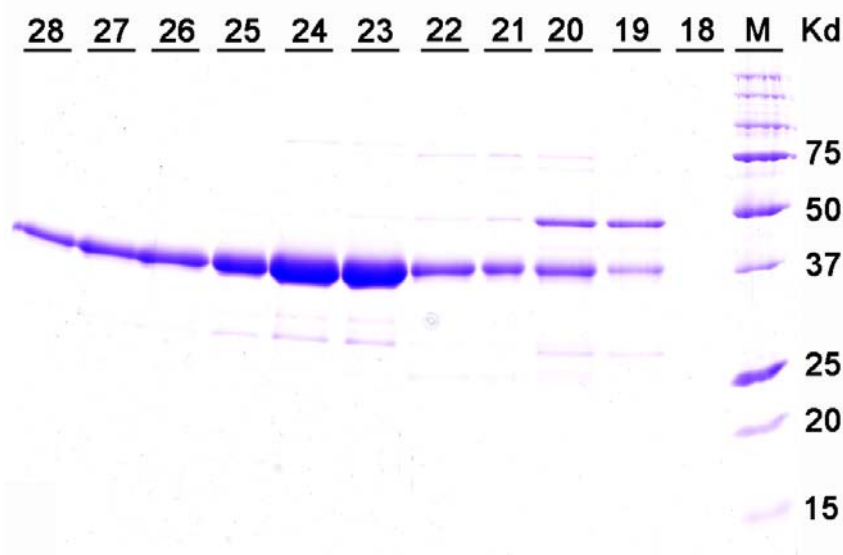


Figure 3.3 Gel filtration (Superdex-75 26/60) chromatography of TEV-digested ZZ-SelDtt. SelDtt enriched fraction from the Ni-NTA column was subjected to a size-exclusion (Superdex-75 26/60) column. A peak was observed from fraction #21 to #28. [Elution buffer: 10 mM Tris pH8.0, 100 mM NaCl and 2 mM DTT. Fraction Size: 3.5 ml] Eluted fractions were collected and examined by SDS-PAGE and Coomassie blue staining. Fraction #21 to #28 were pooled and concentrated for crystallization.

3.1.3 Expression and purification of SelDtt from pETM-10 construct

To seek more opportunities to crystallize SelDtt, various conditions have been tested in terms of expression vectors. SelDtt was cloned on the pETM-10 vector, which contains an un-removable N-terminus fusion His-tag.

As described above, Rosetta (DE3) strain was used for large-scale expression of recombinant M10-SelDtt. The crude cell extract of Rosetta (DE3) cells expressing M10-SelDtt was first applied onto the Ni-NTA agarose column with a bed volume of 0.8ml. The recombinant protein was then eluted by a step-gradient of 0.35 M imidazole (pH8.0) (Fig. 3.4). Next, the eluted M10-SelDtt sample was directly applied through a gel-filtration column (Superdex-75 26/60) in the buffer containing 10 mM Tris pH8.0, 100 mM NaCl and 2 mM DTT and then collected with a fraction size of 5 ml. A significant peak was observed from fraction #17 to #27. A small aliquot of fractions #17 to #27 were taken and run on a 15% gel followed by Coomassie blue staining to ensure the identity of the major protein in the fractions. The SDS-PAGE results were shown in Fig 3.5. Fraction #18 to #23 were pooled and concentrated for crystallization.

Before setting up the crystallization trials, the purified M10-SelDtt was also subjected to a thermostability test. It apparently showed that the purified M10-SelDtt was unstable at 70°C (Fig. 3.6).

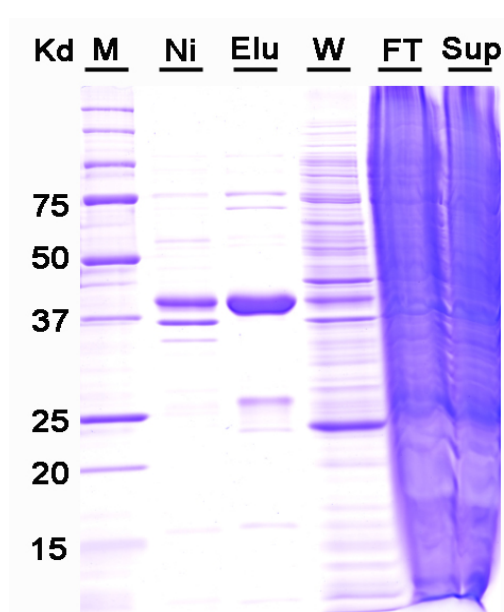


Figure 3.4 SDS-PAGE analysis of the recombinant M10-SelDtt purification. Proteins were visualized by Coomassie blue staining. Sup: supernatant of cell extract. FT: flow-through. W: washed through the affinity column. Ni: Ni-NTA beads after elution. Elu: recombinant M10-SelDtt eluted from the Ni-NTA column.

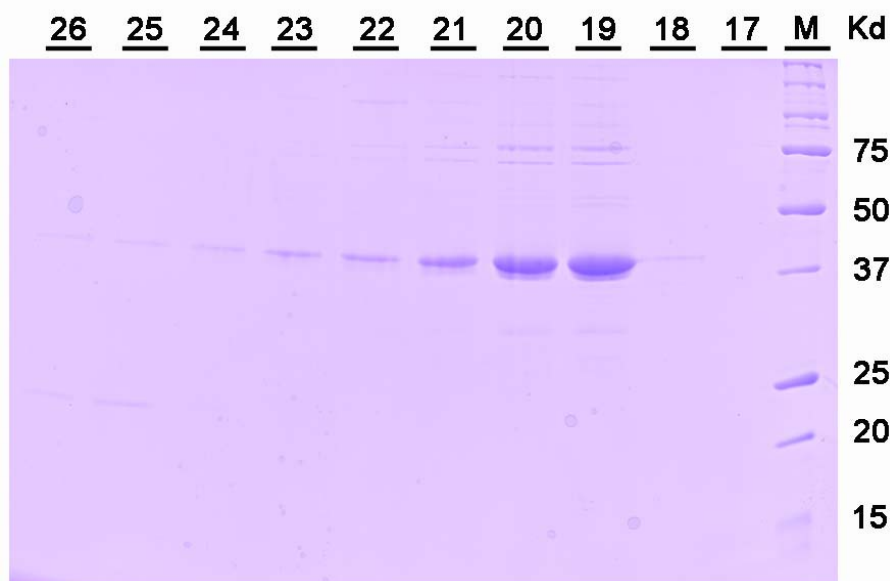


Figure 3.5 Gel filtration (Superdex-75 26/60) chromatography of M10-SeIDtt. M10-SeIDtt enriched fraction from the Ni-NTA column was subjected to a gel filtration (Superdex-75 26/60) column. A peak was observed from fraction #18 to #28. [Buffer: 10 mM Tris pH8.0, 100 mM NaCl and 2 mM DTT. Fraction Size: 5 ml] These fractions were collected and examined by SDS-PAGE and Coomassie blue staining. Fraction #18 to #23 were pooled and concentrated for crystallization.

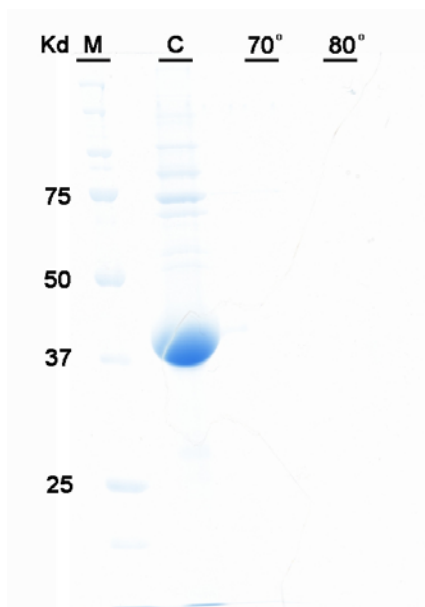


Figure 3.6 SDS-PAGE analysis of the thermostability test of M10-SeIDtt. The protein sample was heated at 70°C and 80°C for 15 min, the pellet was removed by centrifugation. The supernatant was applied onto the gel followed by Coomassie blue staining. C: an unheated purified M10-SeIDtt serves as the control.

3.1.4 Construction and small scale expression of the *Drosophila melanogaster* SPS1 and SPS2 clones

Two SelD homologs, SPS1 and SPS2, have been identified in mammals. In *Drosophila*, three selenophosphate synthetase (SelD) genes were previously identified by homology cloning and genome wide sequence analysis (Hirosawa-Takamori *et al*, 2000; Castellano *et al*, 2001; Martin-Romero *et al*, 2001; Kryukov *et al*, 2003). However, the *Drosophila* gene product, which corresponds to mammalian SPS1 (Persson *et al.*, 1997; Alsina *et al.*, 1999), lacks selenide-dependent SPS activity due to an arginine substitution of the critical Cys (or Sec) residue, which corresponds to the cysteine 17 in *E. coli*, in the catalytic domain of the enzyme. The other two SelD homologs in *Drosophila* are 2 isoforms (370 and 305 residues) of mammalian SPS2 with a Sec residue insertion. The evolutionarily conserved domains of these putative proteins can be aligned well with other SelD proteins (Fig. 3.7).

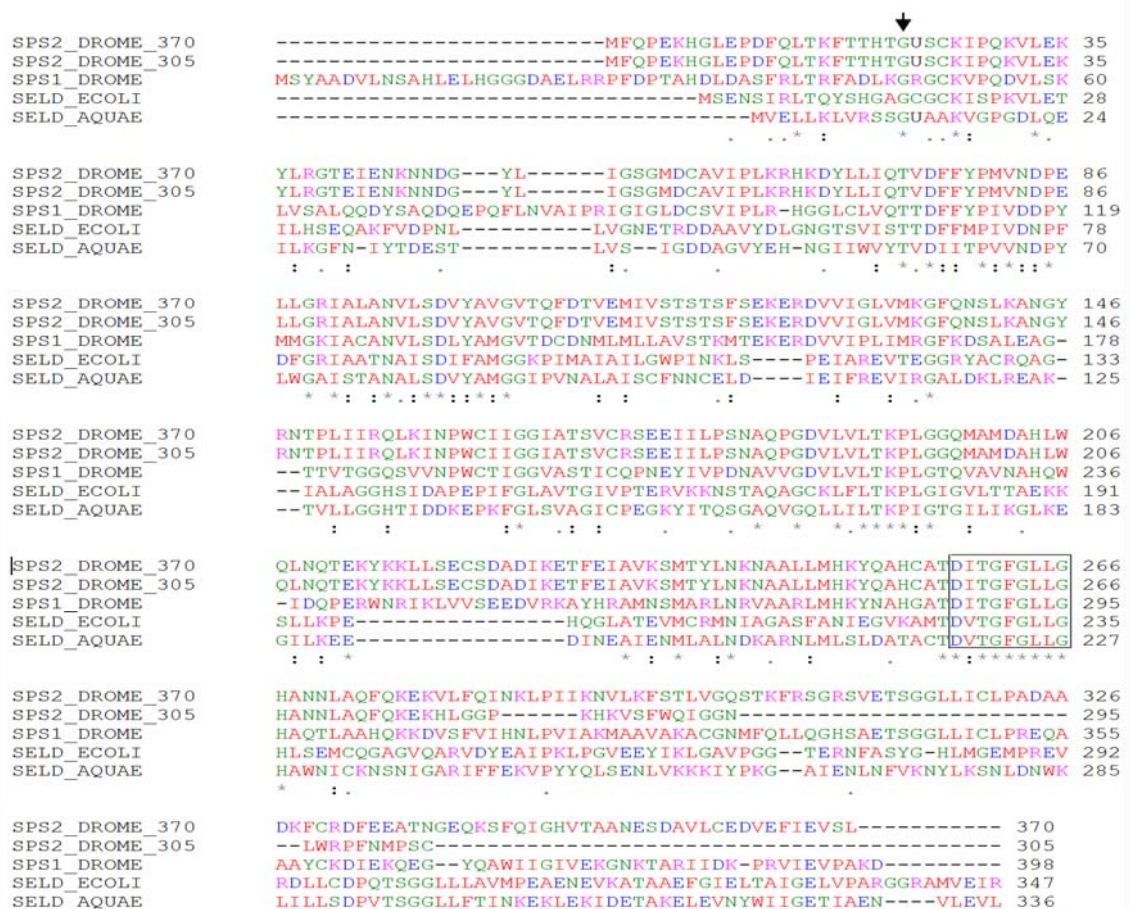


Figure 3.7 Alignments of SelD proteins from *Drosophila melanogaster* (DROME), *Escherichia coli* (ECOLI) and *Aquifex aeolicus* (AQUAE). The residue corresponding to the enzymatic active-site cysteine residue is indicated by an arrow. The sequence motifs which are putatively involved in ATP binding are boxed. Selenocysteine is represented by U.

To understand the structure of *Drosophila* SelD homologs, I cloned both SPS1 and SPS2 genes onto pETM-ZZ and pET22b (+) individually. These two proteins were then expressed in *E. coli* followed by protein purification procedures. However, the results indicated that the *Drosophila* homologs of SPS2 were insoluble when expressed from either expression vector.

3.1.5 Expression and purification of recombinant SPS1

Drosophila SPS1 gene was cloned onto the pET22b (+) T7 expression vector, which provides a C-terminus histidine tag without a proteolytic site between His-tag and the cloned protein. The Rosetta (DE3) strain was used for large-scale expression of recombinant SPS1 protein. The crude extract of Rosetta (DE3) cells expressing SPS1 was first applied onto the Ni-NTA column. The recombinant enzyme was next eluted by a step-gradient of 0.35 M imidazole (pH8.0) followed by another gel-filtration (Superdex-75 26/60) column.

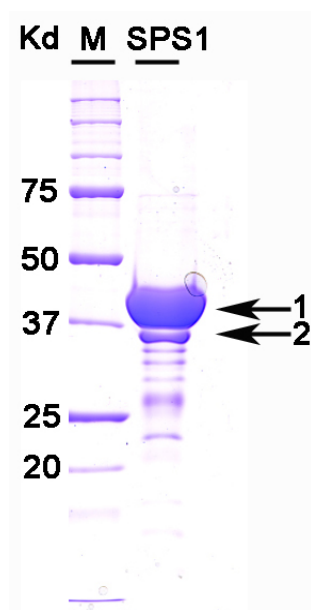


Figure 3.8 SDS-PAGE analysis of the recombinant SPS1.

As shown in Fig. 3.8, the collected sample showed 2 bands on SDS-PAGE. This sample was then analyzed by Mass-Spectroscopy, and the result indicated that both bands were *Drosophila* SPS1 protein. The yield of purified recombinant SPS1 was about 5 mg per 1 liter of LB culture.

3.1.6 Expression and purification of recombinant ZZ-SPS1

Drosophila SPS1 was also cloned onto the pETM-ZZ T7 expression vector and expressed in Rosetta (DE3) strain. The crude extract of Rosetta (DE3) cells expressing SPS1 was first applied to the Ni-NTA column. The recombinant enzyme was then eluted by a step-gradient of 0.35 M imidazole (pH8.0), and then subjected into the IgG-sepharose column (Amersham) for on-column TEV protease digestion. As shown in Fig. 3.9, the collected samples showed one major band on SDS-PAGE. The yield of the purified recombinant SPS1 was about 5 mg per 1 liter of LB culture.

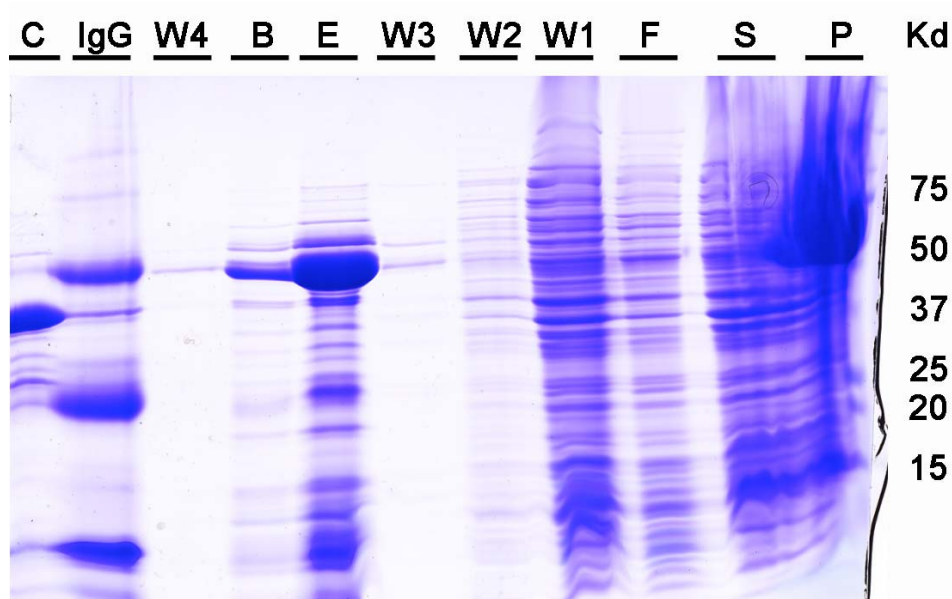


Figure 3.9 SDS-PAGE analysis of the recombinant ZZ-SPS1 purification. Proteins were visualized by Coomassie blue staining. S: supernatant of cell extract. P: pellet of cell extract. F: flow-through. W1-3: washed through the Ni-NTA affinity column. B: Ni-NTA beads after elution. E: recombinant protein purified from a Ni-NTA affinity column. W4: washed through the IgG-sepharose 4B. IgG: IgG beads after removing the TEV-treated SPS1. C: the flow through of the digested SPS1 from the IgG-Sepharose 4B.

To seek the homogeneity of the recombinant SPS1, the partially purified SPS1 subjected to another column to remove the high-salt contamination for further crystallization trials. The recombinant SPS1 protein from the elution fraction described above was applied onto a size-exclusion column, Superdex-75 26/60, and then eluted by the elution buffer. A significant peak was observed in the elution profile (Fig. 3.10). Fractions #26 to #30 were collected and concentrated for further crystallization.

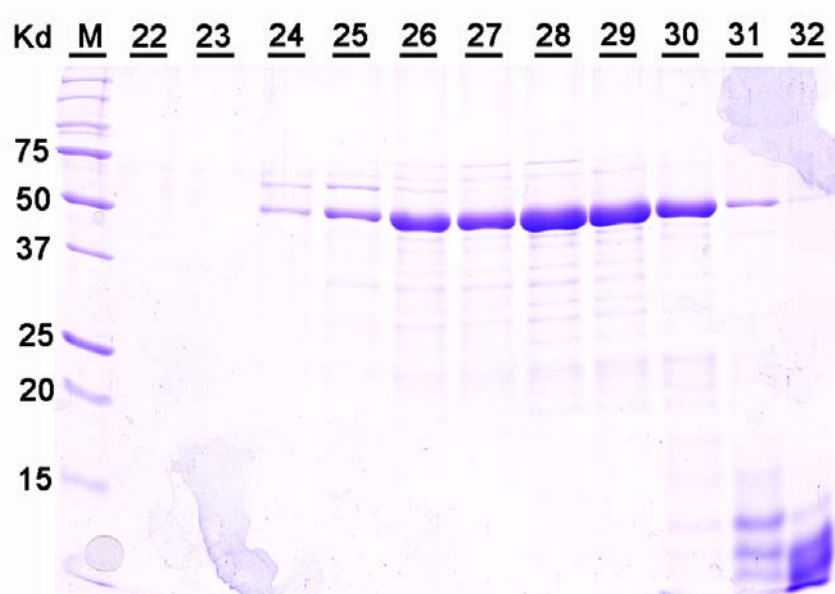


Figure 3.10 Gel filtration (Superdex-75 26/60) chromatography of ZZ-SPS1. SPS1 enriched fraction from the Ni-NTA column was subjected to a gel filtration (Superdex-75 26/60) column. A peak was observed from fraction #22 to #32. [Buffer: 10 mM Tris pH8.0, 100 mM NaCl and 2 mM DTT. Fraction Size: 5 ml] These fractions were collected and examined by SDS-PAGE and Coomassie blue staining. Fraction #26 to #30 were pooled and concentrated for crystallization.

3.1.7 Expression and purification of other recombinant SeID proteins

SeID homologs from other organisms were also cloned and expressed to seek more opportunities to crystallize the SeID proteins. As described above, Rosetta (DE3) strain was used for large-scale expression of the recombinant proteins. The results were briefly shown in Table 3.1.

Organisms	Vectors	Description
<i>Escherichia coli</i>	pETM-11	Expressed; purified
<i>Aquifex aeolicus</i>	pET22b(+)	Expressed; purified
<i>Haemophilus influenzae</i>	pETM-11, & -13	Expressed; insoluble
<i>Methanocaldococcus jannaschii</i>	pET22b(+)	Expressed; insoluble

Table 3.1 Progress in various organisms.

3.1.8 Other recombinant AIR synthase related proteins

In the purine biosynthetic pathway, aminoimidazole ribonucleotide (AIR) synthetase (PurM) is responsible for converting formylglycinamide ribonucleotide (FGAR) and ATP to AIR, ADP, and Pi. Due to the similarity in protein functions, catalytic mechanisms and sequence, SelD and PurM as well as the ATP-dependent enzymes HypE (a NiFe hydrogenase maturation protein) (Reissmann *et al.*, 2003) and thiamine phosphate kinase (ThiL) (Begley *et al.*, 1999) were recently proposed to be belonged to the same structural superfamily (Li *et al.*, 1999).

```

SELD_ECOLI      MSENSIRLTQYSHGAGCGCKISPKVLETILHSEQAKFVDPNLLVGNETRDDAAVYD--LG 58
PURM_ECOLI      TDKTSLSYKDAGVDIDAGNALVGRIKGVVKKTRRPEVMGGLGGFGALCALPKQYREPVLV 60
                . . . * : : : : : : : : : : : : : : : : : : : : : : : : : : : * : *

SELD_ECOLI      NGTSVISTTDFMPDIVDNPFDGRIIAATNAISDIFAMGGKPIMAIAAILGWPINKLSPEIA 118
PURM_ECOLI      SGT DGVGTKLRRLAMD LKRHDTIGIDLVMCVNDLVVQGAELFFLDYY--ATGKLDVDTA 118
                . ** . : * . : : : : * : : : : : : : : : : : : : : : : . . . ** . : *

SELD_ECOLI      REVTEGGRYACRQAGIALAGGHSIDAPEPIFGLAVTGIVPTERVKKNSTAQAGCKLFLT- 177
PURM_ECOLI      SAVISGIAEGCLQSGCSLVGGETAEMP GMYHGEDYDVAGFCVGVVEKSEIIDGSKVSDGD 178
                * . * . * * * : * * * : : * . * * : : * * : *

SELD_ECOLI      KPLGIGVLTAEKKSLLKPEHQGLATEVMCRMNIAGASFANIEGVKAMTDVTFGLLGH 237
PURM_ECOLI      VLIALGSSGPHSNGYSLVRKILEVSGCDPQTTELDGKPLADHLLAPTRIIYVKSVELIEK 238
                : : * . . : * : : : : : * . * : : . : * . . * .

SELD_ECOLI      SEMCQAGVQARVDYEAIPKLPVVEEYIKLGAVPGGTERNFASYGHLMGEMPREVRLLC 297
PURM_ECOLI      VDVHAI AHLTGGGFWENIPRVLPDNTQAVIDESWQWPEVFN---WLQTAGNVEHHEMYR 295
                : : * : . : * * : : : : . . . * : . * * : :

SELD_ECOLI      DPQTSGLLLAVMPEAENEVKATAAEFGIELTAIGELVPARGGRAMVEIR 347
PURM_ECOLI      TFNCGVGMIALPAPEVDKALALLNANGENAWKIGLIKASDSEQRVVEI- 344
                : . * : : : : . : : * * : * : * : : . : : : *

```

Figure 3.11 Alignment of SelD and PurM from *Escherichia coli* (ECOLI).

Few other AIR synthase related proteins were also cloned, expressed and purified for crystallization.

3.1.8.1 Expression and purification of *E. coli* HypE

The sequence similarity between SelD and HypE was shown in Figure 3.12. HypE was cloned onto both pET22b (+) and pETM-ZZ vectors for comparison and followed by overexpression in Rosetta (DE3) strain. Transformants were cultured at 16°C after induction with 0.1 mM IPTG. The inducibility and the expression level were determined by examining the total cell extract, which was taken at different time points after IPTG induction, by SDS-PAGE. However, the results shown on Fig.3.13 indicated that pET22b (+)-harbored HypE could not be expressed very well. In Rosetta (DE3) cells, the expression of ZZ-HypE increased gradually and reached OD₆₀₀ ~ 1.8 twenty-four hours after induction. The ZZ-tag, un-digested fusion protein and TEV protease were then removed after buffer exchange (10 mM Tris pH8.0, 100 mM NaCl, 2 mM DTT) on the PD-10 column (Bio-Rad) followed by the Ni-NTA column as described above. Finally, the sample was subjected onto a gel filtration column (Superdex-75 26/60) and eluted by appropriate buffer. The final purified HypE protein used for crystallization is shown in Fig 3.14.

```

SELD_ECOLI      MSENSIRLTQYSHGAGCGCKISPKVLETIHSEQAKFVDPNLLVGNETRDDAAVYDLNG 60
HYPE_ECOLI      -----MQQLINSLFMEAFANPWLAE---QEDQARLDLAQLVAEGDR-----LAFS 42
                :. . . : * :. . . * : * : : * : * : * : * : * : * : * : * : * : * :
                :. . . : * :. . . * : * : * : * : * : * : * : * : * : * :

SELD_ECOLI      TSVISTTDFMPPIVDNPFDFGRIAATNAISDIFAMGGKPIMAIAILGWPI NK-LSPEIAR 119
HYPE_ECOLI      TDSYVIDPLFFPGGN----IGKLAICGTANDVAVSG--AIPRYLSCGFILEEGLPMETLK 96
                * . . . . . : * : * : * : * : * : * : * : * : * : * : * : * :

SELD_ECOLI      EVTEGGRYACRQAGIALAGGHSIDAPEPIFGLAVTGIVPTERVKKNSTAQAGCKLFLTKP 179
HYPE_ECOLI      AVVT SMAETARAAGIAIVTGDTKVVQRGAVDKLFINTAGMGAIPANIHWGAQTLTAGDVL 156
                * . . . . . : * * * * : * : * : * : * : * : * : * : * : * :

SELD_ECOLI      LGIGVLTTAEEKSLLKPEHQGLATEVMCRMNIAG---ASFANIEGVKAMTDVTGFLLGH 236
HYPE_ECOLI      LVSGTLGDHGATILNLRQLGLDGLVSDCAVLTPLIQTLRDI PGVKALRDATRGGVNAV 216
                * * * * . * * : * * * : * : * : * : * : * : * : * : * : * :

SELD_ECOLI      LSEMCGAGVQARVDYEAIPKLPGVVEEYIKLGAVPGGTERNFASYGHLMGEMPREVRDLL 296
HYPE_ECOLI      VHEFAACGCGIELSEAALPVKPAVRG---VCELLGLDALNFANEGKLVIAVERNAAEQV 273
                : * : . . * . : . * : * * * . . : : * * * * . * : * : * : * :

SELD_ECOLI      CDPQTS GGLLLAVMPEAENEVKATAAEFGIELTAIGELVPARGGRAMVEIR 347
HYPE_ECOLI      LAALHS--HPLGKDAALIGEVVERKGVRLAGLYGKRTLDPHAEPLPRIC 322
                . * . . * . . * * . . * : . : . . . . . *

```

Figure 3.12 Alignments of SelD and HypE from *Escherichia coli* (ECOLI).

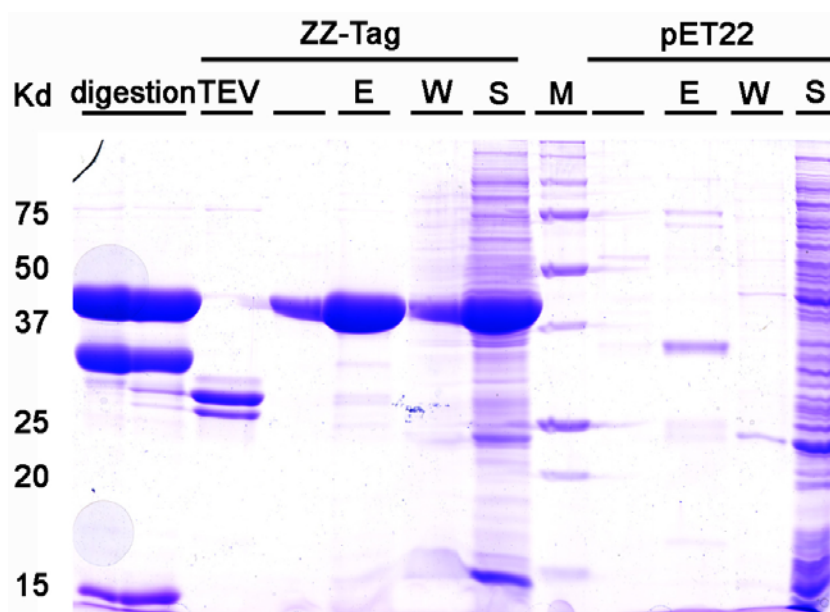


Figure 3.13 SDS-PAGE analysis of the recombinant HypE purification. Proteins were visualized by Coomassie blue staining. S: supernatant of cell extract. E: recombinant protein purified from a Ni-NTA affinity column. W: washed through the Ni-NTA column. M: protein size marker. TEV: TEV protease digested beads. Digestion: TEV-treated HypE flow through.

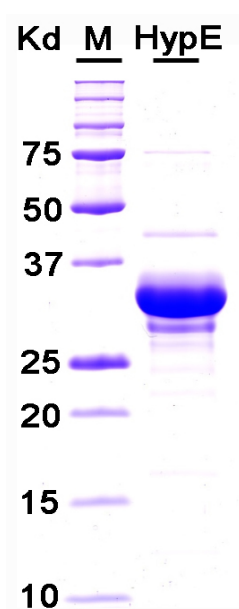


Figure 3.14 SDS-PAGE analysis of the final purity of recombinant HypE after gel-filtration.

3.2 Crystallization

3.2.1 Initial screening

The initial screening was performed with vapor diffusion method using Hampton Crystal Screens 1 & 2, Hampton PEG/ION screen, Salt Rx, Emerald Wizard I & II, Emerald Cryol & II, and Nextal Screening Suites at both 4°C and 20°C. All of the above products were applied by the sparse matrix method, which is based on the successful conditions reported in the literatures. The initial protein solution was 10 mg/ml in 10 mM Tris pH8.0, 100 mM NaCl, and 2 mM DTT. Each drop of solution for crystallized trial was mixed with 100 nl protein and 100 nl crystallization screening solution by using Robot pipetting. The results of the initial crystals are shown in Table 3.2:

Protein	Description
SPS1(C-6xHis)	Crystallized
ZZ-SPS1	Crystallized
SelDaa	Crystallized
SelDec	No crystal
SelDtt	No crystal
SelDtt(N-6xHis)	No crystal
HypE	No crystal

Table 3.2 Initial Crystallization Trials.

3.2.2 Optimization of crystallization conditions

3.2.2.1 The SPS1 crystal

Both SPS1(C-6xHis) and SPS1 always grow under the conditions containing ammonium, malonate, tartrate salts and PEGs. The crystals can be observed within 2-7 days after setting the drops (Fig 3.15). This rod-like crystal form can not diffract and the quality of the crystals needs to be improved.

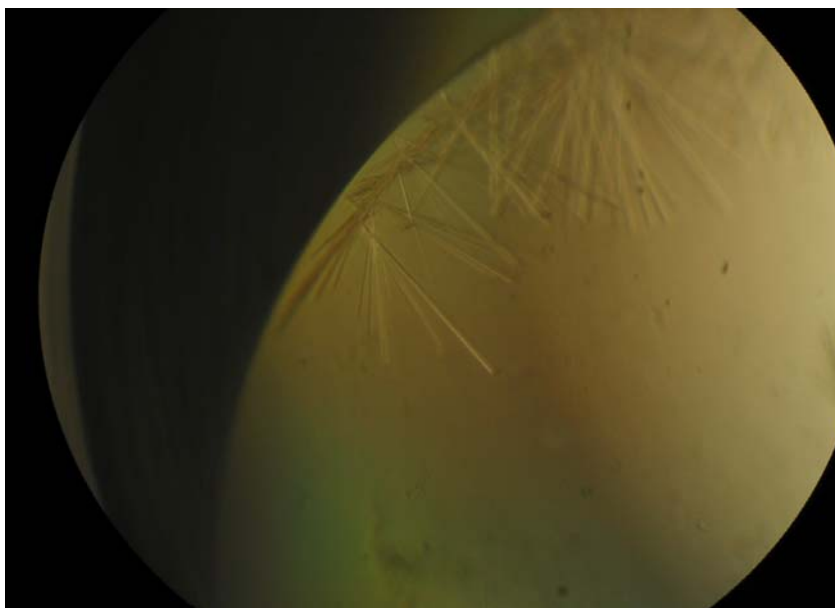


Figure 3.15 SPS1 crystals. Crystals of SPS1 grew under pH7.6, 0.2 M Na-Malonate (pH7.0) and 13 % PEG3350.

3.3 Data Collection of SelDaa

The crystals of SelDaa was grown at 12 % (w/v) PEG4000, 10 % (v/v) Isopropanol, and 0.1 M KCl (Fig. 3.16B).

A native dataset of these crystals to 2.4Å resolution at DESY (Table 3.3) was collected. Despite numerous attempts with co-crystallization and soaking, so far no suitable heavy atom derivatives could be found. Ta₆Br₁₄ seems to bind specifically to the crystals upon prolonged soaking. However, the diffraction power decreases and the derivatized crystals are not isomorphous to the native ones. A three-wavelength MAD dataset with such a derivatized specimen at DESY to about 3.5Å resolution (Table 3.3) was also collected. While we found a likely position for a heavy atom cluster, the data did not suffice to solve the structure, because at the present resolution individual atomic positions within the cluster cannot be resolved.

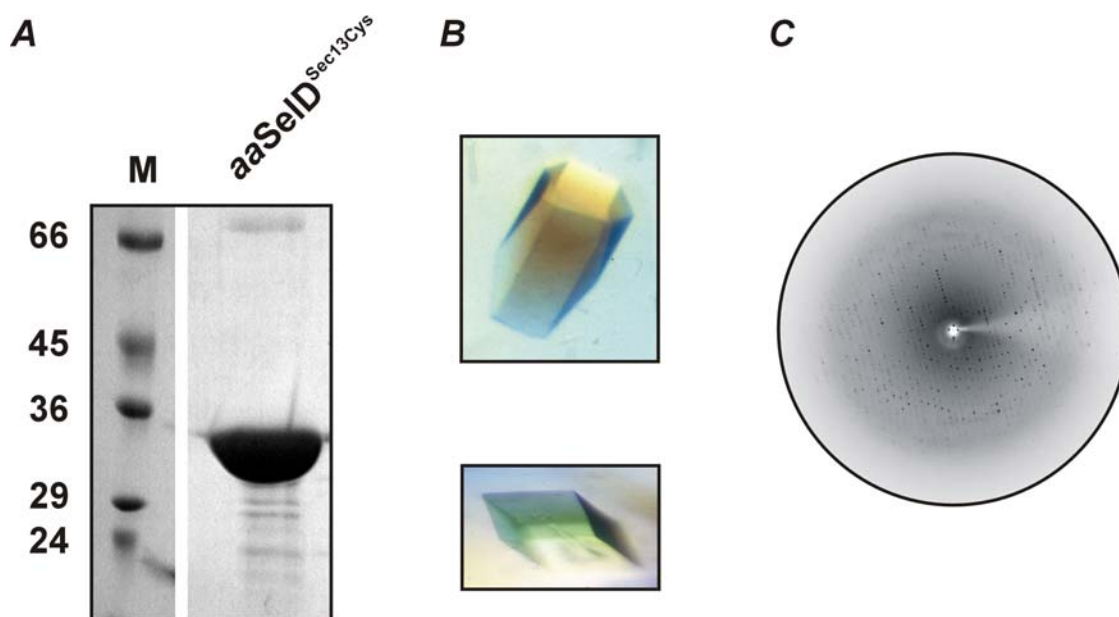


Fig. 3.16 Purified aaSelD^{Sec13Cys} protein and crystals. A: Purified *A. aeolicus* SelD^{Sec13Cys}. B: Crystals of the mutant SelD; top – native; bottom – SeMet. C: Diffraction pattern of the hexagonal SelD^{Sec13Cys} crystals from a rotating anode source. Resolution at the edge of the detector is about 2.5Å.

In parallel, a SeMet derivative of the protein was produced by standard method. SeMet incorporation was verified by N-terminal sequencing and mass spectrometry (data not shown). The SeMet preparation yielded crystals under very similar conditions as the wild type protein. However, these crystals belonged to a new space group, $P2_1$, with an estimated three to four molecules per asymmetric unit (Fig. 3.16 B). A three-wavelength MAD dataset from a specimen at ESRF beamline I14, Grenoble, to about 3.0Å resolution (Table 3.3) was collected. While attempting to interpret the heavy atom positions, a Patterson self rotation analysis revealed the presence of a 222 local symmetry element, indicating four molecules per asymmetric unit. The expected 16 selenium positions are now being sought under the constraint of this local symmetry element.

Crystal	Native	Ta ₆ Br ₁₄	SeMet
Wavelength (Å)	1.05	1.2556 (peak)	0.97894 (peak)
Space Group	P622	P622	P2 ₁
Cell Dimensions			
a, b, c (Å)	117.0, 117.0, 68.4	118.0, 118.0, 68.6	70.5, 88.4, 152.4
α, β, γ (°)	90.0, 90.0, 120.0	90.0, 90.0, 120.0	90.0, 97.7, 90.0
Resolution (Å)	20.0 – 2.4	20.0 – 3.5	30.0 – 3.0
R _{sym}			
All Data	5.7	5.2	8.7
Last 0.1Å	33.0	47.2	18.1
Reflections (last 0.1Å)			
Completeness (%)	97.3 (97.7)	97.9 (96.9)	96.4 (97.2)
Redundancy	3.2	2.9	2.1
Intensity (I/σ(I))			
All Data	12.0	14.3	8.3
Last 0.1Å	1.9	2.7	3.0

Table 3.3. *Aquifex aeolicus* SeID^{Sec13Cys} Crystals Data

4. References

A.

Alsina B, Corominas M, Berry MJ, Baguna J, Serras F. Disruption of selenoprotein biosynthesis affects cell proliferation in the imaginal discs and brain of *Drosophila melanogaster*. *J Cell Sci.* 1999 Sep;112 (Pt 17):2875-84.

B.

Baron C, Böck A. The length of the aminoacyl-acceptor stem of the selenocysteine-specific tRNA(Sec) of *Escherichia coli* is the determinant for binding to elongation factors SELB or Tu. *J Biol Chem.* 1991 Oct 25;266(30):20375-9.

Baron C, Westhof E, Bock A, Giege R. Solution structure of selenocysteine-inserting tRNA(Sec) from *Escherichia coli*. Comparison with canonical tRNA(Ser). *J Mol Biol.* 1993 May 20;231(2):274-92.

Beck MA, Levander OA, Handy J. Selenium deficiency and viral infection. *J Nutr.* 2003 May;133(5 Suppl 1):1463S-7S. Review.

Begley TP, Downs DM, Ealick SE, McLafferty FW, Van Loon AP, Taylor S, Campobasso N, Chiu HJ, Kinsland C, Reddick JJ, Xi J. Thiamin biosynthesis in prokaryotes. *Arch Microbiol.* 1999 Apr;171(5):293-300. Review.

Berry MJ, Banu L, Harney JW, Larsen PR. Functional characterization of the eukaryotic SECIS elements which direct selenocysteine insertion at UGA codons. *EMBO J.* 1993 Aug;12(8):3315-22.

Berry MJ, Harney JW, Ohama T, Hatfield DL. Selenocysteine insertion or termination: factors affecting UGA codon fate and complementary anticodon:codon mutations. *Nucleic Acids Res.* 1994 Sep 11;22(18):3753-9.

Böck A, Forchhammer K, Heider J, Leinfelder W, Sawers G, Veprek B, Zinoni F. Selenocysteine: the 21st amino acid. *Mol Microbiol.* 1991 Mar;5(3):515-20. Review.

Böck A, Forchhammer K, Heider J, Baron C. Selenoprotein synthesis: an expansion of the genetic code. *Trends Biochem Sci.* 1991 Dec;16(12):463-7. Review.

Böck A. (2001) Selenium metabolism in bacteria. In: Hatfield DA, editor. *Selenium: Its molecular biology and role in human health.* Boston: Kluwer Academic Publishers. pp. 7–22.

Briviba K, Roussyn I, Sharov VS, Sies H. Attenuation of oxidation and nitration reactions of peroxynitrite by selenomethionine, selenocystine and ebselen. *Biochem J.* 1996 Oct 1;319 (Pt 1):13-5.

Broome CS, McArdle F, Kyle JA, Andrews F, Lowe NM, Hart CA, Arthur JR, Jackson MJ. An increase in selenium intake improves immune function and poliovirus handling in adults with marginal selenium status. *Am J Clin Nutr.* 2004 Jul;80(1):154-62.

Bult CJ, White O, Olsen GJ, Zhou L, Fleischmann RD, Sutton GG, Blake JA, FitzGerald LM, Clayton RA, Gocayne JD, Kerlavage AR, Dougherty BA, Tomb JF, Adams MD, Reich CI, Overbeek R, Kirkness EF, Weinstock KG, Merrick JM, Glodek A, Scott JL, Geoghagen NS, Venter JC. Complete genome sequence of the methanogenic archaeon, *Methanococcus jannaschii*. *Science.* 1996 Aug 23;273(5278):1058-73.

C.

Carlson BA, Xu XM, Kryukov GV, Rao M, Berry MJ, Gladyshev VN, Hatfield DL. Identification and characterization of phosphoseryl-tRNA^[Ser]Sec kinase. *Proc Natl Acad Sci U S A.* 2004 Aug 31;101(35):12848-53. Epub 2004 Aug 18.

Cone JE, Del Rio RM, Davis JN, Stadtman TC. Chemical characterization of the selenoprotein component of clostridial glycine reductase: identification of selenocysteine as the organoselenium moiety. *Proc Natl Acad Sci U S A*. 1976 Aug;73(8):2659-63.

Copeland PR, Stepanik VA, Driscoll DM. Insight into mammalian selenocysteine insertion: domain structure and ribosome binding properties of Sec insertion sequence binding protein 2. *Mol Cell Biol*. 2001 Mar;21(5):1491-8.

D.

Das KC, Lewis-Molock Y, White CW. Elevation of manganese superoxide dismutase gene expression by thioredoxin. *Am J Respir Cell Mol Biol*. 1997 Dec;17(6):713-26.

Davis CD, Uthus EO. Dietary folate and selenium affect dimethylhydrazine-induced aberrant crypt formation, global DNA methylation and one-carbon metabolism in rats. *J Nutr*. 2003 Sep;133(9):2907-14.

Diamond AM. On the road to selenocysteine. *Proc Natl Acad Sci U S A*. 2004 Sep 14;101(37):13395-6. Epub 2004 Sep 7.

E.

Ehrenreich A, Forchhammer K, Tormay P, Veprek B, Böck A. Selenoprotein synthesis in *E. coli*. Purification and characterisation of the enzyme catalysing selenium activation. *Eur J Biochem*. 1992 Jun 15;206(3):767-73.

F.

Fleischmann RD, Adams MD, White O, Clayton RA, Kirkness EF, Kerlavage AR, Bult CJ, Tomb JF, Dougherty BA, Merrick JM, et al. Whole-genome

random sequencing and assembly of Haemophilus influenzae Rd. Science. 1995 Jul 28;269(5223):496-512.

Forchhammer K, Leinfelder W, Böck A. Identification of a novel translation factor necessary for the incorporation of selenocysteine into protein. Nature. 1989 Nov 23;342(6248):453-6.

Forchhammer K, Leinfelder W, Boesmiller K, Veprek B, Böck A. Selenocysteine synthase from Escherichia coli. Nucleotide sequence of the gene (selA) and purification of the protein. J Biol Chem. 1991 Apr 5;266(10):6318-23.

Forchhammer K, Böck A. Selenocysteine synthase from Escherichia coli. Analysis of the reaction sequence. J Biol Chem. 1991 Apr 5;266(10):6324-8.

G.

Glass R, Singh W, Jung W, Veres Z, Scholz T, Stadtman TC. Monoselenophosphate: synthesis, characterization, and identity with the prokaryotic biological selenium donor, compound SePX. Biochemistry. 1993 Nov 30;32(47):12555-9.

Gromer S, Johansson L, Bauer H, Arscott LD, Rauch S, Ballou DP, Williams CH Jr, Schirmer RH, Arner ES. Active sites of thioredoxin reductases: why selenoproteins? Proc Natl Acad Sci U S A. 2003 Oct 28;100(22):12618-23. Epub 2003 Oct 20.

Guimaraes MJ, Peterson D, Vicari A, Cocks BG, Copeland NG, Gilbert DJ, Jenkins NA, Ferrick DA, Kastelein RA, Bazan JF, Zlotnik A. Identification of a novel selD homolog from eukaryotes, bacteria, and archaea: is there an autoregulatory mechanism in selenocysteine metabolism? Proc Natl Acad Sci U S A. 1996 Dec 24;93(26):15086-91.

H.

Hansen JM, Watson WH, Jones DP. Compartmentation of Nrf-2 redox control: regulation of cytoplasmic activation by glutathione and DNA binding by thioredoxin-1. *Toxicol Sci.* 2004 Nov;82(1):308-17. Epub 2004 Jul 28.

Hatfield D, Portugal FH. Seryl-tRNA in mammalian tissues: chromatographic differences in brain and liver and a specific response to the codon, UGA. *Proc Natl Acad Sci U S A.* 1970 Nov;67(3):1200-6.

Hatfield D, Diamond A, Dudock B. Opal suppressor serine tRNAs from bovine liver form phosphoseryl-tRNA. *Proc Natl Acad Sci U S A.* 1982 Oct;79(20):6215-9.

Hatfield DL, Gladyshev VN. How selenium has altered our understanding of the genetic code. *Mol Cell Biol.* 2002 Jun;22(11):3565-76. Review.

Hirosawa-Takamori M, Jackle H, Vorbruggen G. The class 2 selenophosphate synthetase gene of *Drosophila* contains a functional mammalian-type SECIS. *EMBO Rep.* 2000 Nov;1(5):441-6.

Hoffmann PR, Berry MJ. Selenoprotein synthesis: a unique translational mechanism used by a diverse family of proteins. *Thyroid.* 2005 Aug;15(8):769-75.

Holmgren A. Thioredoxin and glutaredoxin systems. *J Biol Chem.* 1989 Aug 25;264(24):13963-6. Review.

Huenttenhofer A, Westhof E, Böck A. Solution structure of mRNA hairpins promoting selenocysteine incorporation in *Escherichia coli* and their base-specific interaction with special elongation factor SELB. *RNA.* 1996 Apr;2(4):354-66

J.

Jayakumar PC, Musande VV, Shouche YS, Patole MS. The Selenophosphate synthetase gene from *Leishmania major*. *DNA Seq.* 2004 Feb;15(1):66-70.

Jin JS, Baek S, Lee H, Oh MY, Koo YE, Shim MS, Kwon SY, Jeon I, Park SY, Baek K, Yoo MA, Hatfield DL, Lee BJ. A DNA replication-related element downstream from the initiation site of *Drosophila* selenophosphate synthetase 2 gene is essential for its transcription. *Nucleic Acids Res.* 2004 Apr 30;32(8):2482-93. Print 2004.

Jozsef L, Filep JG. Selenium-containing compounds attenuate peroxynitrite-mediated NF-kappaB and AP-1 activation and interleukin-8 gene and protein expression in human leukocytes. *Free Radic Biol Med.* 2003 Nov 1;35(9):1018-27.

K.

Kim IY, Veres Z, Stadtman TC. *Escherichia coli* mutant SELD enzymes. The cysteine 17 residue is essential for selenophosphate formation from ATP and selenide. *J Biol Chem.* 1992 Sep 25;267(27):19650-4.

Kim IY, Veres Z, Stadtman TC. Biochemical analysis of *Escherichia coli* selenophosphate synthetase mutants. Lysine 20 is essential for catalytic activity and cysteine 17/19 for 8-azido-ATP derivatization. *J Biol Chem.* 1993 Dec 25;268(36):27020-5.

Kim SH, Choi CH, Kim SY, Eun JS, Shin TY. Anti-allergic effects of *Artemisia iwayomogi* on mast cell-mediated allergy model. *Exp Biol Med (Maywood).* 2005 Jan;230(1):82-8.

Kim LK, Matsufuji T, Matsufuji S, Carlson BA, Kim SS, Hatfield DL, Lee BJ. Methylation of the ribosyl moiety at position 34 of selenocysteine

tRNA^[Ser]Sec is governed by both primary and tertiary structure. *RNA*. 2000 Sep;6(9):1306-15.

Kohrl J, Brigelius-Flohe R, Böck A, Gartner R, Meyer O, Flohe L. Selenium in biology: facts and medical perspectives. *Biol Chem*. 2000 Sep-Oct;381(9-10):849-64. Review.

Kromayer M, Wilting R, Tormay P, Böck A. Domain structure of the prokaryotic selenocysteine-specific elongation factor SelB. *J Mol Biol*. 1996 Oct 4;262(4):413-20.

Kryukov GV, Castellano S, Novoselov SV, Lobanov AV, Zehtab O, Guigo R, Gladyshev VN. Characterization of mammalian selenoproteomes. *Science*. 2003 May 30;300(5624):1439-43.

Kryukov GV, Gladyshev VN. The prokaryotic selenoproteome. *EMBO Rep*. 2004 May;5(5):538-43. Epub 2004 Apr 23.

L.

Lee BJ, Worland PJ, Davis JN, Stadtman TC, Hatfield DL. Identification of a selenocysteyl-tRNA(Ser) in mammalian cells that recognizes the nonsense codon, UGA. *J Biol Chem*. 1989 Jun 15;264(17):9724-7.

Lacourciere GM, Mihara H, Kurihara T, Esaki N, Stadtman TC. *Escherichia coli* NifS-like proteins provide selenium in the pathway for the biosynthesis of selenophosphate. *J Biol Chem*. 2000 Aug 4;275(31):23769-73.

Leinfelder W, Forchhammer K, Zinoni F, Sawers G, Mandrand-Berthelot MA, Bock A. *Escherichia coli* genes whose products are involved in selenium metabolism. *J Bacteriol*. 1988 Feb;170(2):540-6.

Leinfelder W, Zehelein E, Mandrand-Berthelot M, Böck A. Gene for a novel tRNA species that accepts L-serine and cotranslationally inserts selenocysteine. *Nature*. 1988 Feb 25;331(6158):723-5.

Leinfelder W, Forchhammer K, Veprek B, Zehelein E, Bock A. In vitro synthesis of selenocysteinyl-tRNA(UCA) from seryl-tRNA(UCA): involvement and characterization of the selD gene product. *Proc Natl Acad Sci U S A*. 1990 Jan;87(2):543-7.

Lester RL, DeMoss JA. Effects of molybdate and selenite on formate and nitrate metabolism in *Escherichia coli*. *J Bacteriol*. 1971 Mar;105(3):1006-14.

Li C, Kappock TJ, Stubbe J, Weaver TM, Ealick SE. X-ray crystal structure of aminoimidazole ribonucleotide synthetase (PurM), from the *Escherichia coli* purine biosynthetic pathway at 2.5 Å resolution. *Structure*. 1999 Sep 15;7(9):1155-66.

Longtin R. Selenium for prevention: eating your way to better DNA repair? *J Natl Cancer Inst*. 2003 Jan 15;95(2):98-100.

Low SC, Harney JW, Berry MJ. Cloning and functional characterization of human selenophosphate synthetase, an essential component of selenoprotein synthesis. *J Biol Chem*. 1995 Sep 15;270(37):21659-64.

M.

Martin-Romero FJ, Kryukov GV, Lobanov AV, Carlson BA, Lee BJ, Gladyshev VN, Hatfield DL. Selenium metabolism in *Drosophila*: selenoproteins, selenoprotein mRNA expression, fertility, and mortality. *J Biol Chem*. 2001 Aug 10;276(32):29798-804. Epub 2001 Jun 1.

Morey M, Corominas M, Serras F. DIAP1 suppresses ROS-induced apoptosis caused by impairment of the selD/sps1 homolog in *Drosophila*. *J Cell Sci*. 2003 Nov 15;116(Pt 22):4597-604.

Morey M, Serras F, Baguna J, Hafen E, Corominas M. Modulation of the Ras/MAPK signalling pathway by the redox function of selenoproteins in *Drosophila melanogaster*. *Dev Biol*. 2001 Oct 1;238(1):145-56.

Moosmann B, Behl C. Selenoproteins, cholesterol-lowering drugs, and the consequences: revisiting of the mevalonate pathway. *Trends Cardiovasc Med*. 2004 Oct;14(7):273-81. Review.

Moskovitz J, Stadtman ER. Selenium-deficient diet enhances protein oxidation and affects methionine sulfoxide reductase (MsrB) protein level in certain mouse tissues. *Proc Natl Acad Sci U S A*. 2003 Jun 24;100(13):7486-90. Epub 2003 Jun 5.

Moustafa ME, Carlson BA, El-Saadani MA, Kryukov GV, Sun QA, Harney JW, Hill KE, Combs GF, Feigenbaum L, Mansur DB, Burk RF, Berry MJ, Diamond AM, Lee BJ, Gladyshev VN, Hatfield DL. Selective inhibition of selenocysteine tRNA maturation and selenoprotein synthesis in transgenic mice expressing isopentenyladenosine-deficient selenocysteine tRNA. *Mol Cell Biol*. 2001 Jun;21(11):3840-52.

O.

Olivieri O, Girelli D, Stanzial AM, Rossi L, Bassi A, Corrocher R. Selenium, zinc, and thyroid hormones in healthy subjects: low T3/T4 ratio in the elderly is related to impaired selenium status. *Biol Trace Elem Res*. 1996 Jan;51(1):31-41.

Ogasawara Y, Lacourciere GM, Ishii K, Stadtman TC. Characterization of potential selenium-binding proteins in the selenophosphate synthetase system. *Proc Natl Acad Sci U S A*. 2005 Jan 25;102(4):1012-6. Epub 2005 Jan 14.

P.

Persson BC, Bock A, Jackle H, Vorbruggen G. SelD homolog from *Drosophila* lacking selenide-dependent monoselenophosphate synthetase activity. *J Mol Biol.* 1997 Nov 28;274(2):174-80.

R.

Rafferty TS, Green MH, Lowe JE, Arlett C, Hunter JA, Beckett GJ, McKenzie RC. Effects of selenium compounds on induction of DNA damage by broadband ultraviolet radiation in human keratinocytes. *Br J Dermatol.* 2003 May;148(5):1001-9.

Reissmann S, Hochleitner E, Wang H, Paschos A, Lottspeich F, Glass RS, Böck A. Taming of a poison: biosynthesis of the NiFe-hydrogenase cyanide ligands. *Science.* 2003 Feb 14;299(5609):1067-70.

Romero H, Zhang Y, Gladyshev VN, Salinas G. Evolution of selenium utilization traits. *Genome Biol.* 2005;6(8):R66. Epub 2005 Jul 27.

Roussyn I, Briviba K, Masumoto H, Sies H. Selenium-containing compounds protect DNA from single-strand breaks caused by peroxynitrite. *Arch Biochem Biophys.* 1996 Jun 1;330(1):216-8.

Roy M, Kiremidjian-Schumacher L, Wishe HI, Cohen MW, Stotzky G. Supplementation with selenium restores age-related decline in immune cell function. *Proc Soc Exp Biol Med.* 1995 Sep;209(4):369-75.

Ruan H, Tang XD, Chen ML, Joiner ML, Sun G, Brot N, Weissbach H, Heinemann SH, Iverson L, Wu CF, Hoshi T. High-quality life extension by the enzyme peptide methionine sulfoxide reductase. *Proc Natl Acad Sci U S A.* 2002 Mar 5;99(5):2748-53. Epub 2002 Feb 26. Erratum in: *Proc Natl Acad Sci U S A* 2002 May 14;99(10):7184. Chen, M-L [corrected to Chen, Mai-Lei]; Joiner, MA [corrected to Joiner, Mei-Ling A]; Heinemann, Stephen H [corrected to Heinemann, Stefan H].

S.

Serras F, Morey M, Alsina B, Baguna J, Corominas M. The *Drosophila* selenophosphate synthetase (*selD*) gene is required for development and cell proliferation. *Biofactors*. 2001;14(1-4):143-9

Seo YR, Kelley MR, Smith ML. Selenomethionine regulation of p53 by a ref1-dependent redox mechanism. *Proc Natl Acad Sci U S A*. 2002 Oct 29;99(22):14548-53. Epub 2002 Sep 30.

Sies H, Sharov VS, Klotz LO, Briviba K. Glutathione peroxidase protects against peroxynitrite-mediated oxidations. A new function for selenoproteins as peroxynitrite reductase. *J Biol Chem*. 1997 Oct 31;272(44):27812-7.

Stadtman TC. Selenoproteins--tracing the role of a trace element in protein function. *PLoS Biol*. 2005 Dec;3(12):e421. Epub 2005 Dec 13.

Stewart EJ, Aslund F, Beckwith J. Disulfide bond formation in the *Escherichia coli* cytoplasm: an in vivo role reversal for the thioredoxins. *EMBO J*. 1998 Oct 1;17(19):5543-50.

T.

Taylor PR, Parnes HL, Lippman SM. Science peels the onion of selenium effects on prostate carcinogenesis. *J Natl Cancer Inst*. 2004 May 5;96(9):645-7. Review.

Tamura T, Yamamoto S, Takahata M, Sakaguchi H, Tanaka H, Stadtman TC, Inagaki K. Selenophosphate synthetase genes from lung adenocarcinoma cells: *Sps1* for recycling L-selenocysteine and *Sps2* for selenite assimilation. *Proc Natl Acad Sci U S A*. 2004 Nov 16;101(46):16162-7. Epub 2004 Nov 8.

Turner RJ, Weiner JH, Taylor DE. Selenium metabolism in *Escherichia coli*. *Biometals*. 1998 Sep;11(3):223-7. Review.

U.

Ursini F, Heim S, Kiess M, Maiorino M, Roveri A, Wissing J, Flohe L. Dual function of the selenoprotein PHGPx during sperm maturation. *Science*. 1999 Aug 27;285(5432):1393-6.

V.

Veres Z, Tsai L, Scholz TD, Politino M, Balaban RS, Stadtman TC. Synthesis of 5-methylaminomethyl-2-selenouridine in tRNAs: ³¹P NMR studies show the labile selenium donor synthesized by the selD gene product contains selenium bonded to phosphorus. *Proc Natl Acad Sci U S A*. 1992 Apr 1;89(7):2975-9.

Veres Z, Kim IY, Scholz TD, Stadtman TC. Selenophosphate synthetase. Enzyme properties and catalytic reaction. *J Biol Chem*. 1994 Apr 8;269(14):10597-603.

W.

Warner GJ, Berry MJ, Moustafa ME, Carlson BA, Hatfield DL, Faust JR. Inhibition of selenoprotein synthesis by selenocysteine tRNA[Ser]^{Sec} lacking isopentenyladenosine. *J Biol Chem*. 2000 Sep 8;275(36):28110-9.

Wilting R, Vamvakidou K, Böck A. Functional expression in *Escherichia coli* of the *Haemophilus influenzae* gene coding for selenocysteine-containing selenophosphate synthetase. *Arch Microbiol*. 1998 Jan;169(1):71-5.

X.

Xu XM, Mix H, Carlson BA, Grabowski PJ, Gladyshev VN, Berry MJ, Hatfield DL. Evidence for direct roles of two additional factors, SECp43 and soluble

liver antigen, in the selenoprotein synthesis machinery. *J Biol Chem.* 2005 Dec 16;280(50):41568-75. Epub 2005 Oct 17.

Y.

Yoshizumi M, Kogame T, Suzaki Y, Fujita Y, Kyaw M, Kirima K, Ishizawa K, Tsuchiya K, Kagami S, Tamaki T. Ebselen attenuates oxidative stress-induced apoptosis via the inhibition of the c-Jun N-terminal kinase and activator protein-1 signalling pathway in PC12 cells. *Br J Pharmacol.* 2002 Aug;136(7):1023-32.

Z.

Zhang Y, Fomenko DE, Gladyshev VN. The microbial selenoproteome of the Sargasso Sea. *Genome Biol.* 2005;6(4):R37. Epub 2005 Mar 29.

Zinoni F, Heider J, Böck A. Features of the formate dehydrogenase mRNA necessary for decoding of the UGA codon as selenocysteine. *Proc Natl Acad Sci U S A.* 1990 Jun;87(12):4660-4.

Zhong L, Holmgren A. Essential role of selenium in the catalytic activities of mammalian thioredoxin reductase revealed by characterization of recombinant enzymes with selenocysteine mutations. *J Biol Chem.* 2000 Jun 16;275(24):18121-8.

II. Cloning, Purification and Crystallization of Erp44 from *Mus musculus*

1. Introduction

1.1 The endoplasmic reticulum stress

In eukaryotic cells, the endoplasmic reticulum (ER) is a principle site for protein synthesis and folding as well as calcium storage and signaling. It also serves as a compartment of biosynthesis of steroids, cholesterol and other lipids. In lower eukaryotes, a major portion of the cell wall is also synthesized in the ER. In particular, ER is the first destination for the nascent proteins recruited into the secretory pathway. Several mechanisms are contributed and guaranteed whether or not the unfolded nascent proteins are properly folded. These procedures of protein quality controls are provided to prevent the nascent protein apart from aggregation and leads to the secretory pathway. If the nascent protein is failing to fold, the assembling will not proceed until it is correctly folded or eventually degraded by cytosolic proteasome.

The ER provides a suitable environment and optimal pH for the redox conditions and there are vast array of chaperones and foldases available, including members of protein disulfide isomerase family (PDI), BiP (immunoglobulin heavy chain-Binding Protein) (Kassenbrock *et al.*, 1988), GRp94 (Bose *et al.*, 1996), Calreticulin (Hebert *et al.*, 1996), Calnexin (Bergeron *et al.*, 1994) and Peptidyl-prolyl isomerase (PPIase) (Freskgard *et al.*, 1992). The folding state of proteins is always monitored by the stringent quality control system (Chevet *et al.*, 2001; Ellgaard and Helenius, 2003). If the unfolded or misfolded proteins are abundantly accumulated, a so-called the unfolded protein responses (UPR) signaling pathway will be activated to induce the expression of

transcription factors of more ER chaperones to suit the need (Chapman *et al.*, 1998. Harding *et al.*, 2002).

In principle, proteins with a correct conformation are allowed to leave for the next destination, and in contrast, unfolded, incompletely folded or misfolded proteins will be retained and bound by molecular chaperones or foldases in the ER and go through further attempts to achieve the native conformation. However, if these attempts failed, the misfolded proteins will enter the ER associated degradation pathway (ERAD) through which the unfolded or misfolded proteins will be retro-translocated from the ER to the cytosol and eventually degraded in the proteasome (Ellgaard and Helenius, 2001; Hampton, 2002; Kostova and Wolf, 2003). In all of these mechanisms, the chaperones and foldases play critical roles in response to all the ER stress situation.

In this study, I have investigated the structure of a novel ER resident PDI family member, ERp44, which is induced by ER stress (Anelli *et al.*, 2002).

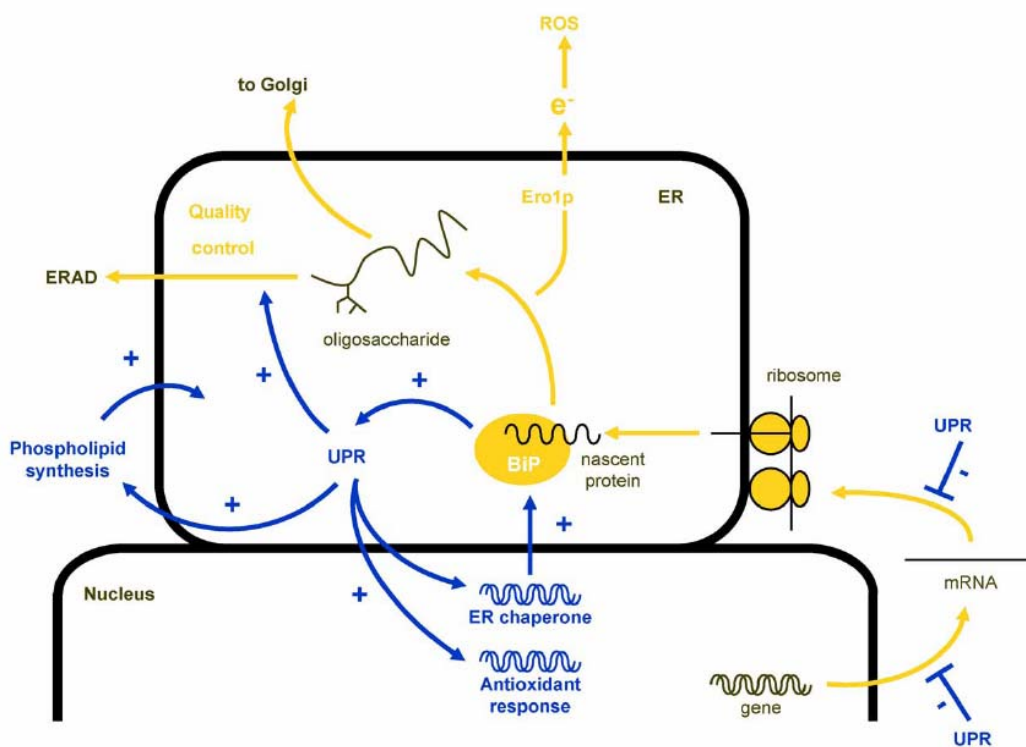


Figure 1.1: Protein flux through the ER (orange) and principal activities of the UPR to couple the ER protein folding capacity with its protein folding burden (blue). ROS: reactive oxygen species (Adapted from Schroeder and Kaufmann; 2005).

1.1.1 Overview of the ER quality control

Almost all proteins secreted from the cell or resident along the secretory pathway begin their journey within the membranes of the ER. They cross or integrate into the ER membrane through a proteinaceous pore called the translocon (Johnson & van Waes, 1999). Being physically separated from the cytosol, the ER maintains its own distinct luminal environment for the specific requirements of secretory protein biogenesis. An extensive collection of factors are critical to carry out essential maturation steps that include signal sequence cleavage, N- and O-linked glycosylation, lysosylphosphatidylinositol (GPI)-anchor addition, folding and oligomerization, disulphide bond formation, and isomerization. Since these protein maturation activities are only found along the secretory pathway, the uncontrolled flux of immature proteins out of the ER would be disastrous. This scenario is avoided by a mechanism termed “ER quality control (ERQC)”, which monitors protein folding and assembly and prevents the transport of immature molecules. The ER must also contend with irreversibly misfolded proteins. The major causes for aberrant protein biogenesis include errors in transcription and translation, environmental stress (including oxidative damage and unfavorable temperatures), and subunit stoichiometric imbalances (Ellgaard & Helenius, 2003; Wickner *et al.*, 1999). Surprisingly, up to 30% of all newly synthesized proteins are estimated to be defective. Most known erroneous proteins are toxic to an organism (Bucciantini *et al.*, 2002). To neutralize them, cells deploy another pathway termed ER-associated degradation (ERAD) to take out offending proteins of folding pathways and aim them for degradation. The protein flux through the ER includes soluble proteins, single and multi-spanning integral membrane proteins, and lipid anchored proteins. Misfolded proteins that appear from any of these populations can be eliminated by ERAD. Regardless of species, they are recognized, targeted, and translocated to the ubiquitylation machinery located on the cytosolic face of the

ER for ubiquitin modification (most substrates). The molecules are next extracted from the membrane and finally degraded by the 26S proteasome. To monitor the wide variety of substrates and decide whether or not a protein is misfolded, multiple cellular pathways were reported to collaborate to accomplish the task. For additional reading, the reader is directed to several excellent reviews recently published (Ellgaard & Helenius, 2003; Kostova & Wolf, 2003; McCracken & Brodsky, 2003; Sitia & Braakman, 2003; Trombetta & Parodi, 2003).

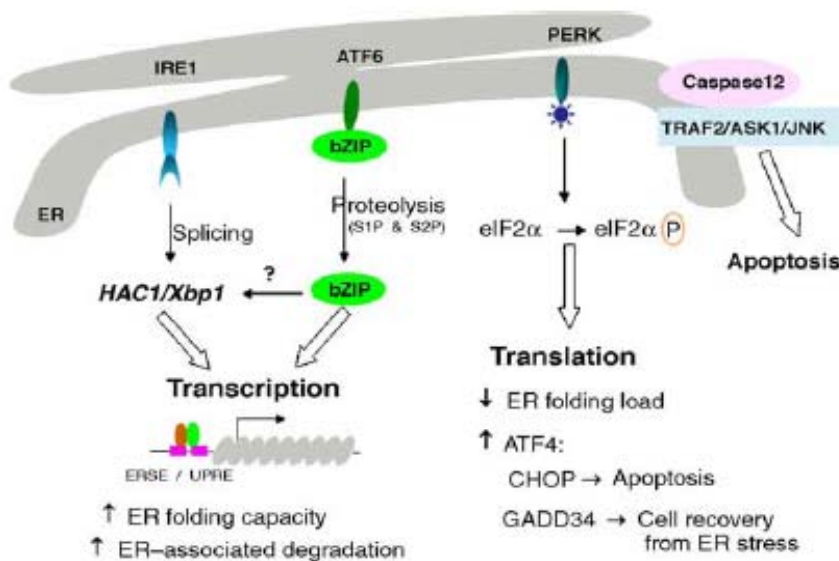


Figure 1.2 Overview of the ER quality control: Tripartite stress signaling from the ER. The UPR is an adaptation of cells to quickly respond to physiological fluctuations in protein folding load and secretion demands that are coupled with differentiation in mammals. PERK-mediated phosphorylation of eIF2 α causes an early and transient response to attenuate translation and hence reduce protein folding load. Paradoxically, phosphorylated eIF2 α preferentially translates *ATF4* mRNA, producing a bZIP transcription factor which upregulates transcription of CHOP and GADD34 that are involved in apoptosis and recovery from translational inhibition. Both IRE1 and ATF6 can mediate transcriptional induction to upregulate ER folding capacity and ER associated degradation (ERAD) machinery. Translocation to the Golgi and proteolytic cleavage mediated by site-1 and site-2 proteases (S1P and S2P) activate ATF6 and release its cytosolic bZIP domain that migrates to the nucleus and activates gene transcription. ATF6 might upregulate transcription of *Xbp1*, a mammalian homologue of yeast *HAC1*, providing *Xbp1* mRNA for splicing

mediated by IRE1 endoribonuclease. Only spliced *Xbp1* mRNA can be translated into a potent bZIP transcription factor. Prolonged ER stress activates ER stress-specific effectors to delete cells with irreparable ER stress. (Adapted from Shen *et al.*, 2004)

1.1.2 The ER-initial cell death (ER Stress)

When every adaptations of the UPR fails, the ER-initiated pathways set alarm by activating NF- κ B, a transcription factor that induces expression of genes encoding mediators of host defense. In multicellular organisms, excessive and prolonged ER stress triggers cell suicide, usually in the form of apoptosis, to dispense of dysfunctional cells. Progress in understanding the mechanisms underlying these 3 phases of adaptation, alarm, and apoptosis has improved our knowledge of ER stress, and its role in disease.

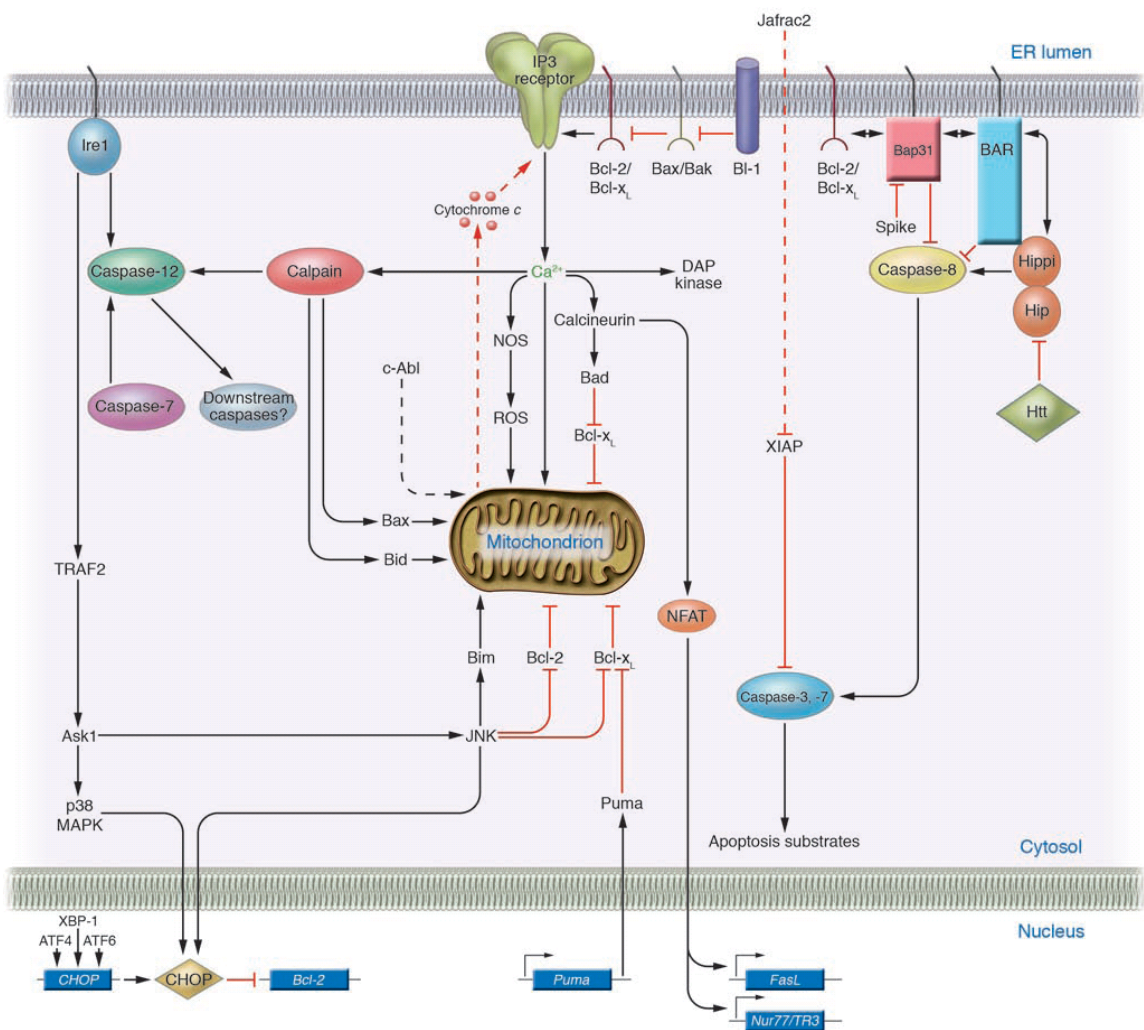


Figure 1.3 Cell death mechanisms induced by ER stress: Several of the proposed pathways that link ER stress to apoptosis. Dashed lines indicate protein translocation process (c-Abl, Jafrac2). The Ca^{2+} sensitive mitochondrial permeability transition pore complex is not shown in the diagram. (Adapted from Xu *et al.*, 2005)

1.2 Protein folding inside the ER lumen

The ER lumen has obvious different topology, chemical composition, and the protein folding machinery from cytoplasm; all of these features affect protein folding in the ER significantly.

1.2.1 The topology and chemical environment of the ER

Since the ER is a membrane surrounded environment. Its luminal space is equivalent to the extracellular environment of Gram-Negative bacteria. Nascent proteins destined for secretory pathway, transverse the ER membrane through the Sec61p complex, which executes signal sequence cleavage, and leads to further folding process.

The pH in the ER is near neutral as well as in the cytosol (Anderson *et al.*, 1984). The ER is the major Ca^{2+} storage site in mammalian cells. The concentrations of Ca^{2+} could reach to 5 mM, compared to 0.1 μM in the cytosol in the ER lumen (Orrenius *et al.*, 2003). The concentrations of Ca^{2+} change rapidly and frequently because the ER Ca^{2+} pool is adjusted during intracellular signaling. Ca^{2+} is also a signal molecule in cells and participates in electrostatic interactions. Therefore the Ca^{2+} fluctuation also effects protein folding in the ER. Besides, most ER-resident molecular chaperones and foldases are strong Ca^{2+} binding proteins. The Ca^{2+} pool perturbation affects folding of either these ER-resident proteins or other chaperones.

Glutathione is the major redox buffer in the cell. The ration of reduced (GSH) to oxidized glutathione (GSSG) in the cytosol is around 30:1 to 100:1

while 1:1 to 3:1 in the ER. This redox energy is generated for protein disulfide bond formation in the ER, and mediated by protein disulfide isomerases (PDI).

1.2.2 N-linked glycosylation

Multiple post-translational modifications take place in the ER including *N*-linked glycosylation, disulfide bond formation, lipidation, hydroxylation and oligomerization. *N*-linked glycosylation starts from transferring a core oligosaccharide from a membrane-bound dolichol phosphate anchor to consensus Asn-X-Ser/Thr residues in the polypeptide chain. The importance of glycosylation in protein folding is described as followed: first, glycosylation enhances the solubility of glycoproteins based on the hydrophilic nature of carbohydrates and help to define the attachment area for the surface of the protein. Second, oligosaccharides can interact with the peptide backbone and hence stabilize its conformation. Third, due to their large hydrated volume, oligosaccharides block the attachment area from surrounding proteins. Lastly, sequential cutting of sugar residues is monitored by a lectin machinery for the folding status of the protein. This calnexin/calreticulin cycle is one major part of the quality-control machinery in the ER that detects protein conformations and decides whether a molecule is exported to the Golgi or targeted for ERAD. The monoglucosylated form of a folding protein shuttles through several cycles of de- and reglucosylation by α -glucosidase II and uridine diphosphate (UDP)-glucose: glycoprotein glucosyl transferase (UGGT) activities. The monoglucosylated form is retained in the ER by interaction with the lectins calnexin (CNX) and calreticulin (CRT). UGGT preferentially recognizes the unfolded conformation. Proteins are removed from this cycle after demannosylation by α (1,2)-mannosidase I. Compared to other oligosaccharide cutting reactions in the ER, this reaction is slow, giving the protein time to go through several folding cycles. If the protein folded properly, the mannose-trimmed protein is exported to the Golgi complex. If incorrectly folded, reglucosylation by UGGT initiates interaction with calnexin, transfer to the lectin Mnl1p/Htm1p/EDEM (ER degradation-enhancing α -mannosidase-like protein; Molinari *et al.*, 2003; Nakatsukasa *et al.*,

2001; Oda *et al.*, 2003.) and retrograde translocation to the cytosol for degradation by the proteasome.

1.2.3 Pathways for proteins disulfate bond formation

The formation of biosynthetic disulfide bonds between two cysteine residues is a critical step in the maturation of both membrane and secreted proteins in eukaryotic and prokaryotic cells. Disulfide bridges are often essential for the stability of a final protein structure. Without the incorrect pairing of cysteine residues, a protein usually cannot fold into its native conformation. The formation of a disulfide bond *in vitro* can be conducted easily by transferring electrons of two cysteines which form a disulfide bond to an available acceptor, such as molecular oxygen. *In vivo*, however, the major mechanism for the formation of protein disulfide bonds is a thiol-disulfide exchange reaction of free thiols (-SH) with an already disulfide-bonded molecules. A thiol-disulfide exchange reaction takes place between a protein and any sulfhydryl-containing substrate, including small thiol-containing compounds, such as glutathione, or a protein containing a disulfide bond. This process is facilitated by a class of proteins known as thiol-disulfide oxidoreductases including DsbA (Bardwell *et al.*, 1991), DsbC (Missiakas *et al.*, 1993; Bardwell *et al.*, 1993) in *E. coli* and protein disulfide isomerase and PDI-like proteins in eukaryotes. Interestingly, the activity of these proteins depends on a pair of cysteines that are usually arranged in a –CXXC- motif within their thioredoxin domain (Sevier and Kaiser, 2003; Hiniker and Bardwell, 2003).

Recent evidence suggests that disulfide bonds are not only an inert structural motif to enhance the stability of proteins but also play a role in regulating the activity of the mature protein by a thiol-disulfide bond exchange reaction (Hogg, 2003). For example, the cytoplasmic enzyme ribonucleotide reductase becomes oxidized during its catalytic cycles, and it requires be recycled to its reduced form to be reactivated (Jordan and Reichard, 1998). In

plants, catabolic and anabolic respiration can be switched by reducing the regulatory disulfide bonds in several photosynthetic enzymes via light-generated reducing equivalents (Dai *et al.*, 2001). Under specific cellular conditions, the oxidation of cysteines that form disulfide bonds can also activate several transcription factors, including the bacterial OxyR (Helmann, 2002) and Hsp33 (Jakob *et al.*, 1999) (Frand, 2000; Sevier and Kaiser, 2003). It is also reported that Thrombospondin-1 (TSP-1), a secreted extracellular glycoprotein which participates in cell-cell and cell-matrix communication, has different disulfide-bonded forms *in vivo* and the disulfide interchange may be critical for controlling its function (Essex and Li, 1999; Essex, 2001; Hogg, 2003).

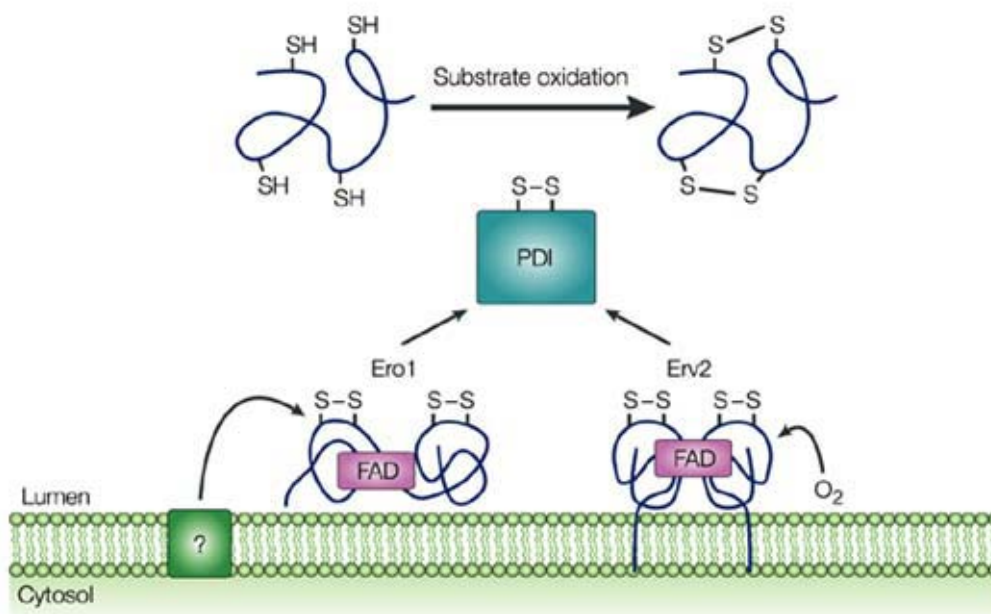


Figure 1.4 Pathways for protein oxidation in the ER of *Saccharomyces cerevisiae*: Two parallel pathways introduce oxidizing equivalents for disulphide-bond formation into the endoplasmic reticulum (ER). In the first pathway, oxidizing equivalents flow from ER oxidoreductin (Ero1) to the thiol-disulphide oxidoreductase protein disulphide isomerase (PDI), and from PDI to secretory proteins through a series of direct thiol-disulphide exchange reactions (thin arrows). Ero1 derives oxidizing equivalents from a flavin adenine dinucleotide (FAD) cofactor, but the ultimate source of oxidizing equivalents for Ero1 oxidation is not yet clear. In the

second pathway, the ER oxidase Erv2 transfers disulphide bonds to PDI before substrate oxidation. Erv2 directly acquires oxidizing equivalents from molecular oxygen via its flavin cofactor. In mammalian cells, two isoforms of Ero1 (Ero1-L and Ero1-L) are present to transfer oxidizing equivalents to PDI. However, the mammalian ER-localized Erv2-like protein has not been identified yet. (Adapted from Sevier & Kaiser)

1.3 The characteristics of protein disulfate isomerase (PDI)

The thioredoxin protein is particularly abundant in the periplasm, ER- or SR-lumen. It was first isolated from liver extract and characterized by Christian Anfinsen in 1963, proving that its ability to catalyse the 4 disulfide bridges formation in ribonuclease A (Golberger., *et al*, 1963). Since then, by several scientists' efforts, the functional roles of the thioredoxin have been intensively investigated, such as the mechanisms of dithiols redox/isomerization ability, and protein chaperonin activity. Up to now, more and more proteins in the ER with the thioredoxin domain have also been identified and classified to a newly established protein family - protein disulfide isomerase (PDI) family. The PDIs have some common features: first, the precursors usually contain a N-terminal hydrophobic signal sequence for translocating into the ER; second, most of them reside in the ER and have a C-terminal ER retrieval or retention signal motifs, such like KDEL, KEEL, HDEL, or QDEL, etc. (MacLennan and Wong, 1971); third, all of these proteins contain one or more thioredoxin domain sharing highly sequence homologies to the cytosolic thioredoxin. These domains structures are also highly conserved at the three dimensional level, exhibiting the similar thioredoxin-fold. As for protein disulfide isomerase in human, it is about 510-amino acid in length and is composed of four thioredoxin-like (trx-like) domains, a C-terminal retrieval signal KDEL and an acidic region in between. The trx-like domain a and a' with CXXC motif are active which are separated by two inactive domain b and b' without CXXC motif (fig 1.5) (Ferrari and Söling, 1999; Freedman *et al*, 2002).

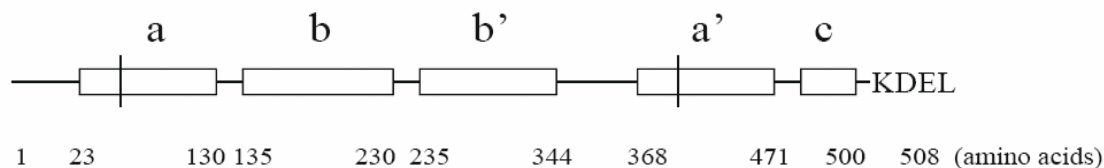


Figure 1.5: PDI model. Boxes represent a, b, b, a' domains and C-terminal acidic region, respectively. Vertical lines are referred to the CGHC redox-active motif. (see details in text).

1.3.1 The achievement of the human PDI structure from its thioredoxin domains

The primary structure of human PDI was sequenced and has been recognized as a multiple thioredoxin domains protein. The achievement of current structural model is based on the combination of the solution structures of each single trx-like domain by NMR analysis. PDI comprises of four structural domains, a, b, b', a', respectively, plus a linker region between b' and a' and a C-terminal acidic region which is a putative low-affinity, high-capacity Ca^{2+} -binding site (fig 1.6) (Ferrari and Söling, 1999; Freedman et al., 2002). Both a and a', with highly sequence identities to cytosolic thioredoxin, containing a conserved redox active site –CGHC-. However, the b and b' domains without the –CXXC- motifs, shows the sequence similarity to each other but without highly similarity to the sequence of cytosolic thioredoxin and the a' or a domain. Interestingly, the NMR studies on both recombinant a and b domains of human PDI have the same characteristic thioredoxin fold, clearly (Kemnick *et al.*, 1995, 1996, 1999).

1.3.1.2 Structural comparison between a and b thioredoxin domains of yeast PDI

The cytosolic thioredoxin is a small (12 kDa), ubiquitous protein with a disulfide reductase activity in the cytosol, where is in favour of reduction. It contains a –CGPC- motif which is critical for the reduction of the disulfide bonds (Holmgren, 1985, 1989). Most of the thioredoxin-like proteins catalyze the redox

reactions which are required the reactive dithiols *in vivo*. Moreover, the thioredoxin superfamily are comprised not only thioredoxin-like, but also glutaredoxin-like, PDI-like proteins, and the bacterial Dsb family (Gilbert, 1998; Holmgren, 1989; Bardwell, 1994). Each thioredoxin-like domain of thioredoxin superfamily always performs the same fold with the cytosolic thioredoxin. They are β , α , β , α , β , α , β , β , α , sequentially. Except the β_4 strand, the other four β strands form the central core, surrounded by four α -helices (Katti *et al.*, 1990; Eklund *et al.*, 1992). The CXXC redox active motif is found in the exposed turn between β_2 and α_2 . The sulfur atom of the N-terminal Cys residue is exposed to the surface of the molecule, while the sulfur atom of C-terminal Cys residue is buried behind it. The core thioredoxin tertiary structure: $\beta\alpha\beta\alpha\beta\alpha$, can also be found in other members of the thioredoxin superfamily, including DsbA (a bacterial periplasmic oxidase) (Martin *et al.*, 1993), and in numbers of enzymes involved in glutathione or sulfur metabolism (Martin, 1995). In cytosolic thioredoxin, the first cysteine of the –CXXC– site, C32 has a pKa of 7.1, much lower than that of the free cysteine (pKa of 8.7 at neutral pH), rendering it highly reactive. At neutral pH the reactive sulfur atom of C32 may share a hydrogen bond to the –SH hydrogen of C35. The pKa of C32 is thought to be decreased by a nearby buried partial charge on D26 (Chivers *et al.*, 1996), which may serve as a general acid/base in thioredoxin-catalysed redox reactions. The C32 thiolate can make a nucleophilic attack on disulfides, generating a mixed disulfide that is then disrupted by C35 to produce a reduced substrate protein. The reactivity of C35 follows upon its loss of a proton to D26 (fig 2.6 A). The thiolate species generated is well poised to attack the intermolecular disulfide-bonded C32. Thioredoxin is then recycled to the reduced state by thioredoxin reductase and NADPH. In close proximity to the reactive-site pocket are the hydrophobic residues G33, P34, I75, P76, G92 and of C35. The pKa of C32 is thought to be decreased by a nearby buried partial charge on D26 (Chivers *et al.*, 1996), which may serve as a general acid/base in thioredoxin-catalysed redox reactions. The C32 thiolate can make a nucleophilic attack on disulfides, generating a mixed disulfide that is then disrupted by C35 to produce a reduced substrate protein.

The reactivity of C35 follows upon its loss of a proton to D26 (fig 2.3 A). The thiolate species generated is well poised to attack the intermolecular disulfide-bonded C32. Thioredoxin is then recycled to the reduced state by thioredoxin reductase and NADPH. In close proximity to the reactive-site pocket are the hydrophobic residues G33, P34, I75, P76, G92 and A93, which may be important for protein-protein interaction (Holmgren, 1995). The a domain of human PDI, in addition to adopting the small overall α/β fold, shares many common features with thioredoxin (fig 2.6 B); first, the active site motif is located at the N-terminus of helix α_2 , which is distorted by a proline residue; second, the peptide bond before the proline residue at the N-terminus of β_4 is in the cis conformation; third, there is a buried acidic residue, E30, in analogous position in the a domain of PDI to that of D26 in thioredoxin (Kemink et al., 1995; 1996) (fig 2.6 B). As in the a-domain, the b-domain of PDI also forms a thioredoxin fold (Kemink et al., 1999), but the characteristic thioredoxin-like active site has been deleted and other residues associated with redox properties have been replaced (fig 2.6 C). Despite a lack of 3-D structural data, based on the sequence similarity between a and a', b and b', and the secondary structure prediction and alignment, the a' and b' domains of PDI should also adopt the thioredoxin fold (Freedman et al., 2002).

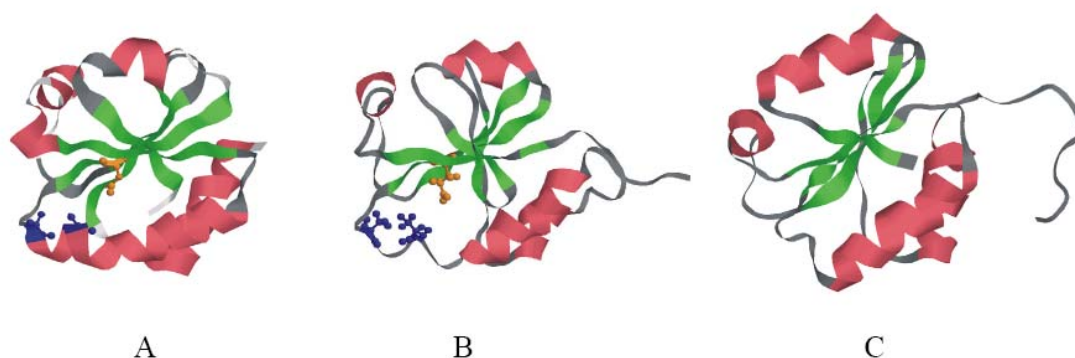


Figure 1.6: Comparison of the tertiary structure of thioredoxin with the thioredoxin fold of the a and b domains of PDI. (A) *E. coli* thioredoxin ribbon model of the crystal structure determined by Katti et al (1990). (B) The a-domain of human PDI, based on a model suggested by NMR

(Kemink et al., 1997). The Cys residues of the active site (blue), D26 (yellow) of thioredoxin (A) and E30 (yellow) of the a-domain of PDI (B) are shown as ball and stick representation. (C) The b-domain of human PDI, based on a model suggested by NMR (Kemmin et al., 1999). α -helical elements are shown in red, and β -strands in green. (see details in text).

1.3.1.3 The importance of the b' domain of PDI

The redox / isomerase activities of PDI, as in thioredoxin, are due to the reactivity of the -CXXC- redox active sites in the a and a' domains. Redox assays by using simple peptide substrates showed that the isolated a and a' domains retain nearly full redox activity (Darby and Creighton, 1995a, b). However, neither of them could fulfill the isomerase activity of the full length PDI, as neither is able to catalyse the isomerisation of the disulfide bonds in BPTI (the bovine pancreatic trypsin inhibitor), lysozyme and ribonuclease (Darby and Creighton, 1995c). This suggests that other parts of PDI are required for its activity. Recently, the b' domain of PDI attracted special attention. Through the intensive studies of a series of combinations of different domains, it was revealed that the simple thiol-disulfide reaction only requires the a or a' domains, that simple isomerization requires one of these in a linear combination of domains including b', while complex isomerization (isomerizations that would require substantive conformational change in the substrate as well as thiol-disulfide reactions), suggesting all of these PDI domains were required (but not the C-terminal acidic extension) (Darby and Creighton, 1995c; Darby et al., 1998). The b' domain is also crucial for the peptide binding activity of PDI. For small peptides testing, the isolated b' domain is essential and sufficient for the binding. However, the binding of larger peptide or non-native protein substrates requires at least the b'-a'-c fragment. Thus it appears that the b' domain of PDI provides the principal peptide binding site of PDI, but all domains contribute to the binding of larger substrates such as non-native proteins (Klappa et al., 1998). These observations explain the importance of the b' domain in the catalysis of complex isomerization reactions by PDI, apparently, suggesting that it holds the substrate protein in a partially unfolded conformation while the catalytic sites act synergetically to

perform the chemical processes of thiol-disulfide exchange (Freedman et al., 2002).

1.3.2 Other PDI like proteins

In the last few years, the PDI family has expanded by the addition of several new members. Currently, 12 known mammalian proteins are likely to belong to this family. The number is much bigger if the homologues from other species are included (Fig 2.7). Most of these proteins are redox active and involved in thiol-disulfide exchanges with the notable exception of the most recently found members. Although no direct structural information is available for all of them, by sequence alignment and secondary structure prediction, their domain organization can be deduced. Based on the domain compositions, the PDI family can be divided into a classical PDI-L subfamily which contains only thioredoxin domains (redox active or inactive) and a unique PDI-L subfamily which contains other unique domains apart from the thioredoxin domains. These subfamilies can be divided further into α (redox active) and β (redox inactive) sub-subfamilies (reviewed by Ferrari and Söling, 1999).

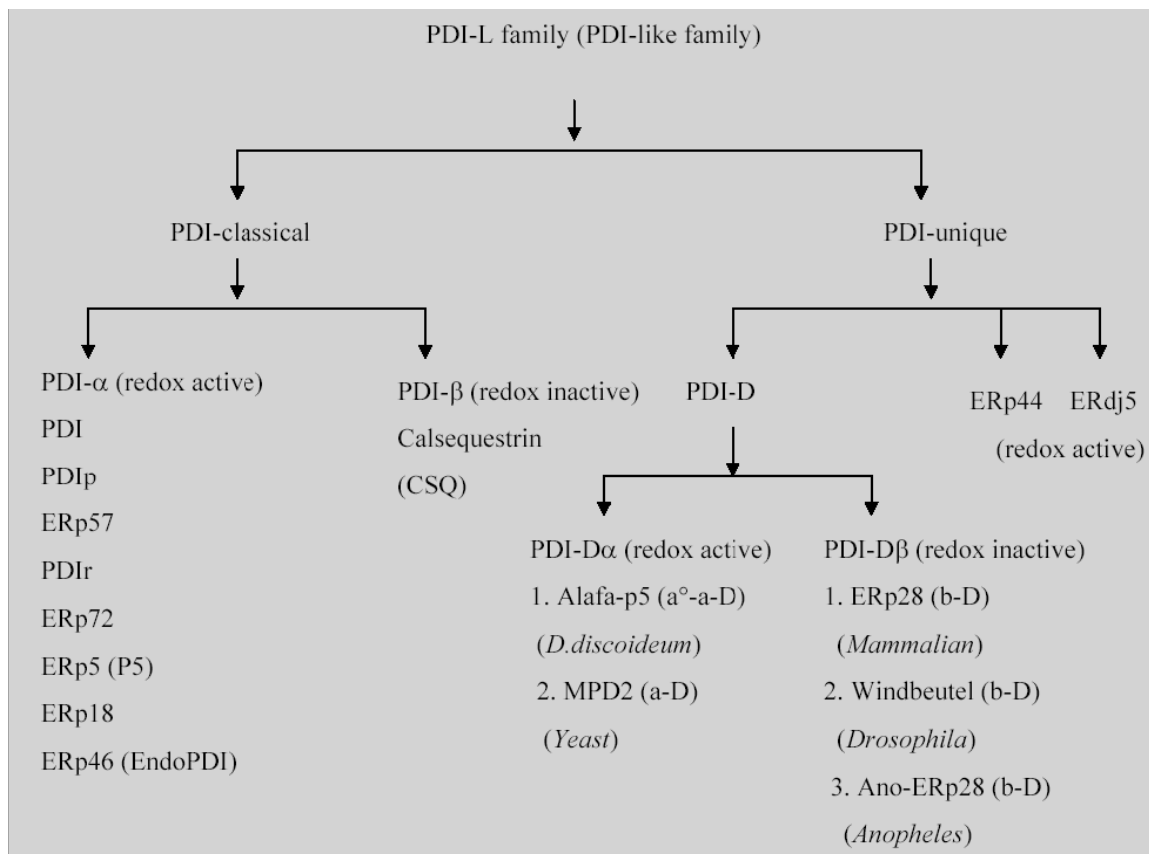


Figure 1.7: The PDI-like family.

1.3.3 A novel protein of PDI superfamily- ERp18

The recently identified ERp18 (Alanen *et al.*, 2003) is the smallest member of the PDI family. It only contains a single thioredoxin domain with the –CGAC-motif resembles the –CGPC-site of thioredoxin instead of –Cys-Gly-His-Cys of PDI. According to that, it was strongly assumed that ERp18 is likely to be a reductase rather than an oxidase inside ER. However, the reduced form of ERp18 is more stable than its oxidised form, similar to PDI. From this point of view, it seems to be an oxidase. It is worth noting that there is a very acidic region within its thioredoxin domain. This feature is unique among the PDI family although PDI has an acidic region at the C-terminus outside the a' domain.

1.4 The structure of Ero1p

The functional roles of the seven conserved cysteine residues of Ero1p have been examined by site-directed mutagenesis (Frand & Kaiser, 2000.). This work suggests that there are at least two disulfide bonds in Ero1p and that each has a unique role: Cys352 and Cys355 are essential to maintain Ero1p in a fully oxidized form, pointing to their central role in the de novo formation of disulfide bonds, whereas Cys100 and Cys105 are probably involved in interactions with PDI, because a Cys100Ala mutation abolishes the ability of Ero1p to oxidize PDI in vivo [11]. Consistent with this, the crystal structure shows that the disulfide pairings are Cys352–Cys355, Cys100–Cys105 and Cys90–Cys349, and that Cys208 is in an unpaired thiol form. This disulfide connectivity corroborates the model suggested by Frand and Kaiser in which electrons are transferred from PDI to Cys100–Cys105 of Ero1p, and then within Ero1p to Cys352–Cys355.

Further crystallographic evidence supports this intramolecular disulfide relay. Cys100 and Cys105 are positioned on a flexible loop that can change its conformation by at least 17 Å. A slight modification of the protein backbone in this region would position Cys105 within disulfide-bonding distance of Cys352, which is a requirement for dithiol–disulfide exchange. The Cys352–Cys355 disulfide is positioned on a more rigid part of Ero1p, adjacent to the FAD cofactor, which probably enables Cys352–Cys355 to be readily reoxidized. Thus, electrons could be transferred from PDI to the Cys100–Cys105 disulfide, then to the Cys352–Cys355 disulfide, and then to FAD.

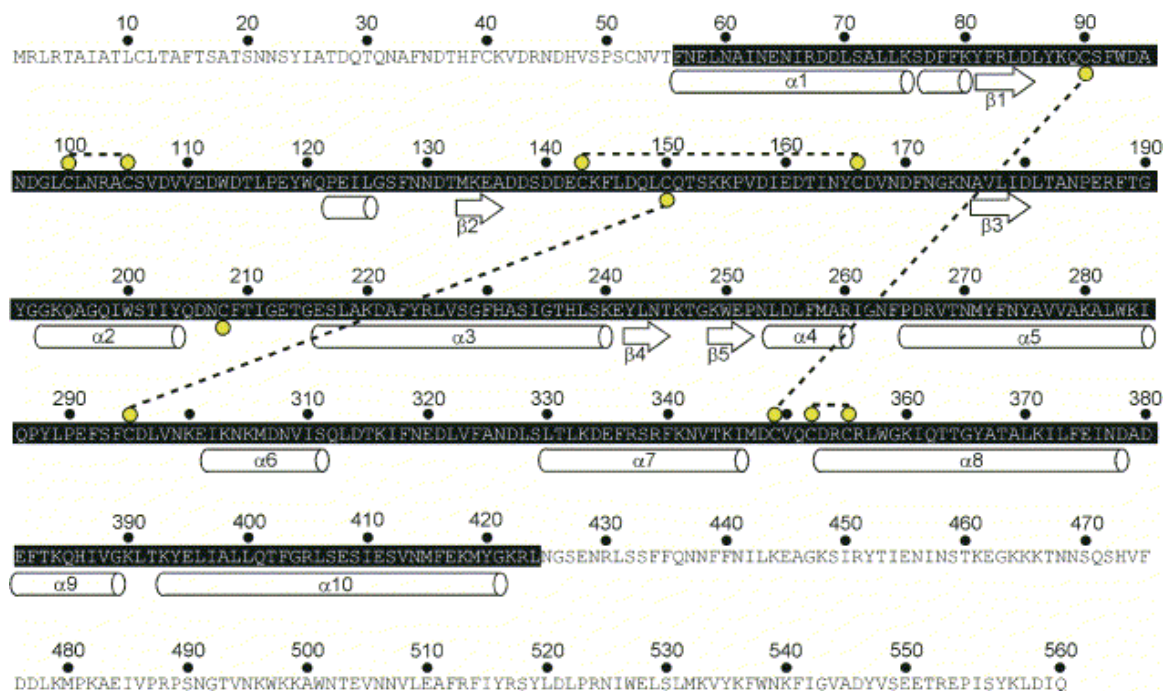


Figure 1.8 Ero1p Sequence, Secondary Structure, and Disulfide Connectivity: The crystallized fragment Ero1p-c, highlighted in black, is shown within the complete amino acid sequence of *S. cerevisiae* Ero1p. Below the sequence, cylinders represent α helices and arrows β sheets. Yellow balls above or below the sequence highlight cysteine residues, and dotted lines indicate disulfide bond connectivity.

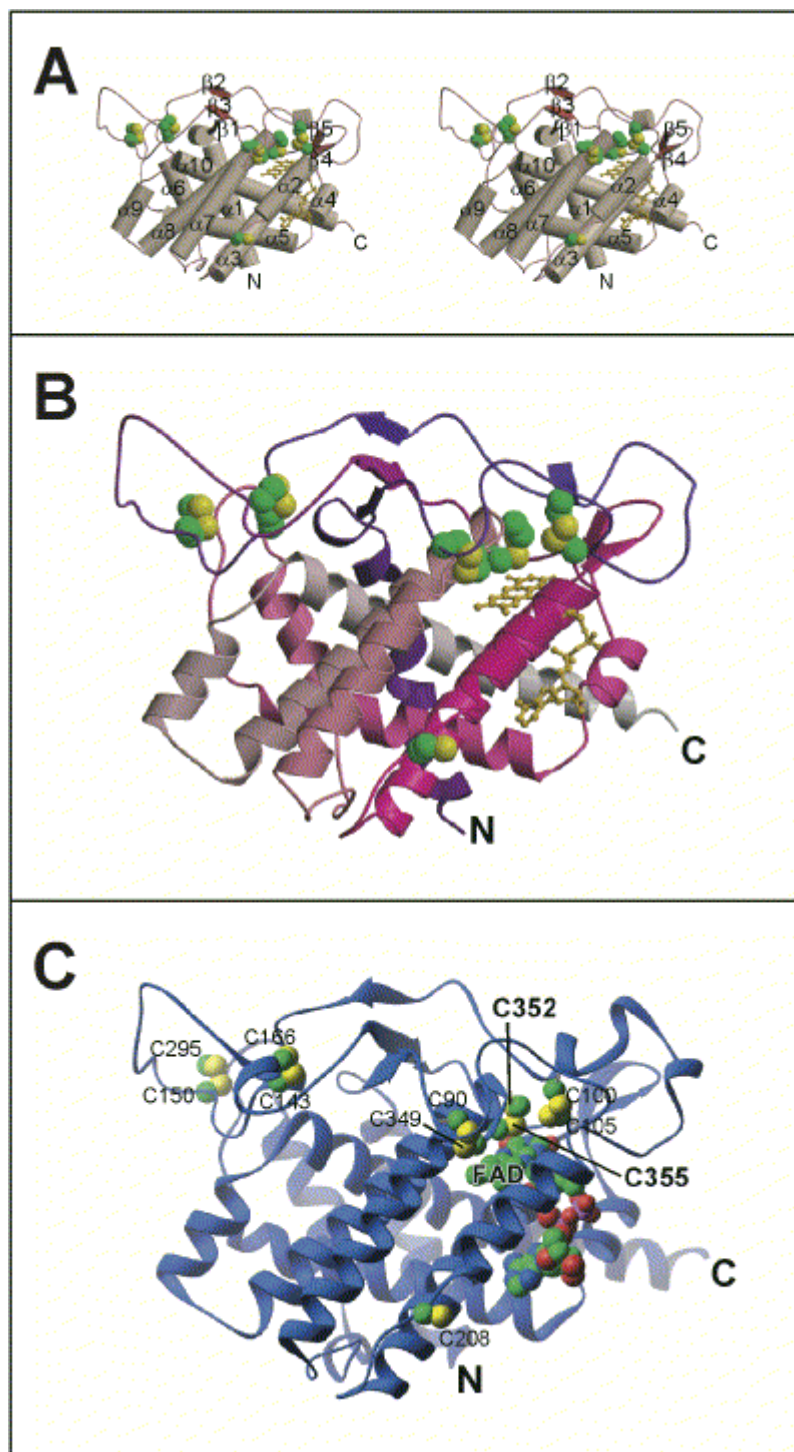


Figure 1.9 Structure of Ero1p: (A) Stereo view of Ero1p with α helices represented as cylinders and β strands as arrows. Secondary structure elements are numbered from N-terminus to C-terminus, corresponding to Figure 1.7. Side chains of cysteine residues are shown in space-filling representation and the FAD cofactor in gold ball-and-stick representation. (B) The same view of Ero1p is shown in ribbons representation and colored in a gradient from purple (N terminus)

through magenta to white (C terminus). (A) and (B) were generated with the programs molscript and raster3d (Kraulis, 1991). (C) The cysteine residues are numbered according to their positions in the full-length Ero1p sequence, with the active-site cysteine pair indicated in boldface. This figure was prepared using the program Ribbons (Carson, 1997). (from Gross *et al.*, 2004)

1.4.1 The **-CXXCXXC-** motif

The CXXCXXC sequence motif in other proteins can bind metal clusters (e.g., Jung *et al.*, 2000), and it was previously suggested that this motif in Ero1p might play a similar role (Pollard *et al.*, 1998). However, using optical emission spectrometry, we were unable to detect any metal specifically associated with Ero1p (our unpublished data), and each of the cysteines in this motif participates in disulfide bonds in the crystal structures. The first CXXCXXC cysteine, C349, is almost 14 Å away (sulfur-to-sulfur distance) from the C352/C355 cysteine pair, which forms a disulfide bond in the first turn of the $\alpha 8$ helix, a local conformation that is shared by the active sites of thioredoxin-like proteins. The C90/C349 disulfide bond tethers the flexible loop that contains the C100/C105 disulfide bond to the vicinity of the active site.

The FAD cofactor is held between helices $\alpha 2$ and $\alpha 3$ in a bent conformation with the isoalloxazine and adenine rings buried in the protein. Through this packing, the isoalloxazine ring system is presented to the active-site cysteines (Figure 3C). The ribityl 5' phosphate (on the FMN portion of the FAD) contacts H231, whereas the AMN ribose 5' phosphate may be associated with R260 but is largely solvent exposed. The ribose ring is also largely solvent exposed, and the adenine ring is sandwiched between H231 and R267. Two mutants that impair Ero1p function have changes at or near H231: in the temperature-sensitive mutation *ero1-1*, glycine 229 is mutated to serine, and in the DTT-hypersensitive mutant *ero1-2*, histidine 231 itself is mutated to tyrosine (Figure 2.9).

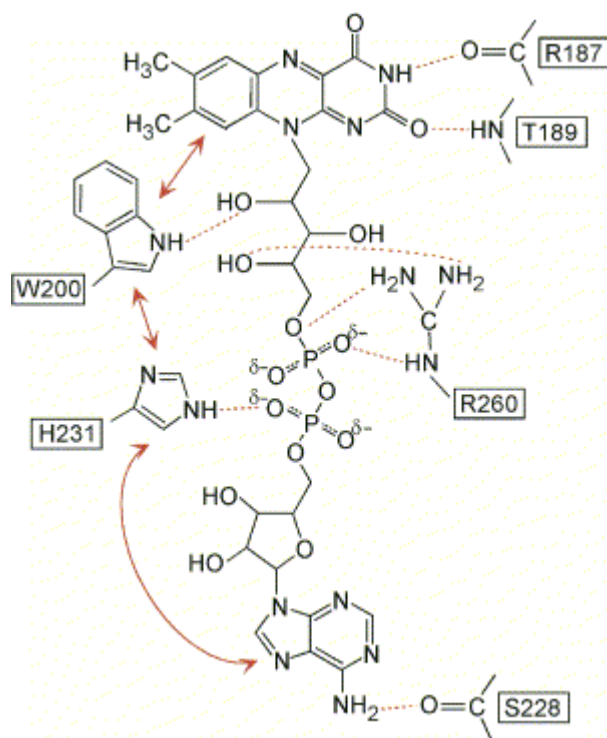


Figure 1.10 Enzyme-FAD Contacts Contacts made by the Ero1p-c protein to the FAD cofactor are shown in a schematic diagram. Dashed lines indicate putative hydrogen bonds or salt bridges, and double-headed arrows represent stacking interactions between amino acid side chains and ring systems in the FAD.

1.5 The role of ERp44

ERp44, a novel UPR induced ER protein, was first identified from the co-immunoprecipitation and mass spectrometry. The precursor of ERp44 contains about 30-amino-acid signal peptides. The molecular weight of matured ERp44 is about 43.9 kDa after cleavage. ERp44 was reported to form mixed disulfides with various proteins including both human Ero1 homologues, Ero1-L α and Ero1-L β , as well as with partially unfolded Ig subunits. ERp44 contains a thioredoxin-like domain followed by a fragment showing weaker similarities with the second domain of calsequestrin and a long sequence with no obvious sequence homologies with other proteins. In the thioredoxin-like domain, the second cysteine in the canonical -CXXC- motif is found replaced by a serine, resulting the sequence -CRFS-. The CRFS motif and the surrounding sequences of

ERp44 are extremely conserved in all species, suggesting an important functional role for this region. Mass-spectroscopy analysis indicates that the cysteine of the CRFS motif is involved in the formation of mixed disulfides with Ero1-L α . Two dominant redox isoforms of Ero1-L α , OX1 and OX2, have been reported and they possibly represent different structural conformers of Ero1-L α in its functional cycle. Overexpression of ERp44 alters the relative amounts of the two Ero1-L α isoforms, shifting the equilibrium towards OX2. This observation suggests that ERp44 may play an important role in controlling the function of human Ero1 by accumulation of OX2 and hence the redox state of the ER (Anelli *et al.*, 2002).

1.5.1 Thiol-mediate retention of ERO1 in the ER

The biochemical studies show that ERp44 utilizes cysteine 29 (C29) to physically interact with Ero1-L α and other client proteins. Sequence alignments and computer modeling imply that C29 lies in the position normally occupied by the most reactive residue of thioredoxin (trx) domains, the first cysteine of the canonical CxxC motif. When C29 is replaced by a serine, ERp44 fails to form mixed disulphides with Ero1 α , Ig subunits and other client proteins. In contrast, replacing C63 with other amino acids has minor effects on the formation of the covalent complexes, while the covalent ERp44 homodimers become more abundant. This result suggests that C63 might be important to destabilize ERp44 homodimers. In contrast, the presence of an additional cysteine in the interacting surface of ERp44 CxxC facilitates the ERp44 homodimer formation. However, the C29 mutant displays a significantly reduced number of stable covalent interactions, perhaps it is because C29 is also involved in intra-molecular interactions with the downstream cysteine.

Even though both human Ero1 α and Ero1 β can complement an Ero1 defective yeast strain (Cabibbo *et al.*, 2000; Pagani *et al.*, 2000) due to the

similarities between yeast and mammalian oxidative folding pathways, ERp44 homolog was surprisingly not yet found in yeast.

Besides the similarities, however, there are critical differences between yeast and human Ero1 members. For example, yeast Ero1 has an essential C-terminal ER-retention sequence that serves to associate the molecule to the ER membrane. This C-terminal sequence is absent from human Ero1 proteins (hEROs), which nonetheless associate with the membranes (Cabibbo et al., 2000; Pagani et al., 2000). Since hEROs do not contain hydrophobic regions to mediate membrane interaction, they may interact with ERp44 and other proteins to achieve proper localization and function. It is somehow unexpectedly that, the major oxidase activity is evolutionarily conserved in the two distant species, yeast and human, the localization mechanisms diverged. One speculation is that to utilize trans molecules for mediating localization of Ero1 may allow further levels of regulation, controlling its topology and/or function in mammalian cells (Anelli et al., 2002; Tsai et al., 2002).

1.5.2 Redoxing calcium by IP3 receptor

Many signals from the extracellular environment, from adjacent cells, or from a distant part of the cell itself can cause a calcium transient, a sharp rise of Ca^{2+} concentration in the cell. Calcium transients can be achieved through Ca^{2+} channels in the plasma membrane (PM) or those in the ER which functions as an intracellular Ca^{2+} storage compartment. In the case of Ca^{2+} release from the ER, inositol 1,4,5 trisphosphate (IP3), which is generated through the hydrolysis of phosphatidylinositol 4,5-bisphosphate (PIP2) by phospholipase C (PLC), plays an important role because it opens a specific calcium channel in the ER termed the IP3 receptor (IP3R).

The IP3R is regulated by other molecules, including calmodulin, IRAG, and Ca^{2+} itself. It has been reported to regulate various physiological events,

including fertilization, cell division, and synaptic plasticity. When the cytoplasmic Ca^{2+} concentration rises, cells quickly respond to counteract the increase of Ca^{2+} to prevent toxicity caused by continuous high concentration of intracellular Ca^{2+} . This response is conducted by pumping Ca^{2+} out of the cell, taking it up into the ER, or chelating it with certain proteins. One can easily imagine that repetitive or robust calcium transients from the ER would consume the total Ca^{2+} content within ER, but cells are able to manage not to let this happen; when the Ca^{2+} concentration in the ER decreases, some Ca^{2+} channels in the PM open to maintain the Ca^{2+} content within the cell. However, the molecular identification of such Ca^{2+} channels and the mechanism of their activation is not yet clear.

1.5.3 ERp44 and type 1 InsP3R

A novel InsP3R accessory protein, ERp44, which confers upon the receptor calcium, pH, and redox sensitivity was identified by Mikoshiba and colleagues by using a proteomic approach (Higo et al., 2005). In this study, a polypeptide fragment of the InsP3R which contains the consensus glycosylation sites—and cysteine residues that are sensitive to thiol modification—was used as the bait to fish for interacting proteins in a brain lysate. One of the isolated proteins was identified as ERp44. Furthermore, although there is significant homology in this region, which was used as the bait, between the three InsP3R isoforms, the authors determined that the interaction of ERp44 was specific for the type 1 InsP3R. ERp44 is identified as an ER luminal protein that and belongs to the thioredoxin protein family, members of which also include protein disulphide isomerase (PDI) and ERp57. PDI family members assist in oxidative protein folding and catalyzing the formation of disulphide bonds (Anelli et al., 2002).

The ERp44-InsP3R interaction requires the presence of reduced cysteine residues of InsP3R, indicating the interaction with ERp44 is regulated by the thiol modification status of InsP3R. Furthermore, the interaction was sensitive to the

concentration of ER luminal calcium with concentrations above 100 μM resulting dissociation of ERp44 from the InsP3R in vitro. This places the calcium sensitivity of the association of ERp44 and InsP3R within the physiological range of ER luminal calcium concentration, which ranges between 80 and 200 μM when full and decreasing to between 10 and 100 μM after stimulation.

The functional effect of ERp44 on InsP3R activity was demonstrated by using two different approaches. First, the previous studies showed that agonist-induced calcium release was inhibited by overexpression of ERp44 and potentiated by siRNA-mediated knockdown of endogenous ERp44 in HeLa cells. No effect of ERp44 overexpression was found on agonist-induced calcium release from COS-7 cells which do not express endogenous type 1 InsP3R, supporting the biochemical data. In addition, inhibition of agonist-induced calcium release was not observed by overexpressing altered InsP3R which carries mutation of the critical in InsP3R knockout DT40 cells.

2. Materials and Methods

2.1 Materials

2.1.1 Chemicals

Acrylamide solution	Roth, Kalsruhe
Acetic Acid	Merck, Darmstadt
Agarose	Invitrogen, USA
Amonium persulfate (APS)	Merck, Darmstadt
Ampicilin	Sigma, Deisenhofen
Bradford solution	Biorad, Muenchen
Bromophenol blue	Merck, Darmstadt
Choloramphenicol	Boehringer, Mannheim
Coomassie Brillant Blau R250	Serva, Heidelberg
Dimethyl sulfoxide (DMSO)	Sigma, Deisenhofen
Dithiothreitol (DTT)	Roth, Kalsruhe
Ethanol	Merck, Darmstadt
Ethidium bromide solution	Roth, Kalsruhe
Glutathion (reduced)	Sigma, Deisenhofen
Glycerol	Merck, Darmstadt
Guanidinium hydrochloride	Fluka, Schweiz
HEPES	Calbiochem, USA
Imidazole	Merck, Darmstadt
Isopropyl- β -D-thiogalactoside (IPTG)	Sigma, Deisenhofen
Kanamycin	Boehringer, Mannheim
Lysozyme	Boehringer, Mannheim
1 kb DNA ladder	Invitrogen, USA
Polyethleneglycol 3350	Fluka, Schweiz
Polyethleneglycol 4000	Fluka, Schweiz
Polyethleneglycol 8000	Fluka, Schweiz
Potassium chloride	Merck, Darmstadt

Precision protein standard marker	Biorad, Muenchen
Sodium Chloride	Merck, Darmstadt
Sodium dodecyl sulfate (SDS)	Merck, Darmstadt
N, N, N', N'-tetramethylethyldiamin (TEMED)	Sigma, Deisenhofen
Tris-(hydroxymethylen) aminomethan (TRIS)	Roth, Karlsruhe

2.1.2 Bacterial strains

<i>E. coli</i> BL21(DE3)	Novagen, Darmstadt
<i>E. coli</i> DH5 α	Invitrogen, USA
<i>E. coli</i> Rossetta (DE3)	Novagen, Darmstadt
<i>E. coli</i> BL21(DE3)-RIL	Stratagene, Heidelberg
<i>E. coli</i> B834(DE3)	Stratagene, Heidelberg

2.1.3 Nucleotides

Deoxynucleoside-5'-Triphosphate, 100 mM (dATP, dCTP, dGTP, dTTP)

Nucleoside-5'-Triphosphate, 100 mM (ATP, CTP, GTP, UTP)

2.1.4 Oligonucleotide primers for PCR (Table 2.1)

Protein	Oligo	Description	Sequence (5'→3')
ERp44	ER44/Ncol/fw	ERp44; <i>Mus musculus</i>	ACGTACCCATGGCAAGTCTTGATTC AGAGAATATAGATG
	ER44/Kpnl/rv		ACGTACGGTACCTTACAGCTCATCT CGATCCCTCAATAAAG
ERO1A	ERO1A/Ncol/fw	ERO1-Lalpha; <i>Mus musculus</i>	TCAAACCATGGAGGAGCGGCGGCC GGAGACAGCGGCACA

	ERO1A/KpnI/rv		CTTGGGTACCTCAGTGAACATTCTG TAACAAGTGCTGAA
1L3V	1L3V/NcoI/fw	IP3R-1L3V; <i>Mus musculus</i>	ACGTACCCATGGTCTTCAAGGATG ACTTTATCTTGGAAGTA
	1L3V/KpnI/rv		ACGTACGGTACCTTAGTCGTAGATC ACCCTTGCAGCAAACAG
ERp18	ER18/NcoI/fw	ERp18; <i>Mus musculus</i>	ACGTACCCATGGGACGCACTGGGC TTGGAAAGG
	ER18/KpnI/rv		ACGTACGGTACCTCACAACTCATCC TGAAAGTGTTTC

2.1.6 Vectors and plasmids (Table 2.2)

Plasmid	Description	Source
pETM-ZZ	zz-domain of protein A fusion expression vector, T7 promoter, Kan ^r	Dr. Guenter Stier
pCH-ZZ	zz-domain of protein A fusion expression vector, T7 promoter, Amp ^r	Constructed by Li-Chi Chang
pGEX-6P-2	GST expression vector, Amp ^r	AP Biotech
pQE-60	C-terminus 6xHis expression vector, Amp ^r	Qiagen

2.1.7 Reaction sets (Kits)

ABI PRISM™ Dye Deoxy Cycle Sequencing Kit	Applied Biosystems, Weiterstadt
Amicon Centriplus Concentrator	Millipore, France
ECL Western Blot Detection Kit	Amersham Biosciences, Freiburg
GFX Purification Kit	Amersham Biosciences, Freiburg

Mouse 18-day embryonic cDNA Library	Clontech, Heidelberg
QIAprep Spin Miniprep Kit	Qiagen, Hilden
QIAquick Gel Extraction Kit	Qiagen, Hilden
QIAquick PCR Purification Kit	Qiagen, Hilden
TNT [®] T7 Coupled Reticulocyte Lysate System	Promega, USA

2.1.8 Equipments

ABI PRISM™ 310 Genetic Analyzer	Applied Biosystems, Weiterstadt
Biofuge (pico/fresco)	Heraeus, Hanau
Electrophorese apparaturen	BiorRad, München
Gel documentation system	Biorad, München
Gradient Master Modell 106	BioComp Instruments, Canada
Heating block Hybaid	Biometra, UK
Head over tail Rotor 7637-01	Cole-Parmer, USA
Hybridisation oven	Hybaid, Biometra
Incubator BK-600	Heraeus, Hanau
Incubation shaker	Multitron Infors, Switzerland
pH Meter	Molecular Dynamics
Replica plater	Qbiogene, Eschwege
SMART System	Pharmacia Biotech
Sonifier	Heinemann Labortechnik
Sorvall Rotor	Kendro, USA
Speed Vac Concentrator 5301	Eppendorf, Hamburg
Spectrophotometer Ultropsec 300 pro	Amersham Biosciences, Freiburg
SW60 Rotor	Beckman, USA
Ultra centrifuge	Sorvall/Beckman, USA
UV Lamp 254nm	Bachofer, Reutlingen
Thermal Cycler Hybaid	Omni Gene, UK

2.1.9 Special materials

Cuvettes for Monolight 3010	Pharmingen, USA
Collodium Bags	Sartorius GmbH, Göttingen
Dialysis cassettes	Pierce, USA
Falcon tubes (5, 15, 50 ml)	Greiner, Kremsmünster
Glass Beads (425-600 microns)	Sigma, Deisenhofen
Glutathione Sepharose 4B	Amersham Biosciences, Freiburg
N ⁺ -NTA Agar	Qiagen, Hilden
Pipettes	Eppendorf, Hamburg
Protein A Sepharose	Amersham Biosciences, Freiburg
Protran Nitrocellulose Membrane	Schleicher & Schuell, Dassel
Reaction tubes (0.5; 1.5; 2 ml)	Eppendorf, Hamburg
Sterile filter (0.22 & 0.45 µm)	Millipore, France
Vivaspin concentrators	Vivascience, Sartorius

2.2 Methods

2.2.1 Molecular Cloning

DNA fragments used for the plasmids construction were amplified with the desired restriction enzyme sites introduced at the 5' end by PCR (section 2.2.1.1). The PCR products were first purified from the agarose gel (section 2.2.1.2); the purified DNA was then digested by appropriate enzymes and ligated with target vectors after purification (section 2.2.1.3). 1-2 µl ligation reaction was used for transformation (section 2.2.1.4). The positive colonies were inoculated in LB medium and the plasmid DNA was prepared (section 2.2.1.5). 2 µl DNA sample from mini-preparation was digested with appropriate enzymes and examined on

the agarose gel. The clones which have right-sized insert DNA fragment were verified by sequencing (2.2.1.6).

2.2.1.1 PCR amplification

Polymerase chain reaction (PCR) was mostly used as a tool for cDNA cloning and plasmid construction in this work. For this purpose, forward and reverse primers were designed to introduce compatible restriction enzyme sites and 3-6 additional bases were added at the 5' ends to allow efficient digestion by restriction enzymes (table 2.1). The following text describes a typical PCR reaction and a PCR cycling programme. The annealing temperature can be chosen on the basis of the melting temperature of the primers. This may work, but sometimes the results may not match up to expectations. Therefore, a simple procedure used many times in this work was to use an initial annealing temperature of 55°C (usually good for most primers with a length around 20 bp or more). If non-specific products resulted, this temperature was increased. If there were no products, the temperature was decreased.

PCR reaction mixture (50 µl)

2.0 µl DNA sample (~20ng)

1.0 µl 5' oligo (100 pmol/µl)

1.0 µl 3' oligo (100 pmol/µl)

5.0 µl 10x cloned *Pfu* buffer

5.0 µl DMSO

5.0 µl dNTP (2.5 mM)

1.0 µl *Pfu* polymerase

30.0 µl H₂O

PCR cycling programme

92°C 3 min,

55°C 4 min,
68°C 1 min/kb,
25 cycles of [92°C 30 sec, 60°C 30 sec/kb, 68°C 1 min/kb],
92°C 30 sec,
60°C 30 sec/kb,
68°C 10 min,
hold temperature at 4°C

2.2.1.2 Agarose gel electrophoresis and DNA fragment isolation

For analysis of plasmid DNA, a 0.8% agarose gel was usually used in this study. A 1-kb DNA ladder at a concentration of 0.05 mg/ml was loaded in one lane as a marker. Gel was run in 1 x TBE buffer and stained in 0.5 µg/ml ethidium bromide (EtBr). DNA was visualized under UV light.

10x TBE buffer (pH 8.3)

1 M Tris base
0.83 M Boric acid
10 mM EDTA

5x DNA loading buffer

30% glycerol (v/v)
0.25% bromophenol blue (w/v)
0.25% xylene cyanol FF (w/v)

A QIAquick gel extraction kit (Qiagen, Hilden, Germany) was used for isolation of DNA fragments from agarose gel. The samples (PCR products or enzyme-digested DNA samples) were electrophoresed through 0.8% agarose gel and stained with EtBr. The band of interest was identified using a UV-illuminator and cut out of the gel. The gel slice containing the DNA fragment was placed in

the prepared tube and weighed. Every 100 mg of gel was dissolved in 300 μ l buffer QG at 50°C for 10 minutes. After the gel slice has dissolved completely, it was applied to a QIAquick column and spun down for 1 minute. The column was washed once with 0.75 ml wash buffer PE and the DNA sample was eluted with 30 μ l elution buffer EB(10 mM Tris-HCl, pH 8.5).

2.2.1.3 Enzyme digestion and ligation

For the ligation reaction, the vector DNA and the insert DNA have to be prepared by digesting with appropriate restriction enzymes and then purified with either a GFX purification kit (Amersham Biosciences) or a QIAquick PCR purification kit (Qiagen) according to the manufacture's protocol. The ligation reaction was established as follows. For the optimal ligation efficiency, two DNA molecules were added in the reaction in the range of 3:1 to 5:1 molar ratio of insert to vector. The reaction mixture was incubated at 16°C for 3 hours or more and was then incubated at 65°C for 15 minutes to inactivate the enzyme. The sample was spun down briefly and 2 μ l was used for transformation.

20 μ l ligation reaction mixture

2.0 μ l 10x buffer for T4 DNA ligase

2.0 μ l linearised vector DNA

8.0 μ l insert DNA

7.5 μ l H₂O

0.5 μ l T4 DNA ligase (400 U/ μ l)

2.2.1.4 Bacterial transformation

Two methods were used for the bacterial transformation in this work.

2.2.1.4.1 Transformation of *E. coli* cells by electroporation

- **Preparation of competent cells**

One liter of culture was incubated until an OD₆₀₀ of 0.4-0.6 was reached. The culture was centrifuged at 4000 x g for 15 minutes. The pellet was washed twice with 500 ml ice-cooled, sterile water, once with 200 ml ice-cooled, sterile 10% glycerol and once with 50 ml ice-cooled, sterile 10% glycerol. The last pellet was resuspended in 4 ml of ice-cooled sterile 10% glycerol. 50 µl aliquots were prepared and were shock-frozen in liquid nitrogen and placed in the -70°C freezer for storage.

- **Transformation**

Before transformation, a 50 µl aliquot of competent cells was thawed on ice. The DNA to be transformed was then added to competent cells and the cell mixture was transferred to a pre-chilled electroporation cuvette (BioRad). After a brief incubation on ice, the cells were exposed to a voltage of 1.8 kV (for cuvettes with 0.1 mm width) using the *E. coli* Pulser (BioRad). 950 µl of LB medium was added to the cuvette after electroporation. The cells were transferred to a 1.5-ml microcentrifuge tube, incubated at 37°C for 40-60 minutes, spread on LB plates containing appropriate antibiotics and incubated at 37°C overnight.

2.2.1.4.2 Transformation of *E. coli* cells by heat shock

- **Preparation of competent cells (rubidium chloride method)**

250 ml culture was incubated until an OD₆₀₀ of 0.4-0.6 was reached. To collect cells, the culture was centrifuged at 4000 x g for 15 minutes at 4°C. Next, the cell pellet was resuspended in 100 ml ice-cooled TFBI buffer and incubated on ice for 10 minutes. The resuspension was then centrifuged at 4000 x g for 5 minutes at 4°C, and the pellet was resuspended in 10 ml ice-cooled TFBII buffer

and incubated on ice for at least 15 minutes. 100 µl aliquots were prepared and were shock-frozen in liquid nitrogen and placed in the -70°C freezer for storage.

TFBI

30 mM potassium acetate

100 mM rubidium chloride

10 mM calcium chloride

50 mM manganese chloride

15% v/v glycerol

Adjust to pH 5.8 with acetic acid and filter (0.20 µm, Millipore) to sterilize.

TFBII

10 mM MOPS

75 mM calcium chloride

10 mM rubidium chloride

15% v/v glycerol

Adjust pH to 6.5 with KOH and filter to sterilize.

• Transformation

Before transformation, a 100 µl aliquot of competent cells was thawed on ice. The DNA or ligation reaction to be transformed was then added to the competent cells and the cell mixture was incubated on ice for 20-30 minutes and then at 42°C for 90 seconds for heat shock. 900 µl of LB medium was added and incubated at 37°C for 45 minutes and then spread on the LB plates containing appropriate antibiotic and incubated at 37°C overnight.

2.2.1.5 Mini-preparation of plasmid DNA

QIAprep spin miniprep kit (Qiagen, Hilden, Germany) was used for this purpose. The purification of plasmid DNA was performed following the methods

described by the manufacturer. A single colony was inoculated into 5 ml of LB liquid medium containing appropriate antibiotic and grown overnight at 37°C with shaking. 2 ml of overnight culture was transferred to a 2-ml microcentrifuge tube and centrifuged at 13,000 rpm at 4°C for 10 minutes. The cell pellet was resuspended in 250 µl buffer P1, and then 250 µl buffer P2 was added and mixed gently by inverting the tube 4-6 times. After 5 minutes incubation at room temperature, 350 µl buffer P3 was added and mixed immediately but gently by inverting the tube 4-6 times. The tube was centrifuged at 13,000 rpm for 10 minutes. The supernatant was applied to a QIAprep spin column by decanting. The column was spun down for 1 minute to remove the liquid and washed once with 0.75 ml buffer PB and subsequently with 0.75 ml buffer PE. The residual wash buffer was removed by additional centrifugation for 1 minute and air-dried for 1 minute. To elute DNA, 50 µl of elution buffer EB was added to the center of each column and the column was allowed to stand for 1 minute at room temperature and centrifuged for 1 minute to collect the DNA sample. For checking the desired insert DNA fragment, 2 µl DNA sample was used for enzyme digestion and run on a 0.8 % agarose gel.

2.2.1.6 DNA sequencing

To minimize potential misincorporation during PCR, I used high-fidelity *Pfu* DNA polymerase to perform DNA amplification. In addition, the sequence accuracy of PCR products for each construct and cDNA was confirmed by DNA sequencing. The sequencing reaction and the PCR cycling program were established as follows:

20 µl sequencing reaction

10.0 µl H₂O

6.0 µl BigDye(Applied Biosystems, Weiterstadt, Germany)

3.0 µl DNA sample(~250 ng)

1.0 μ l sequencing oligo(10 pmol/ μ l)

PCR cycling program

96°C 1 min

25 cycles of [96°C 30 sec, 55°C 30 sec, 60°C 4 min],

hold temperature at 4°C

Following the temperature cycling, the reaction was spun down briefly. To precipitate the sample, 15 μ l of 3 M NaAc pH 5.3, 65 μ l of H₂O and 300 μ l of 100% ethanol were added and mixed. The tube was centrifuged at 13,000 rpm at 15°C for 20 minutes. The pellet was washed once with 750 μ l 70% ethanol, dried in air and resuspended in 25 μ l of template suppression reagent (Applied Biosystems, Weiterstadt, Germany). The DNA sample was sequenced by ABI PRISM™ 310 Genetic Analyzer (Applied Biosystems).

Table 2.3. List of the original constructs used in this study

Mouse protein	Construction	Description
ERp44-GST	pGEX-6p-2/BamHI-EcoRI	The GST fusion protein could be cleaved by Procission Protease (Amersham Biotech).
ERp44-ZZ	pCH-ZZ/NcoI-KpnI	With n-terminus His-tag; the ZZ fusion with the target protein could be cleaved by TEV protease.
ERO1p-ZZ	pETM-ZZ/NcoI-KpnI	With n-terminus His-tag; the ZZ fusion with the target protein could be cleaved by TEV protease.

1L3V-ZZ	pETM-ZZ/NcoI-KpnI	With n-terminus His-tag; the ZZ fusion with the target protein could be cleaved by TEV protease.
ERp18	pQE-60/NcoI-KpnI	With c-terminus His-tag.

2.3 Protein expression and purification

2.3.1 Small scale expression

The *E. coli* host strains Rosetta (DE3) and BL21 (DE3) were transformed with different expression plasmids. Transformants of both strains were selected on Luria–Bertani (LB) plates supplemented with either ampicillin (100 µg /mL) or kanamycin (35 µg /mL). Well-grown single colonies from the selection plate were inoculated into 100 mL of LB medium containing either 100 µg /mL of ampicillin or 35 µg /mL kanamycin and the culture was incubated overnight at 37°C in an INNOVA 4330 shaker (New Brunswick Scientific, Edison, NJ) (180 rpm). Twenty milliliters of this culture was then added into 1 liter of fresh culture medium and the culture was grown in the shaker (180 rpm) at 37°C. When the absorbance at 600 nm reached around 0.7, expression of recombinant protein was induced by adding isopropyl b-D-thiogalactopyranoside (IPTG) to a concentration of 0.1 mM and incubation was continued at 18°C for various time periods. Ten milliliters of the culture medium was sampled after different culture times and the cell pellets were collected by centrifugation. The cell pellets were resuspended in 1 ml of 1 x PBS buffer. Each suspension was sonicated 10 times for 10 second on ice with a Branson Sonifier 250 (Branson Ultrasonics, Danbury, CT), and was then centrifuged at 19,000 x g for 10 min at 4°C to separate the soluble and insoluble fractions. Both fractions were finally analyzed by using different concentrations of Sodium Dodecyl Sulphate-PolyAcrylamide Gel Electrophoresis (SDS–PAGE) followed by Coomassie Blue staining.

2.3.2 Protein assay

Protein concentration was determined in accordance with Lowry et al. using a Bovine Serum Albumin (BSA) standard. SDS-PAGE and Western Blotting SDS-PAGE was performed by the method of Laemmli. Proteins separated in the polyacrylamide gels were stained with the GelCode Blue Stain Reagent (Pierce Biotechnology), which is based on Coomassie Brilliant Blue G250 staining. The molecular weight markers were obtained from Bio-Rad.

2.3.3 Large scale expression and purification of recombinant proteins

Escherichia coli Rosetta (DE3) transformants which carry the desired protein-expression plasmids were cultured in 6 liter of LB broth containing either 100 µg /mL ampicillin or 35 µg /mL Kanamycin at 37°C. When the absorbance at 600 nm reached 0.7, 1 mM IPTG was added to induce the inducible promoter. For the production of endoPGI, the culture was incubated for another 24 hours at 20°C. After centrifugation, the bacterial pellets were stored at -80°C. The bacterial pellets were resuspended in 50 ml of 1 x PBS buffer. The suspension was sonicated for 30 sec 10 times on ice with a Branson Sonifier 250, and was centrifuged at 20,000 x g for 30 min at 4°C. The supernatant was dialyzed against 20 mM phosphate buffer (pH 6.2) and then applied to an open-column (Bio-rad, 20 ml) with affinity resin pre-equilibrated with the same buffer. The recombinant protein was purified by a standard procedure of affinity chromatography.

2.3.3.1 GST-ERp44

A 1131bp DNA fragment of the *Mus musculus ERP44* gene's conserved region (coding for amino acid residues 30-406) was inserted into the pGEX-6p-2 expression vector (Amersham Pharmacia Biotech). The resulting construct was transformed into Rossette (DE3) (Novagen) cells. Transformants were grown in LB medium containing 0.4% (w/v) glucose, 100 µg/mL ampicillin, and 34 µg/mL chloramphenicol. Cultures were grown at 37°C to an optical density of A600 ~ 0.7 to 1.0. Isopropyl-D-thiogalactoside (IPTG) was added to the cultures to a final concentration of 0.1 mM, and the cultures were shaken for an additional 4 hours at 37°C. Cells were harvested by centrifugation at 2600 x g for 30 min; resuspended in PBS buffer (20 mM potassium phosphate buffer, 150 mM NaCl, pH 7.4) supplemented with protease inhibitors tablets (Roche), and lysed by sonication. To remove cell debris, the resulting lysate was centrifuged for 45 min at 15,500 x g, and the supernatant was collected and gently mixed with Glutathione-Sepharose 4B beads (Amersham Pharmacia Biotech) at 4°C for 2 hr. The protein:bead mixture was collected by centrifugation, loaded into a column, and washed with four volumes PBS buffer, four volumes of high salt buffer (0.5 M Tris-HCl [pH 8.0]), and then four volumes PBS buffer. The Glutathione-Sepharose 4B beads were mixed and incubated with Prescission Protease at 4°C over night. The digested protein was concentrated and applied to a Superdex-75 26/60 column (Amersham Pharmacia Biotech) that had been preequilibrated with [10 mM Tris pH 8.0, 100 mM sodium chloride, 2 mM Dithiothreitol (DTT)]. The fractions of pure protein which were verified by SDS-PAGE, were directly pooled together and concentrated to 10 mg/ml. The final sample was aliquoted into enppendorf at 50 µl, and stored at -80°C.

2.3.3.2 ZZ-ERp44

A 1131bp DNA fragment of the *Mus musculus ERP44* gene's conserved region (coding for amino acid residues 30-406) was inserted into the pCHM-ZZ expression vector. The resulting construct was transformed into Rossette (DE3) (Novagen) cells. Transformants were grown in LB medium containing 0.4% (w/v) glucose, 100 µg/mL ampicillin, and 34 µg/mL chloramphenicol. Cultures were grown at 37°C to an optical density of A600 ~ 0.7 to 1.0. IPTG was added to the cultures to a final concentration of 0.1 mM, and the cultures were shaken for an additional 4 hours at 37°C. Cells were harvested by centrifugation at 2600 x g for 30 min; resuspended in lysis buffer [20 mM Tris pH8.0, 150 mM sodium chloride, and 0.2% of NP40 (w/v)] with 10 mM Imidazole (pH8.0) supplemented with protease inhibitors tablets (Roche); and lysed by sonication. To remove cell debris, the resulting lysate was centrifuged for 45 min at 15,500 x g, and the supernatant was collected and gently mixed with Ni-NTA beads (Qiagen) at 4°C for 2 hours. The protein:bead mixture was collected by centrifugation, loaded into a column, and washed with four volumes of lysis buffer, four volumes of high salt buffer (lysis buffer plus 0.5 M sodium chloride), and then four volumes of lysis buffer with 20 mM Imidazole (pH8.0). The column was then eluted with buffer containing 350 mM Imidazole (pH8.0). The eluted protein was collected and applied to an IgG sepharose column (Amersham Pharmacia Biotech) followed by incubation with TEV protease at 4°C overnight. The digested protein was concentrated and applied onto a Superdex-75 26/60 column (Amersham Pharmacia Biotech) that had been preequilibrated with [10 mM Tris pH 8.0, 100 mM sodium chloride, 2 mM Dithiothreitol (DTT)]. The fractions of pure protein which were verified by SDS-PAGE, were directly pooled together and concentrated to 10 mg/ml. The final sample was aliquoted into enppendorf at 50 µl, and stored at -80°C.

2.3.3.3 ZZ-ERO1A

A 1323bp DNA fragment of the *Mus musculus ERO1* gene's conserved region (coding for amino acid residues 24-464) was inserted into the pETM-ZZ expression vector. The resulting construct was transformed into Rossette (DE3) (Novagen) cells. Transformants were grown in LB medium containing 0.4% (w/v) glucose, 100µg/mL ampicillin, and 34 µg/mL chloramphenicol. Cultures were grown at 37°C to an optical density of A600 ~ 0.7 to 1.0. IPTG was added to the cultures to a final concentration of 0.1 mM, and the cultures were shaken for an additional 4 hours at 37°C. Cells were harvested by centrifugation at 2600 x g for 30 min; resuspended in lysis buffer [20 mM Tris pH8.0, 150 mM sodium chloride, and 0.2% of NP40 (w/v)] with 10 mM Imidazole (pH8.0) supplemented with protease inhibitors tablets (Roche); and lysed by sonication. To remove cell debris, the resulting lysate was centrifuged for 45 min at 15,500 x g, and the supernatant was collected and gently mixed with Ni-NTA beads (Qiagen) at 4°C for 2 hours. The protein:bead mixture was collected by centrifugation, loaded into a 20-ml open column (Bio-Rad), and washed with four volumes of lysis buffer, four volumes of high salt buffer (lysis buffer plus 0.5 M sodium chloride), and then four volumes of lysis buffer with 20 mM Imidazole (pH8.0). The column was eluted with buffer with 350 mM Imidazole (pH8.0). The eluted protein was collected and applied to an IgG sepharose column (Amersham Pharmacia Biotech) followed by incubation with TEV protease at 4°C overnight. The digested protein was concentrated and applied onto a Superdex-75 26/60 column (Amersham Pharmacia Biotech) that had been preequilibrated with [10 mM Tris pH 8.0, 100 mM sodium chloride, 2 mM Dithiothreitol (DTT)]. The fractions of pure protein which were verified by SDS-PAGE, were directly pooled together and concentrated to 10 mg/ml. The final sample was aliquoted into eppendorf at 50 µl, and stored at -80°C.

2.3.3.4 ZZ-1L3V

A 327bp DNA fragment of the *Mus musculus IP3R* gene's conserved region (coding for amino acid residues 2461-2569) was inserted into the pETM-

ZZ expression vector. The resulting construct was transformed into Rossette (DE3) (Novagen) cells. Transformants were grown in LB medium containing 0.4% (w/v) glucose, 100 µg/mL ampicillin, and 34 µg/mL chloramphenicol. Cultures were grown at 37°C to an optical density of A₆₀₀ ~ 0.7 to 1.0. IPTG was added to the cultures to a final concentration of 0.1 mM, and the cultures were shaken for an additional 18 hours at 16°C. Cells were harvested by centrifugation at 2600 x g for 30 min; resuspended in lysis buffer [20 mM Tris pH8.0, 150 mM sodium chloride, and 0.2% of NP40 (w/v)] with 10 mM Imidazole (pH8.0) supplemented with protease inhibitors tablets (Roche); and lysed by sonication. To remove cell debris, the resulting lysate was centrifuged for 45 min at 15,500 x g, and the supernatant was collected and gently mixed with Ni-NTA beads (Qiagen) at 4°C for 2 hours. The protein:bead mixture was collected by centrifugation, loaded into a column, and washed with four volumes of lysis buffer, four volumes of high salt buffer (lysis buffer plus 0.5 M sodium chloride), and then four volumes of lysis buffer with 20 mM Imidazole (pH8.0). The column was eluted with buffer containing 350 mM Imidazole (pH8.0). The eluted protein was collected and applied to an IgG sepharose column (Amersham Pharmacia Biotech) followed by incubation with TEV protease at 4°C overnight. The digested protein was concentrated and applied onto a Superdex-75 26/60 column (Amersham Pharmacia Biotech) that had been, preequilibrated with [10 mM Tris pH 8.0, 100 mM sodium chloride, 2 mM Dithiothreitol (DTT)]. The fractions of pure protein which were verified by SDS-PAGE, were directly pooled together and concentrated to 10 mg/ml. The final sample was aliquoted into eppendorf at 50 µl, and stored at -80°C.

2.3.3.5 ERp18

A 438bp DNA fragment of the *Mus musculus ERP18* gene's conserved region (coding for amino acid residues 25-170) was inserted into the pQE-60 expression vector (Qiagen). The resulting construct was transformed into

Rossette (DE3) (Novagen) cells. Transformants were grown in LB medium containing 0.4% (w/v) glucose, 100 µg/mL ampicillin, and 34 µg/mL chloramphenicol. Cultures were grown at 37°C to an optical density of A600 ~ 0.7 to 1.0. IPTG was added to the cultures to a final concentration of 0.1 mM, and the cultures were shaken for an additional 18 hours at 16°C. Cells were harvested by centrifugation at 2600 x g for 30 min; resuspended in lysis buffer [20 mM Tris pH8.0, 150 mM sodium chloride, and 0.2% of NP40 (w/v)] with 10 mM Imidazole (pH8.0) supplemented with protease inhibitors tablets (Roche); and lysed by sonication. To remove cell debris, the resulting lysate was centrifuged for 45 min at 15,500 x g, and the supernatant was collected and gently mixed with Ni-NTA beads (Qiagen) at 4°C for 2 hours. The protein:bead mixture was collected by centrifugation, loaded into a 20-ml open column (Bio-Rad), and washed with four volumes of lysis buffer, four volumes of high salt buffer (lysis buffer plus 0.5 M sodium chloride), and then four volumes of lysis buffer containing 20 mM Imidazole (pH8.0). The column was then eluted with buffer containing 350 mM Imidazole (pH8.0). The eluted protein was collected and applied to an IgG sepharose column (Amersham Pharmacia Biotech) followed by incubation with TEV protease at 4°C overnight. The digested protein was concentrated and applied onto a Superdex-75 26/60 column (Amersham Pharmacia Biotech) that had been preequilibrated with [10 mM Tris pH 8.0, 100 mM sodium chloride, 2 mM Dithiothreitol (DTT)]. The fractions of pure protein which were verified by SDS-PAGE, were directly pooled together and concentrated to 10 mg/ml. The final sample was aliquoted into eppendorf at 50 µl, and stored at -80°C.

2.4 Crystallization

2.4.1 Screening

The initial screening was performed with vapor diffusion method by using Hampton Crystal Screens 1 & 2, Hampton PEG/ION screen, Emerald Wizard I &

II, Emerald Cryol & II, and Nextal Screening Suites at both 4°C and 20°C. All of the above products used the sparse matrix method which is based on the successful conditions reported in the literatures. The initial protein solution was 10 mg/ml in 10 mM Tris pH8.0, 100 mM sodium chloride, and 2 mM DTT. Each drop of solution for crystallized trial was mixed with 100 nl of protein and 100 nl of crystallization screening solution by using Robot peptting.

2.4.2 Optimization

All of the initial conditions were optimized and the initial conditions gave the good crystal (Fig. 2-2b). Several parameters were tuned to grow better crystals for diffraction.

(1) Protein concentration: finding an appropriate protein concentration is important for crystallization. The protein concentration (i.e. 10 mg/ml) in the screening worked fine. Very little was changed on this parameter.

(2) Temperature: crystals can grow under several temperatures such as 4°C, 15°C, 20°C and 25°C. In general, the lower the temperature the crystallization was conducted, the more crystal nuclei and hence the smaller final size one would observe. However, the nucleation process is very difficult to control under low temperature even by adjusting other parameters. The crystallization seems to be sensitive to temperature variations and no crystals were observed in a quiet and temperature-uncontrolled room.

(3) pH and buffer: crystals were also reported appeared in buffers such as imidazol, ADA and cacodylate...etc. However, the crystals I observed looked much worse in the buffer systems other than what I documented here.

(4) Precipitant: adjusting either the concentration or the usage of different molecular weighted PEGs, e.g. PEG600, PEG400, PEG300...etc also helped to optimize the environment for crystallization.

(5) Salts: salts can be used as additives even though the crystallization is sensitive to the salt concentration which should be lower than 0.2M.

(6) Other factors: crystals prefer to grow from a material surface, e.g. the slide surface. Smearing a thin layer of silicon grease on the slide surface helped to grow better crystals and diminish mechanical damages to the crystals when mounting.

2.4.3. Cryo solutions

Several cryo-protectants were optimized for best results (table 2-1) (Rodgers, 2001). Finally, the buffer containing either [0.1M MES pH 6.1, 0.1M CsCl, 20% PEG300, 10% Glycerol] or [0.1M MES pH6.1, 0.1M sodium chloride, 20% PEG300, 10% Glycerol] was used as the cryo-solution.

Cryo-protectant	Suggested Concentration
DMSO	2-20%
Erythritol	>50%(w/v)
Ethylene glycol	15-45%
Glycerol	15-45%
Inositol	20-50%
MPD	25-40%
PEG 200-600	30-50%
Raffinose	>50%(w/v)
Sucrose	>50%(w/v)
(NH ₄) ₂ SO ₄	50% saturation
2-propanol	>70%
Xylitol	20-50%

Table 2.4 Commonly used cryo-protectants.

2.4.4. Heavy atom derivatives

Since the thioredoxin domain contains 3 cysteines and Hg^{2+} ions have a good affinity to sulfur atoms, Hg compounds are good candidates for heavy atom derivatation. In summary, several commonly used heavy atom compounds such as K_2PtCl_4 , HgCl_2 , PbAc , ZnI_2 and some lanthanide compounds etc. had been tried (table 3.5). The long soaking time is not necessary and could be shortened to 3 days. However, the very low concentration (0.05mM) of HgCl_2 is critical for successful crystallization since the derived crystals were somewhat crashed and diffracted badly when higher concentration was used.

Used times	Compound
287	Potassium tetrachloroplatinate(II)
111	Potassium dicyanoaurate(I)
103	Uranyl acetate
101	Mercury(II) acetate
98	Mercury(II) chloride
85	Ethylmercurythiosalicylate (EMTS)
82	Potassium tetraiodomercurate(II)
81	para-Chloromercuriobenzenesulfonate(PCMBS)
75	Trimethyllead(IV) acetate
73	Potassium pentafluorooxyuranate(VI)
73	Phosphatotris(ethylmercury)
61	Potassium tetranitroplatinum(II)
60	Uranyl nitrate
58	Potassium tetracyanoplatinate(II)
57	Dichlorodiammineplatinum(II)
51	Potassium hexachloroplatinate(IV)
51	Methylmercury chloride
44	Potassium tetrachloroaurate(III)
42	para-Chloromercurybenzoate(PCMB)

39	Lead(II) acetate
----	------------------

Table 2.5 The 23 most commonly used heavy-atom compounds reagents. The first column gives the number of times the reagent has appeared in the heavy-atom data bank. (Carvin et al.,2001)

2.5. X-ray data collection and processing

All the diffraction experiments were carried out at low temperature (100K). The crystals were soaked in the cryo solution for a short time (seconds or minutes), then plunged directly into liquid nitrogen (rather than flash cooling in the nitrogen gas).

The native data were collected on a Mar CCD detector at the synchrotron beamline X11 at the EMBL Hamburg outstation/DESY. The dose mode was used in collection. High resolution data were collected first with a high dose and fine oscillation angle, while subsequently the low resolution data were collected with low dose and wide oscillation angle. The radiation damage became apparent in the latter stage of the high resolution data collection, judged by the resolution decreasing. Hg derivative data were collected on Mar345 image plate in house. In order to overcome the non-isomorphism problem between the synchrotron and the in house data, one native dataset was also collected in house. The X-ray data were indexed & integrated with DENZO, and scaled with SCALEPACK (Otwinowski and Minor, 1997).

3. Results and Discussions

2.1 Protein expression and purification

2.1.1 Construction of the GST-ERp44 expression plasmid and small scale expression

In *M. musculus*, ERp44 is initially expressed as a precursor consisting of 406 amino acid residues, and the first 30 residues at the N-terminus are proteolytically removed to form a mature enzyme subsequently. The cDNA fragment encoding the amino acid residues 30-406 (total 377 residues) of the mature *M. musculus* ERp44 was cloned into a pGEX-6p-2 vector, which provides a GST tag at the N-terminus of the recombinant protein, for expressing the mature *M. musculus* ERp44 protein in *E. coli*. A codon corresponding to the translational initiation methionine was engineered to the N-terminus of the cloned ERp44 to fulfill translational requirements.

Among the six cysteine residues which *M. musculus* ERp44 consists, four cysteine residues form two disulfide bonds and the other two sulfhydryls are left free. Therefore, correct disulfide bonds formation between the six cysteine residues is critical to obtain a correct conformation thus an active enzyme. To this end, I attempted to purify the native form of ERp44 protein from *E. coli* Rosetta (DE3) directly. Rosetta (DE3) strain is one of BL21 derivatives and is designed for enhancing the expression of eukaryotic proteins containing codons which are rarely used in *E. coli*. Rosetta (DE3) strain contains a compatible chloramphenicol-resistant plasmid which carries six tRNA genes for the rare

codons AUA, AGG, AGA, CUA, CCC and GGA to achieve this purpose. A parallel protein-overexpression experiment in BL21 (DE3) cells was also conducted for comparison of the yield of the recombinant protein. After introducing the GST-ERp44 plasmid into Rosetta (DE3) and BL21 (DE3), transformants of both hosts were cultured at 16°C after induction with 0.1 mM IPTG. The inducibility and the expression level were determined by examining the total cell extract taken at different time points after induction by SDS-PAGE. In Rosetta (DE3) cells, the expression increased gradually and reached $OD_{600} \sim 1.8$ twenty-four hours after induction. Indeed, Rosetta (DE3) produced more recombinant protein than BL21 (DE3), and therefore Rosetta (DE3) was chosen for the following large scale expression of GST-ERp44.

3.1.1.1 Purification of recombinant GST-ERp44

As described above, Rosetta (DE3) was used for large-scale (6 liters) expression of the recombinant GST-ERp44. The crude cell extract of Rosetta (DE3) cells expressing GST-ERp44 was lysed in 1 x PBS buffer and then applied onto the Glutathione-Sepharose 4B column. The recombinant enzyme was then eluted by a step-gradient of 0.1 M GSH (reduced form) at 4°C and all the collected fractions are subjected to SDS-PAGE followed by Coomassie Blue staining. As shown in Fig. 3.1, the eluted fraction shows a major single 70 kDa band (arrow) on the 15 % gel.

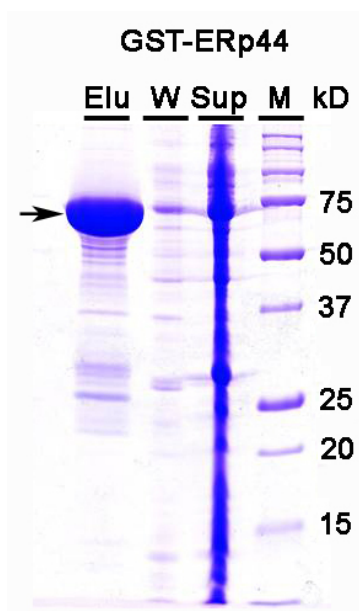


Figure 3.1 One-step purification of the recombinant GST-ERp44 protein by the Gluthathione-Sepharose 4B column. Purification fractions were subjected to a 15% acrylamide gel and stained by Coomassie Blue. Sup: supernatant of the total cell extract. W: washed fraction from the affinity column. Elu: eluted fraction from the affinity column. Arrow: GST-ERp44 protein.

This is a simple and efficient purification which was done by one step while the recombinant protein is not visible in the total cell extract via Coomassie Blue staining on the gel. The concentration of the purified protein was determined by Bradford method. The yield of purified recombinant GST-ERp44 was about 15 mg per 1 liter of the cell culture (either in LB or M9 medium).

3.1.1.2 The size-exclusion chromatography of GST-ERp44

Because ERp44 protein has 2 free sulfhydryls, a size-exclusion column was able to be employed in the second-step purification to seek the homogeneity of the recombinant protein and to remove the high-salt contamination as well for further crystallization trials. The recombinant GST-ERp44 protein from the elution fraction described above was applied onto a size-exclusion column, Superdex-75 26/60, was then eluted by the elution buffer and revealed a very

significant peak in the elution profile (Fig. 3.2). Fractions #23 to #27 were collected and concentrated for further crystallization trials.

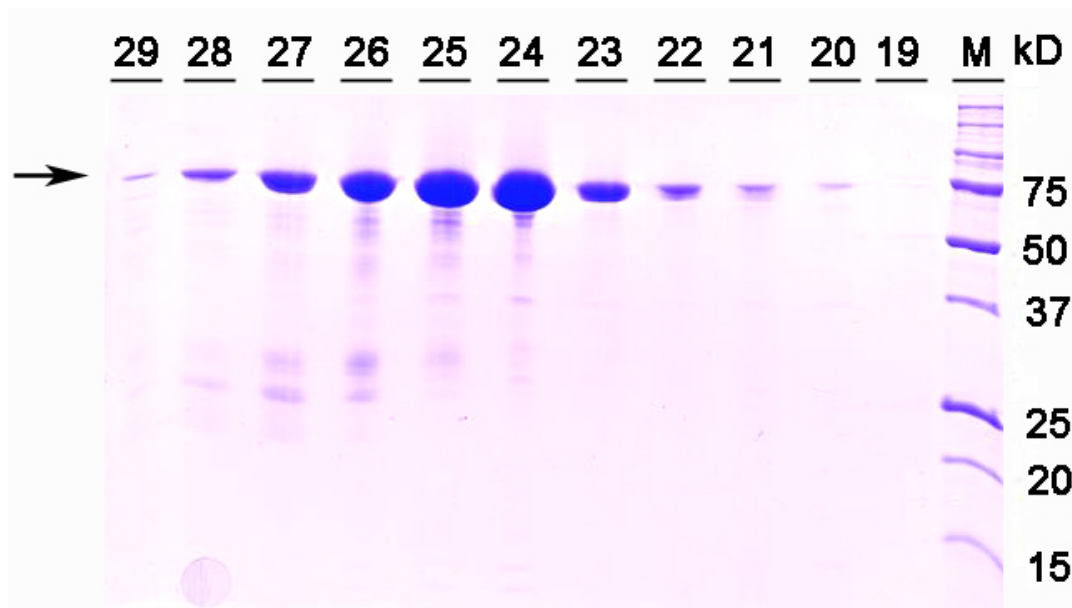


Figure 3.2 The elution profile of the GST-ERp44 from a size-exclusion column (Superdex-75 26/60). The GST-ERp44 enriched elution fraction from the Gluthathione-Sepharose 4B column was applied onto a Superdex-75 26/60 column for further purification. After eluted by the elution buffer, fraction #23 to #27 were pooled and concentrated for crystallization trials.

3.1.2 Construction of the ERp18 (6xHis) expression plasmid and small scale expression

In *M. musculus*, ERp18 is initially expressed as a precursor consisting of 170 amino acid residues, and the first 25 residues at the N-terminus are proteolytically removed to form a mature enzyme subsequently. The cDNA fragment encoding the 146 amino acid residues of the mature *M. musculus* ERp44 was cloned into a pQE-60 vector, which provides a 6xHis tag at the C-terminus of the recombinant protein, for expressing the mature *M. musculus* ERp18 protein in *E. coli*. A codon corresponding to the translational initiation

methionine was engineered to the N-terminus of the cloned ERp18 to fulfill translational requirements.

ERp18 protein contains two cysteine residues which form one disulfide bond. To express the enzyme in its active form, I also selected *E. coli* Rosetta (DE3) as the host. BL21 (DE3) expression was also attempted for parallel comparison. After introducing the 6xHis-ERp18 plasmid into Rosetta (DE3) and BL21 (DE3), transformants of both hosts were cultured at 16°C after induction with 0.1 mM IPTG, and the inducibility and the expression level were determined by examining the total cell extract fraction by SDS-PAGE followed by Coomassie Blue staining. In Rosetta (DE3) cells, the expression increased gradually and reached $OD_{600} \sim 1.8$ twenty-four hours after induction and Rosetta (DE3) was again chosen for the large scale expression. The crude cell extract of Rosetta (DE3) cells expressing 6xHis-ERp18 was lysed by lysis buffer with 10 mM Imidazole (pH8.0) supplemented with protease inhibitors tablets (Roche). The supernatant was then applied to a Ni-NTA column for purification. As shown in Fig. 3.3, the eluted fraction does not show bands with anticipated size of the mature ERp18 protein on the 15% gel.

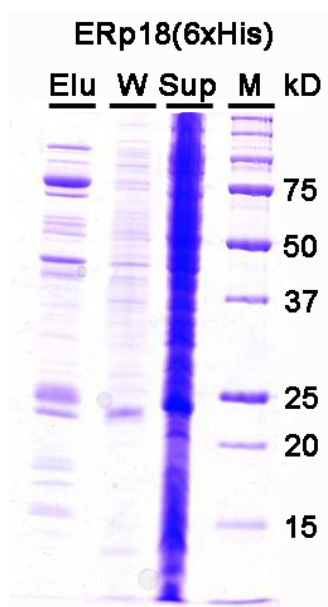


Figure 3.3 Purification of the recombinant ERp18 (6xHis) protein by the Ni-NTA column. Purification fractions were subjected to a 15% acrylamide gel and stained by Coomassie Blue. Sup: supernatant of the total cell extract. W: washed fraction from the affinity column. Elu: eluted fraction from the affinity column. No overexpressed recombinant ERp18 (6xHis) protein was observed.

3.1.3 The construction and purification of ZZ-ERp44

To improve the protein solubility and yielding, ERp44 was sub-cloned onto a different vector, pCH-ZZ. The pCH-ZZ T7 expression vector is inserted with a leading peptide, the ZZ domain of protein A, for facilitating a better productivity and solubility of the recombinant protein while overexpressing in *E. coli*. A specific proteolytic site between the leading peptide (the ZZ tag) and the desired protein was inserted, and the proteolytic site can be easily recognized and digested by TEV protease. As described above, Rosetta (DE3) was used for large-scale expression of recombinant ZZ-Erp44. The crude extract of Rosetta (DE3) cells expressing ZZ-ERp44 was lysed and then applied onto the Ni-NTA agarose column with a bed volume of 0.8ml for purification. The recombinant enzyme was then eluted by a step-gradient of 0.35 M imidazole (pH8.0). As shown in Fig. 3.4, the collected fraction shows a single band on the gel after single step purification. The concentration of purified protein was determined by Bradford method. The yielding of purified recombinant ZZ-Erp44 was about 15 mg per 1 liter of cell culture (either in LB or M9 medium).

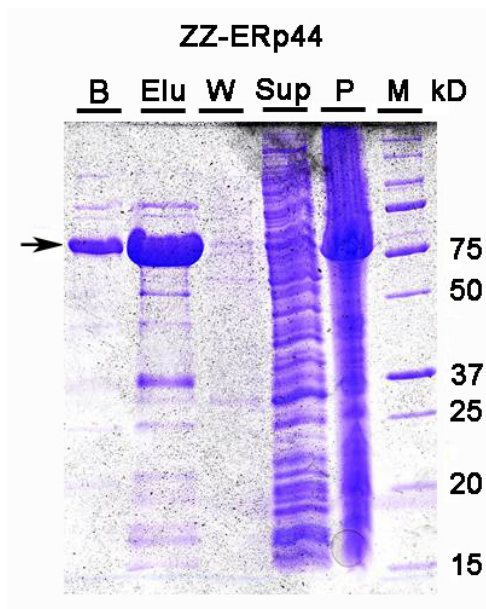


Figure 3.4 Purification of the recombinant ZZ-Erp44 by a Ni-NTA column. All fractions were analyzed by SDS-PAGE and Coomassie Blue staining. Sup: supernatant of the cell extract. W: washing fraction through the Ni-NTA column. Elu: eluted fraction from the Ni-NTA column. B: the protein that remained on the Ni-beads after elution. P: pellet of the cell extract.

3.1.3.1 Removing the ZZ-tag from ZZ-ERp44

The ZZ-tag was removed by incubating with TEV protease at 4°C overnight. Since both the ZZ-tag and TEV protease contain a 6xHis tag, they can be separated from the ERp44 protein easily by a Nickel column after the digestion of TEV protease. The previous collected protein fraction was applied onto a PD-10 column (Bio-Rad) for buffer exchange (10 mM Tris pH8.0, 100 mM NaCl, 2 mM DTT). Next, the TEV protease digested protein fraction was subjected to a Ni-NTA agarose column with a bed volume of 0.8ml again to remove the ZZ-tag and TEV protease. Non-ZZ-tag containing and ERp44 protein enriched fraction was eluted by wash buffer followed by protein concentration. The concentrated sample was applied onto another gel-filtration column, Superdex-20 10/30 for further purification. Unfortunately, the elution profile showed that the ZZ-tag of ZZ-ERp44 was uncleavable (Fig. 3.5), possibly due to the proteolytic site of TEV protease is too rigid for the TEV protease to interact with.

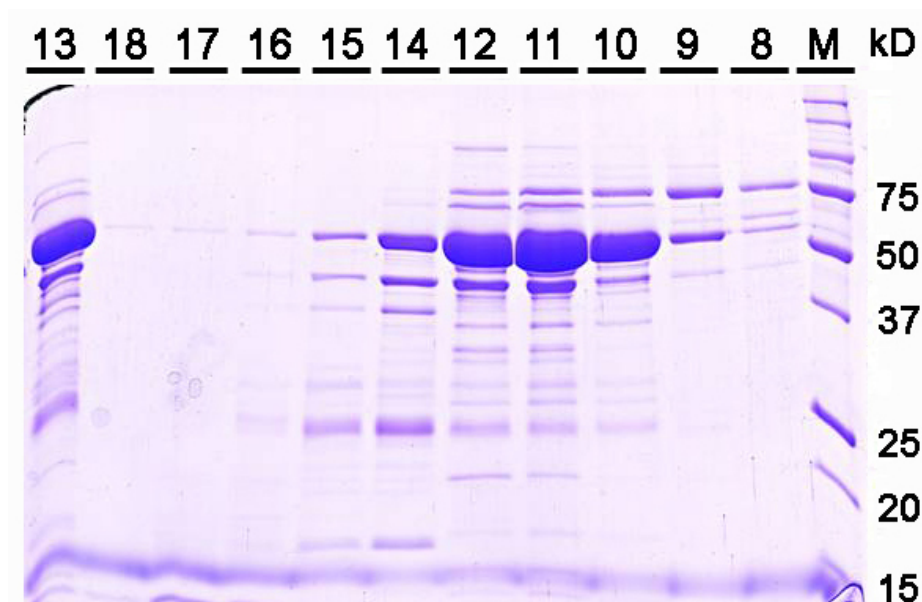


Figure 3.5 Purification of the ZZ-tag-removed ERp44 protein by gel filtration (Superdex-200 10/30) chromatography. After TEV protease digestion and the purification by a Ni-NTA column, ERp44 protein enriched fractions were subjected to a gel filtration column (Superdex-200 10/30) column for further purification of ERp44 protein. However, the major band has a size of ~60 kDa and it apparently showed that the ZZ-tag was un-cut (ZZ-tag: 19 kDa, ERp44: 42 kDa). Fractions # 10 to #13 were pooled and concentrated for crystallization.

3.1.3.1 Purification of ZZ-ERp44 without removing the ZZ-tag

Since ZZ-tag was unable to be cut by TEV protease but it indeed enhanced the protein solubility and yielding, the second batch purification preparation was not subjected to the treatment of TEV protease attempting to get purer protein for crystallization. As described above, Rosetta (DE3) was used for large-scale expression of recombinant ZZ-Erp44. The crude extract of Rosetta (DE3) cells expressing ZZ-ERp44 was first applied to the Ni-NTA agarose column with a bed volume of 0.8ml. The recombinant enzyme was then eluted by a step-gradient of 0.35 M imidazole (pH8.0). ZZ-ERp44 enriched fractions were collected and underwent a buffer exchange step. Next, the ZZ-ERp44 sample was directly applied though a gel-filtration column (Superdex-75 26/60) in

the buffer containing 10 mM Tris pH8.0, 100 mM NaCl and 2 mM DTT with a fraction size of 3.5 ml. The gel-filtration column fraction profile was shown in Fig 3.6. A significant peak was observed from fraction #46 to #56. A small aliquot of fractions #46 to #56 were taken and run on a 15% gel followed by Coomassie Blue staining to ensure the identity of the major protein in the fractions.

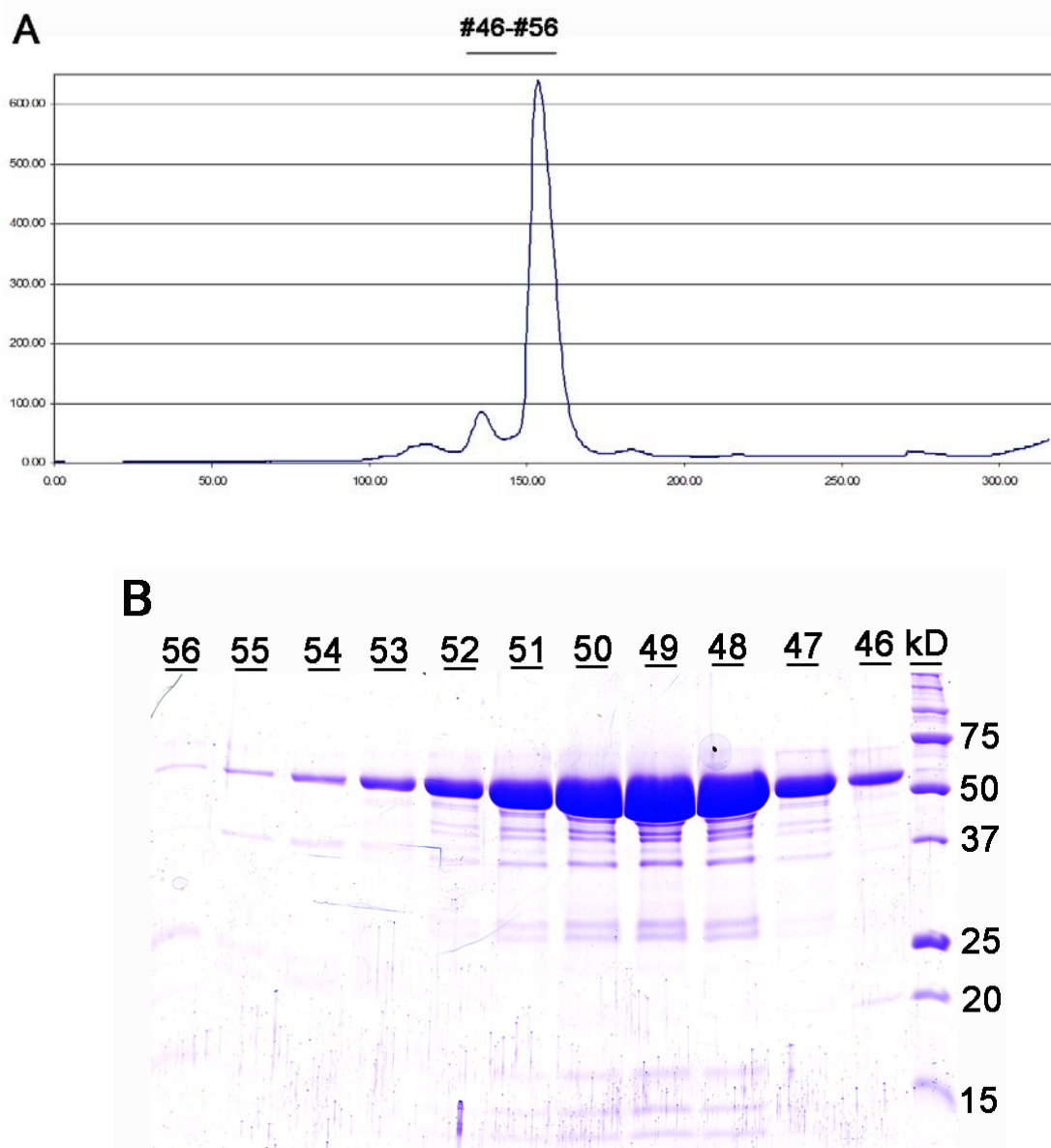


Figure 3.6 Gel filtration (Superdex-75 26/60) chromatogram of non-TEV-digested ZZ-ERp44. ZZ-ERp44 enriched fraction from the Ni-NTA column was subjected to a gel filtration (Superdex-75 26/60) column. (A) A peak was observed from fraction #46 to #56. [Buffer: 10 mM Tris pH8.0, 100 mM NaCl and 2 mM DTT; Fraction Size: 3.5 ml] (B) These fractions were collected and

examined by SDS-PAGE and Coomassie Blue staining. Fraction #46 to #54 were pooled and concentrated for crystallization.

The SDS-PAGE results were shown in Fig 3.7. A major band with an estimated size of 60 kDa was observed in every fraction of #46 to #56. Those fractions were then pooled and concentrated for crystallization.

3.1.4 The construction and purification of ZZ-ERO1A

In *M. musculus*, ERO1A is initially expressed as a precursor consisting of 464 amino acid residues, and the first 30 residues at the N-terminus are proteolytically removed to form a mature enzyme subsequently. The cDNA fragment encoding the amino acid residues 31-464 (total 434 residues) of the mature *M. musculus* ERO1A was cloned into a pETM-ZZ vector, which provides a ZZ tag at the N-terminus of the recombinant protein, for expressing the mature *M. musculus* ERO1A protein in *E. coli*. A codon corresponding to the translational initiation methionine was engineered to the N-terminus of the cloned ERp44 to fulfill translational requirements.

Transformants of BL21 (DE3) were cultured in 2 liter of LB medium at 18°C after induction with 0.1 mM IPTG. The supernatant of the crude cell extract was applied onto a Ni-NTA agarose column with a bed volume of 0.8ml. After elution, the fractions were examined by SDS-PAGE and Coomassie Blue staining (Fig 3.7). The yielding was estimated about 15 mg per 2 liter LB medium culture by the standard Bradford method. The ZZ-tag was then removed from the fusion protein after incubation with the TEV protease. Finally, the ERO1A enriched samples were applied onto a gel-filtration column (Superdex-75 26/60) after the removal of the ZZ-tag and the TEV protease by Ni-cycling procedure. A small amount of aliquot was examined by SDS-PAGE and Coomassie Blue staining (Fig. 3.8).

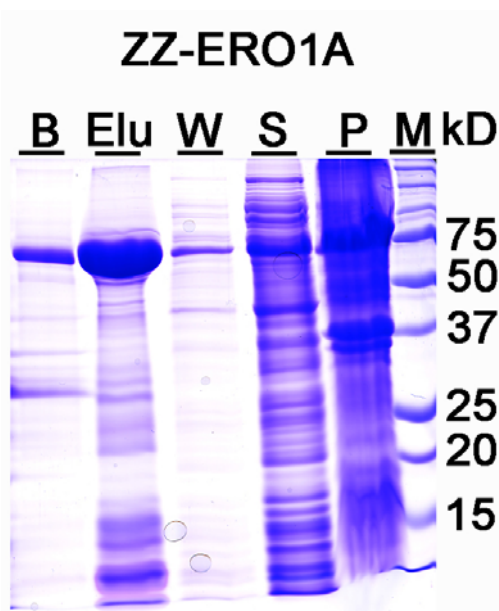


Figure 3.7 Purification of the recombinant ZZ-ERO1A protein by the Ni-NTA column All fractions were analyzed by SDS-PAGE and Coomassie Blue staining. Sup: supernatant of the cell extract. W: washing fraction through the Ni-NTA column. Elu: eluted fraction from the Ni-NTA column. B: the protein that remained on the Ni-beads after elution.

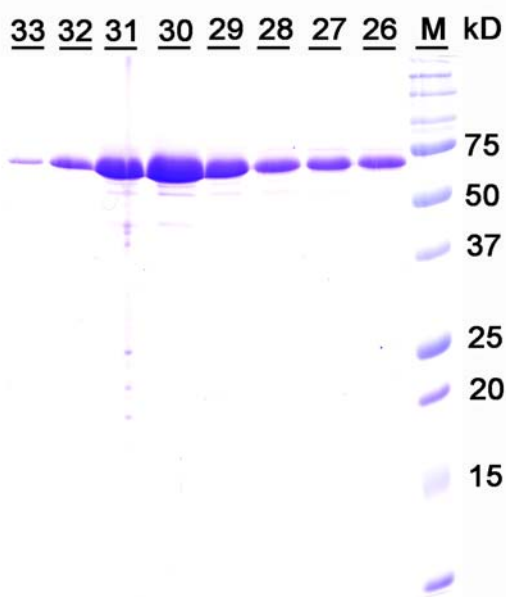


Figure 3.8 Gel filtration (Superdex-75 26/60) chromatography of the ZZ-tag-removed ERO1A protein. ERO1A protein was observed enriched from fraction #26 to #32 by SDS-PAGE and Coomassie Blue staining. [Buffer: 10 mM Tris pH8.0, 100 mM NaCl and 2 mM DTT; Fraction Size: 5 ml] These fractions were pooled and concentrated for crystallization.

3.1.4.1 The co-expression and co-purification of ERp44-ERO1A complex

The ERp44 protein and ERO1A protein were first reported to form a protein dimer covalently linked by a disulfide bridge in mammalian cells (Anelli *et al.*, 2002 & 2003). It is possible these two proteins can be copurified and crystallized together in their native forms. To this end, both ZZ-ERp44 and ZZ-ERO1A plasmids were transformed into BL21 (DE3) cells and selected by both antibiotics, ampicillin and kanamycin. Transformants of BL21 (DE3) were cultured in 2 liter of LB medium at 28°C after induction with 0.1 mM IPTG for 2 hours. The supernatant of the crude cell extract was applied onto a Ni-NTA agarose column with a bed volume of 0.8ml. After elution, the fractions were examined by SDS-PAGE and Coomassie Blue staining (Fig 3.9). The yielding was estimated about 6 mg per 2 liter LB medium culture by the standard Bradford method.

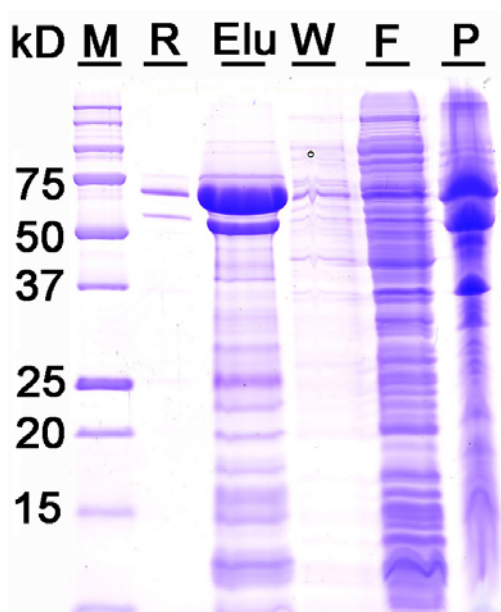


Figure 3.9 Co-expression and co-purification of the recombinant ZZ-ERp44 protein and ZZ-ERO1A protein by the Ni-NTA column. All fractions were analyzed by SDS-PAGE and

Coomassie Blue staining. Sup: supernatant of the cell extract. W: washing fraction through the Ni-NTA column. Elu: eluted fraction from the Ni-NTA column. B: the protein that remained on the Ni-beads after elution. P: pellet of the cell extract.

The ZZ-tag of both recombinant proteins was removed by TEV protease at 4°C overnight. The concentrated eluted sample was applied onto a gel filtration column (Superdex-200 10/30). Eluted fractions showed that apparently the ZZ-tag of both ERp44 and ERO1A proteins was un-cut by TEV protease (Fig. 3.10).

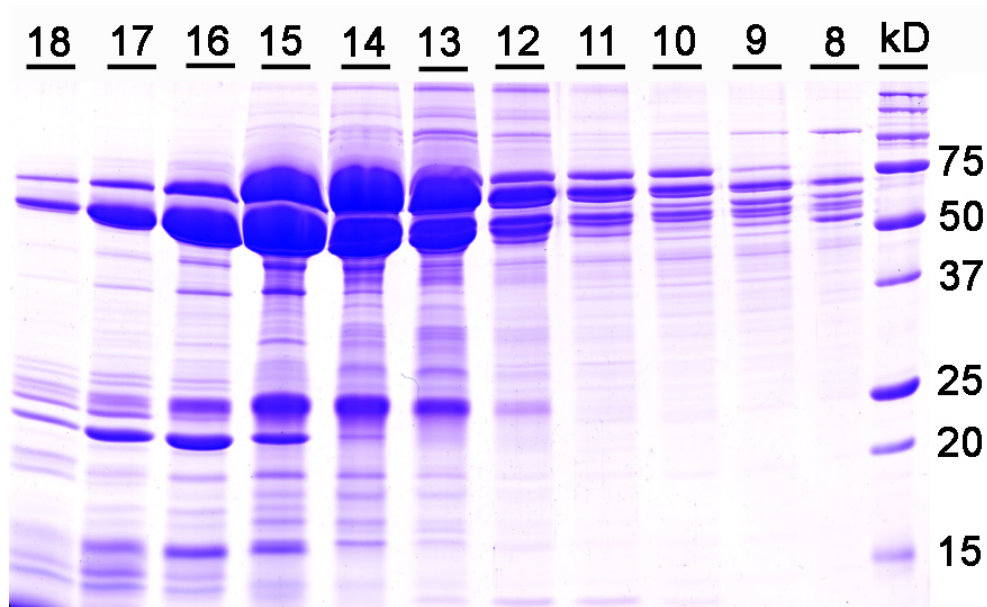


Figure 3.10 Gel filtration (Superdex-200 10/30) chromatogram of TEV protease treated ZZ-ERp44/ZZ-ERO1A proteins. ZZ-ERp44 enriched fraction from the Ni-NTA column was subjected to a gel filtration (Superdex-200 10/30) column. [Buffer: 10 mM Tris pH8.0, 100 mM NaCl, 2.5 mM DTT; Fraction Size: 0.8 ml] However, the ZZ-tag of both ERp44 and ERO1A proteins were not able to be cut by TEV protease. (ZZ-ERp44: 60 kDa; ZZ-ERO1A: 75 kDa) Fraction #13 to #16 pooled and concentrated for crystallization.

3.1.4 The construction and purification of ZZ-1L3V

The cDNA fragment encoding the amino acid residues (total 109 residues) of the mature *M. musculus* 1L3V domain of IP3 receptor type I was cloned into a

pETM-ZZ vector, which provides a ZZ tag at the N-terminus of the recombinant protein, for expressing the mature *M. musculus* 1L3V protein in *E. coli*.

Transformants of BL21 (DE3) were cultured in 2 liter of LB medium at 18°C after induction with 0.1 mM IPTG overnight. The supernatant of the crude cell extract was applied onto a Ni-NTA agarose column with a bed volume of 0.8ml. After elution, the fractions were examined by SDS-PAGE and Coomassie Blue staining (Fig 3.11). The yielding was estimated about 15 mg per 2 liter LB medium culture by the standard Bradford method.

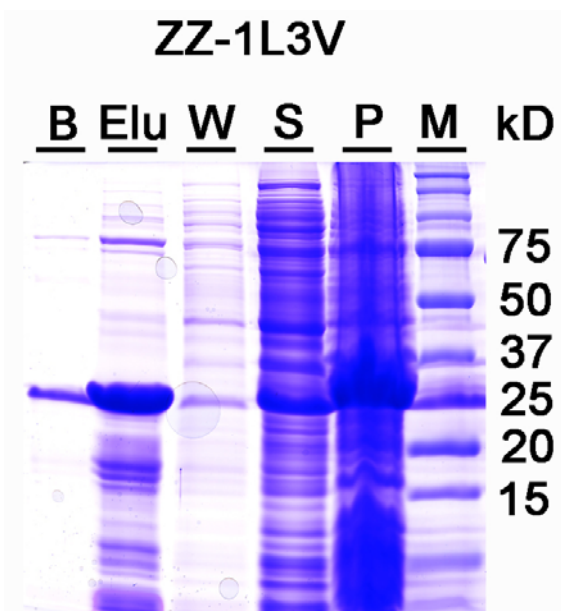


Figure 3.11 Purification of the recombinant ZZ-1L3V protein by the Ni-NTA column All fractions were analyzed by SDS-PAGE and Coomassie Blue staining. Sup: supernatant of the cell extract. W: washing fraction through the Ni-NTA column. Elu: eluted fraction from the Ni-NTA column. B: the protein that remained on the Ni-beads after elution.

3.1.4.1 The co-expression and co-purification of ERp44-1L3V complex

The ERp44 protein and the 1L3V domain of IP3 receptor type I were first reported to physically interact for releasing the calcium from ER lumen in mammalian cells (Higo et al., 2005). It is possible these two proteins can be

copurified and crystallized together in their native forms. To this end, both ZZ-ERp44 and ZZ-1L3V plasmids were transformed into BL21 (DE3) cells and selected by both antibiotics, ampicillin and kanamycin. Transformants of BL21 (DE3) were cultured in 2 liter of LB medium at 28°C after induction with 0.1 mM IPTG for 2 hours. The supernatant of the crude cell extract was applied onto a Ni-NTA agarose column with a bed volume of 0.8ml. After elution, the fractions were examined by SDS-PAGE and Coomassie Blue staining (Fig 3.9). The yielding was estimated about 6 mg per 2 liter LB medium culture by the standard Bradford method. The ZZ-tag of both recombinant proteins was removed by TEV protease at 4°C overnight. The concentrated eluted sample was applied onto a gel filtration column (Superdex-200 10/30). Eluted fractions showed that apparently the ZZ-tag of both ERp44 and 1L3V proteins was un-cut by TEV protease (Fig. 3.10).

3.2 Crystallization

3.2.1 Initial screening

The initial screening was performed with the vapor diffusion method by using Hampton Crystal Screens 1 & 2, Hampton PEG/ION screen, Salt Rx, Emerald Wizard I & II, Emerald Cryol & II, and Nextal Screening Suites at both 4°C and 20°C. All of the above products were tested by the sparse matrix method, which is based on the successful conditions reported in literatures. The initial protein solution was 10 mg/ml in 10 mM Tris pH8.0, 100 mM NaCl, and 2 mM DTT. Each drop of the solution for crystallization trials was mixed with 100 nl protein and 100 nl crystallization screening solution by Robot peptting. The results of the initial crystals are shown on Table 3.1:

Protein	Result
GST-ERp44	No crystal
ZZ-ERp44	Crystallized

ERp44	Crystallized
ERO1A	No crystal
ZZ-ERO1A	No crystal
ERp44- ERO1A complex	No crystal
ERp44-1L3V complex	No crystal

Table 3.1 Initial Crystallization Trials.

3.2.2 Optimization of crystallization conditions

3.2.2.1 The ZZ-ERp44

The ZZ-ERp44 crystals were always observed under the condition containing ammonium and tartrate salts (Fig 3.11). The crystals can be observed within 2-7 days after setting the drops (Fig 3.12). The crystals usually degraded within 1 week from the day they have been observed. The crystal was also examined by SDS-PAGE and Coomassie Blue staining (Fig 3.14) and MASS-SPEC.

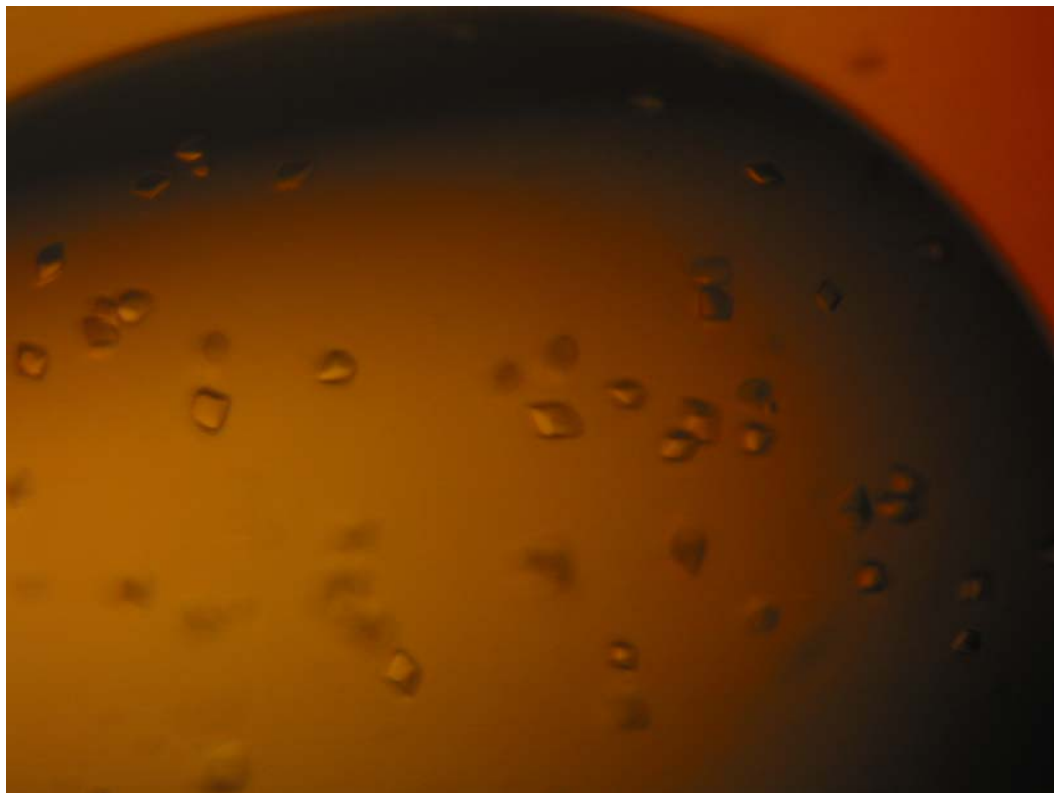


Figure 3.12 The initial crystal of ZZ-ERp44.

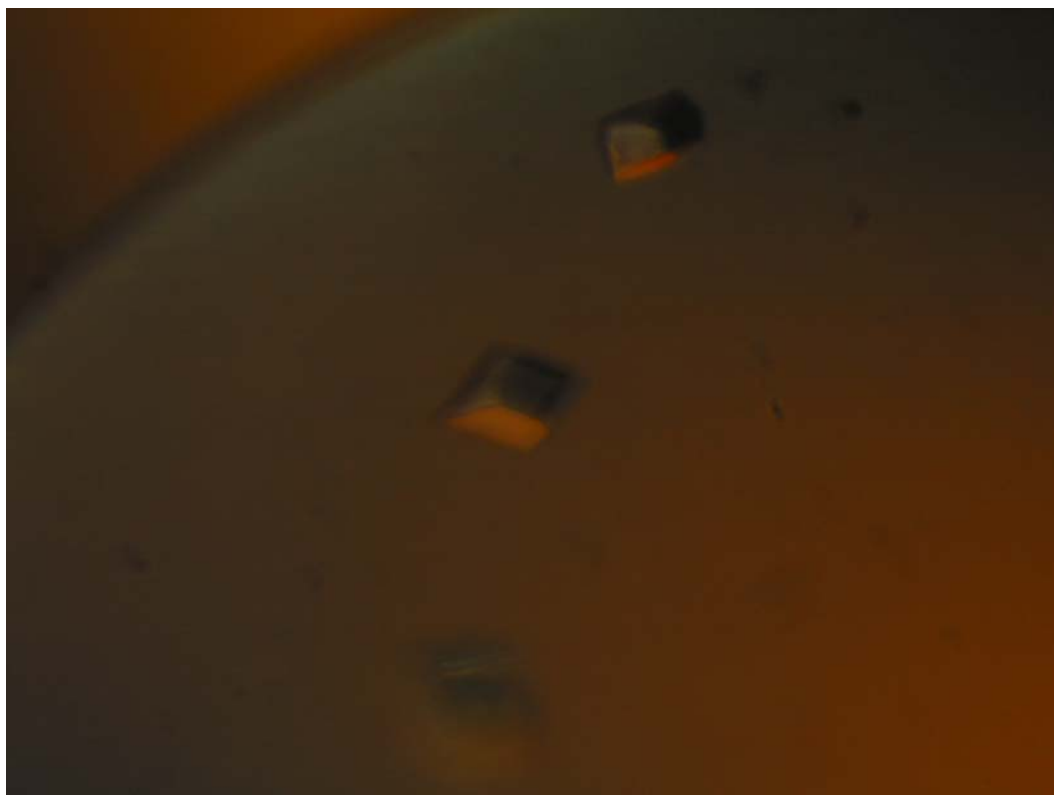


Figure 3.13 The optimization of ZZ-ERp44 crystals (1.5 M di-amonium hydrogen phosphate, pH8.2).

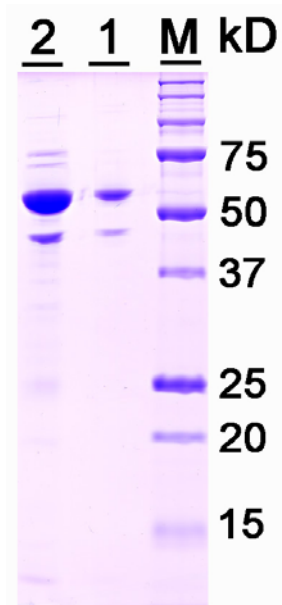


Figure 3.14 SDS-PAGE analyses of the ZZ-ERp44 crystals. ZZ-ERp44 crystals were dissolved and subjected to SDS-PAGE followed by Coomassie Blue staining. 1: ZZ-ERp44 crystals. 2: Purified ZZ-ERp44 protein (control).

3.2.2.2 The ERp44

The ERp44 crystals were observed under the condition containing Taccimate, malonate, and tartrate salts (Fig 3.14). The crystals can be observed within 2-7 days after setting the drops (Fig 3.15). The crystals usually degraded within 1 week from the day they have been observed. The crystal was also examined by SDS-PAGE and Coomassie Blue staining and MASS-SPEC.

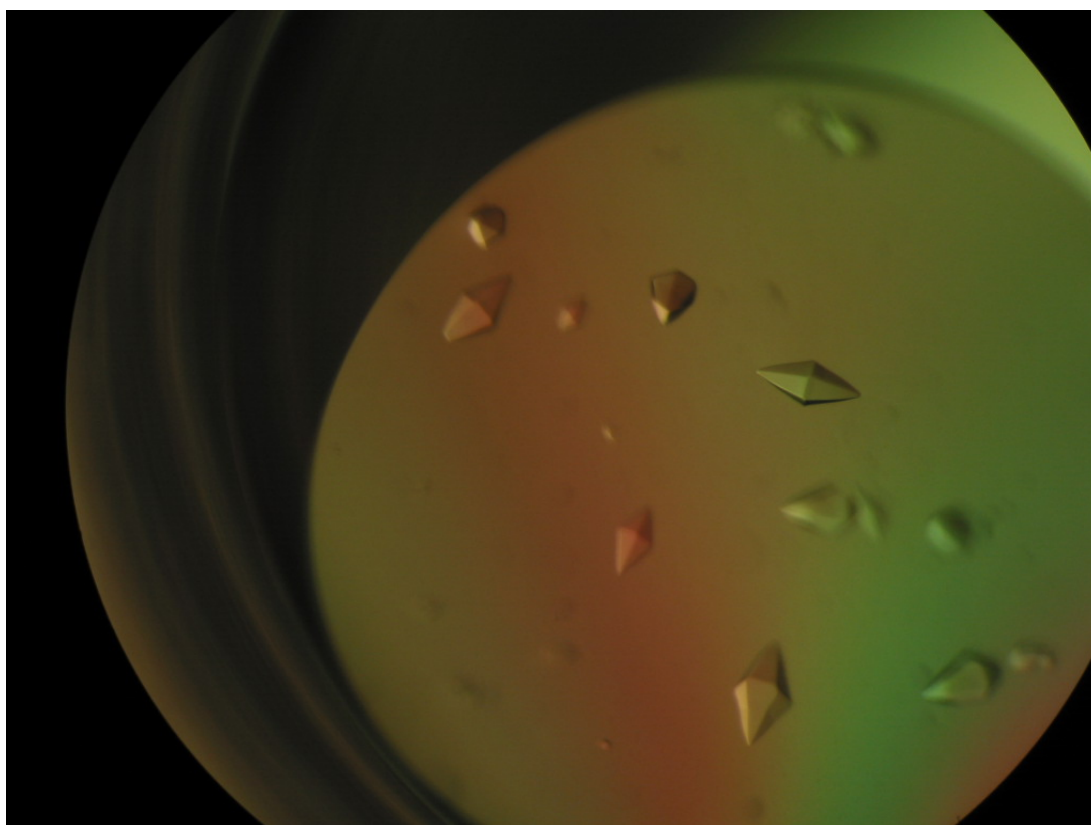


Figure 3.15 The initial crystals of ERp44.

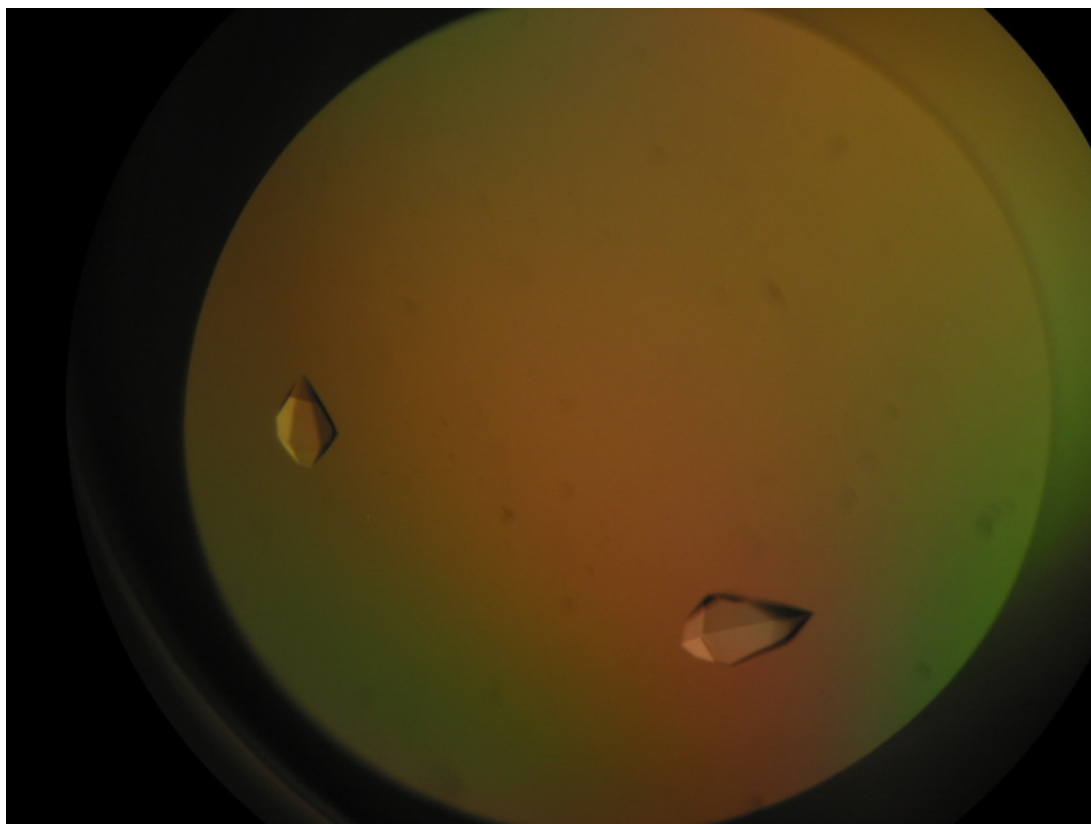


Figure 3.16 The optimization of ERp44 crystals (40% Tacsimate).

4. References

A.

Alanen HI, Williamson RA, Howard MJ, Lappi AK, Jantti HP, Rautio SM, Kellokumpu S, Ruddock LW. Functional characterization of ERp18, a new endoplasmic reticulum-located thioredoxin superfamily member. *J Biol Chem.* 2003 Aug 1; 278 (31):28912-20.

Anderson RG, Falk JR, Goldstein JL, Brown MS. Visualization of acidic organelles in intact cells by electron microscopy. *PNAS* 81 (1984) 4838-4842.

Anelli T, Alessio M, Mezghrani A, Simmen T, Talamo F, Bachi A, Sitia R. ERp44, a novel endoplasmic reticulum folding assistant of the thioredoxin family. *EMBO J.* 2002 Feb 15;21 (4):835-44.

Anelli T, Alessio M, Bachi A, Bergamelli L, Bertoli G, Camerini S, Mezghrani A, Ruffato E, Simmen T, Sitia R. Thiol-mediated protein retention in the endoplasmic reticulum: the role of ERp44. *EMBO J.* 2003 Oct 1;22(19):5015-22.

B.

Bader M, Muse W, Ballou DP, Gassner C, Bardwell JC. Oxidative protein folding is driven by the electron transport system. *Cell.* 1999 Jul 23;98 (2):217-27.

Bader M, Muse W, Zander T, Bardwell J. Reconstitution of a protein disulfide catalytic system. *J Biol Chem.* 1998 Apr 24; 273 (17):10302-7.

Bader MW, Xie T, Yu CA, Bardwell JC. Disulfide bonds are generated by quinone reduction. *J Biol Chem.* 2000 Aug 25; 275 (34):26082-8.

Barbouche R, Miquelis R, Jones IM, Fenouillet E. Protein-disulfide isomerase-mediated reduction of two disulfide bonds of HIV envelope glycoprotein 120 occurs post-CXCR4 binding and is required for fusion. *J Biol Chem.* 2003 Jan 31; 278 (5):3131-6.

Bardwell JC. Building bridges: disulphide bond formation in the cell. *Mol Microbiol.* 1994 Oct; 14 (2):199-205.

Bardwell JC. Disulfide bond formation, a race between FAD and oxygen. *Dev Cell.* 2002 Dec; 3 (6):758-60.

Bardwell JC, Lee JO, Jander G, Martin N, Belin D, Beckwith J. A pathway for disulfide bond formation in vivo. *Proc Natl Acad Sci U S A.* 1993 Feb 1; 90 (3):1038-42.

Bardwell JC, McGovern K, Beckwith J. Identification of a protein required for disulfide bond formation in vivo. *Cell.* 1991 Nov 1; 67 (3):581-9.

Benham AM, Cabibbo A, Fassio A, Bulleid N, Sitia R, Braakman I. The CXXCXXC motif determines the folding, structure and stability of human Ero1-Lalpha. *EMBO J.* 2000 Sep1; 19 (17):4493-502.

Bergeron JJ, Brenner MB, Thomas DY, Williams DB. Calnexin: a membrane-bound chaperone of the endoplasmic reticulum. *Trends Biochem Sci.* 1994 Mar; 19 (3):124-8.

Bertoli G, Simmen T, Anelli T, Molteni SN, Fesce R, Sitia R. Two conserved cysteine triads in human Ero1alpha cooperate for efficient disulfide bond formation in the endoplasmic reticulum. *J Biol Chem.* 2004 Jul 16; 279 (29):30047-52. Epub 2004 May 10.

Bose S, Weikl T, Bugl H, Buchner J. Chaperone function of Hsp90-associated proteins. *Science*. 1996 Dec 6; 274 (5293):1715-7.

Bradford MM. A rapid and sensitive method for the quantitation of microgram quantities of protein utilizing the principle of protein-dye binding. *Anal Biochem*. 1976 May 7; 72: 248-54.

Bu G. The roles of receptor-associated protein (RAP) as a molecular chaperone for members of the LDL receptor family. *Int Rev Cytol*. 2001; 209:79-116.

Bu G, Geuze HJ, Strous GJ, Schwartz AL. 39 kDa receptor-associated protein is an ER resident protein and molecular chaperone for LDL receptor-related protein. *EMBO J*. 1995 May 15; 14 (10):2269-80.

Bu G, Schwartz AL. RAP, a novel type of ER chaperone. *Trends Cell Biol*. 1998 Jul; 8 (7):272-6.

Bucciantini M, Giannoni E, Chiti F, Baroni F, Formigli L, Zurdo J, Taddei N, Ramponi G, Dobson CM, Stefani M. Inherent toxicity of aggregates implies a common mechanism for protein misfolding diseases. *Nature*. 2002 Apr 4;416(6880):507-11.

Bullock SL, Fletcher JM, Beddington RS, Wilson VA. Renal agenesis in mice homozygous for a gene trap mutation in the gene encoding heparan sulfate 2-sulfotransferase. *Genes Dev*. 1998 Jun 15; 12 (12):1894-906.

C.

Cai H, Wang CC, Tsou CL. Chaperone-like activity of protein disulfide isomerase in the refolding of a protein with no disulfide bonds. *J Biol Chem*. 1994 Oct; 269 (40):24550-2.

Chanas-Sacre G, Rogister B, Moonen G, Leprince P. Radial glia phenotype: origin, regulation, and transdifferentiation. *J Neurosci Res.* 2000 Aug 15; 61 (4):357-63.

Chapman, R. Sidrauski, C. and Walter, P: Intracellular signaling from the endoplasmicreticulum to the nucleus. *Annu. Rev. Cell Dev. Biol.* 14: 459–85 (1998).

Charbonnier JB, Belin P, Moutiez M, Stura EA, Quemeneur E. On the role of the cis-proline residue in the active site of DsbA. *Protein Sci.* 1999 Jan; 8 (1):96-105.

Cheung PY, Churchich JE. Recognition of protein substrates by protein-disulfide isomerase. A sequence of the b' domain responds to substrate binding. *J Biol Chem.* 1999 Nov 12; 274 (46):32757-61.

Chivers PT, Laboissiere MC, Raines RT. The CXXC motif: imperatives for the formation of native disulfide bonds in the cell. *EMBO J.* 1996 Jun 3; 15 (11):2659-67.

Chodobski A, Szmydynger-Chodobska J. Choroid plexus: target for polypeptides and site of their synthesis. *Microsc Res Tech.* 2001 Jan 1; 52 (1):65-82.

Cresswell P, Bangia N, Dick T, Diedrich G. The nature of the MHC class I peptide loading complex. *Immunol Rev.* 1999 Dec; 172: 21-8.

Cuozzo JW, Kaiser CA. Competition between glutathione and protein thiols for disulphidebond formation. *Nat Cell Biol.* 1999 Jul; 1 (3):130-5.

Cunnea PM, Miranda-Vizuete A, Bertoli G, Simmen T, Damdimopoulos AE, Hermann S, Leinonen S, Huikko MP, Gustafsson JA, Sitia R, Spyrou G. ERdj5,

an endoplasmic reticulum (ER)-resident protein containing DnaJ and thioredoxin domains, is expressed in secretory cells or following ER stress. *J Biol Chem.* 2003 Jan 10; 278 (2):1059-66.

D.

Dai S, Schwendtmayer C, Schurmann P, Ramaswamy S, Eklund H. Redox signaling in chloroplasts: cleavage of disulfides by an iron-sulfur cluster. *Science.* 2000 Jan 28; 287 (5453):655-8.

Darby NJ, Creighton TE. Catalytic mechanism of DsbA and its comparison with that of protein disulfide isomerase. *Biochemistry.* 1995 Mar 21; 34 (11):3576-87. (a)

Darby NJ, Creighton TE. Characterization of the active site cysteine residues of the thioredoxin-like domains of protein disulfide isomerase. *Biochemistry.* 1995 Dec 26; 34 (51):16770-80. (b)

Darby NJ, Creighton TE. Functional properties of the individual thioredoxin-like domains of protein disulfide isomerase. *Biochemistry.* 1995 Sep 19; 34 (37):11725-35.(c)

Darby NJ, Penka E, Vincentelli R. The multi-domain structure of protein disulfide isomerase is essential for high catalytic efficiency. *J Mol Biol.* 1998 Feb 13; 276 (1):239-47.

Delom F, Mallet B, Carayon P, Lejeune PJ. Role of extracellular molecular chaperones in the folding of oxidized proteins: Refolding of colloidal thyroglobulin by protein disulfide isomerase and immunoglobulin heavy chain-binding protein. *J Biol Chem.* 2001 Jun 15; 276 (24):21337-42.

Demmer J, Zhou C, Hubbard MJ. Molecular cloning of ERp29, a novel and widely expressed resident of the endoplasmic reticulum. *FEBS Lett.* 1997 Feb 3; 402 (2-3):145-50.

Desilva MG, Lu J, Donadel G, Modi WS, Xie H, Notkins AL, Lan MS. Characterization and chromosomal localization of a new protein disulfide isomerase, PDIp, highly expressed in human pancreas. *DNA Cell Biol.* 1996 Jan; 15(1):9-16.

Desilva MG, Notkins AL, Lan MS. Molecular characterization of a pancreas-specific protein disulfide isomerase, PDIp. *DNA Cell Biol.* 1997 Mar; 16(3):269-74.

Dredge BK, Polydorides AD, Darnell RB. The splice of life: alternative splicing and neurological disease. *Nat Rev Neurosci.* 2001 Jan; 2(1):43-50.

Dziegielewska KM, Ek J, Habgood MD, Saunders NR. Development of the choroid plexus. *Microsc Res Tech.* 2001 Jan 1;52(1):5-20.

E.

Eckert DM, Kim PS. Mechanisms of viral membrane fusion and its inhibition. *Annu Rev Biochem.* 2001;70:777-810.

Edwards MA, Yamamoto M, Caviness VS Jr. Organization of radial glia and related cells in the developing murine CNS. An analysis based upon a new monoclonal antibody marker. *Neuroscience.* 1990;36(1):121-44.

Eklund H, Ingelman M, Soderberg BO, Uhlin T, Nordlund P, Nikkola M, Sonnerstam U, Joelson T, Petratos K. Structure of oxidized bacteriophage T4 glutaredoxin (thioredoxin): Refinement of native and mutant proteins. *J Mol Biol.* 1992 Nov 20;228(2):596-618.

Ellgaard, L and Helenius, A. ER quality control: towards an understanding at the molecular level. *Current Opinion in Cell Biology*. 13:431–437 (2001)

Ellgaard, L and Helenius, A. Quality control in the endoplasmic reticulum. *Nat Rev Mol Cell Biol*. 2003 Mar;4(3):181-91. Review.

Ellis RJ, van der Vies SM, Hemmingsen SM. The molecular chaperone concept. *Biochem Soc Symp*. 1989;55:145-53.

Epp O, Ladenstein R, Wendel A. The refined structure of the selenoenzyme glutathione peroxidase at 0.2-nm resolution. *Eur J Biochem*. 1983 Jun 1; 133(1):51-69.

Essex DW, Li M. Protein disulphide isomerase mediates platelet aggregation and secretion. *Br J Haematol*. 1999 Mar;104(3):448-54.

Essex DW, Li M, Miller A, Feinman RD. Protein disulfide isomerase and sulfhydryl-dependent pathways in platelet activation. *Biochemistry*. 2001 May 22;40(20):6070-5.

F.

Farwell AP, Lynch RM, Okulicz WC, Comi AM, Leonard JL. The actin cytoskeleton mediates the hormonally regulated translocation of type II iodothyronine 5'-deiodinase in astrocytes. *J Biol Chem*. 1990 Oct 25; 265(30):18546-53.

Fassio A, Sitia R. Formation, isomerisation and reduction of disulphide bonds during protein quality control in the endoplasmic reticulum. *Histochem Cell Biol*. 2002 Feb;117(2):151-7.

Feng W, Bedows E, Norton SE, Ruddon RW. Novel covalent chaperone complexes associated with human chorionic gonadotropin beta subunit folding intermediates. *J Biol Chem*. 1996 Aug 2; 271(31):18543-8.

Ferrari DM, Nguyen Van P, Kratzin HD, Soling HD. ERp28, a human endoplasmicreticulum-lumenal protein, is a member of the protein disulfide isomerase family but lacks a CXXC thioredoxin-box motif. *Eur J Biochem*. 1998 Aug 1;255(3):570-9.

Ferrari DM, Soling HD. The protein disulphide-isomerase family: unravelling a string of folds. *Biochem J*. 1; 339 (Pt 1):1-10 (1999) .

Fewell SW, Travers KJ, Weissman JS, Brodsky JL. The action of molecular chaperones in the early secretory pathway. *Annu Rev Genet*. 2001; 35:149-91.

Fishell G, Kriegstein AR. Neurons from radial glia: the consequences of asymmetric inheritance. *Curr Opin Neurobiol*. 2003 Feb;13(1):34-41.

Frand AR, Cuozzo JW, Kaiser CA. Pathways for protein disulphide bond formation. *Trends Cell Biol*. 2000 May;10(5):203-10.

Frand AR, Kaiser CA. The ERO1 gene of yeast is required for oxidation of protein dithiols in the endoplasmic reticulum. *Mol Cell*. 1998 Jan; 1(2):161-70.

Frand, A. R. Kaiser, C. A. Ero1p oxidizes protein disulfide isomerase in a pathway for disulfide bond formation in the endoplasmic reticulum. *Mol Cell*. 1999 Oct;4(4):469-77.

Freedman RB, Hirst TR, Tuite MF. Protein disulphide isomerase: building bridges in protein folding. *Trends Biochem Sci*. 1994 Aug;19(8):331-6.

Freedman, R. B. Klappa, P. Ruddock, L. W. Protein disulfide isomerases exploit synergy between catalytic and specific binding domains. *EMBO Rep.* 3(2):136-40 (2002).

Freskgard PO, Bergenheim N, Jonsson BH, Svensson M, Carlsson U. Isomerase and chaperone activity of prolyl isomerase in the folding of carbonic anhydrase. *Science.* 1992 Oct 16;258(5081):466-8.

G.

Gallina A, Hanley TM, Mandel R, Trahey M, Broder CC, Viglianti GA, Ryser HJ. Inhibitors of protein-disulfide isomerase prevent cleavage of disulfide bonds in receptor-bound glycoprotein 120 and prevent HIV-1 entry. *J Biol Chem.* 2002 Dec 27;277(52):50579-88.

Garcia-Verdugo JM, Doetsch F, Wichterle H, Lim DA, Alvarez-Buylla A. Architecture and cell types of the adult subventricular zone: in search of the stem cells. *J Neurobiol.* 1998 Aug;36(2):234-48.

Gerber J, Muhlenhoff U, Hofhaus G, Lill R, Lisowsky T. Yeast ERV2p is the first microsomal FAD-linked sulfhydryl oxidase of the Erv1p/Alrp protein family. *J Biol Chem.* 2001 Jun 29;276(26):23486-91.

Gilbert HF. Protein disulfide isomerase. *Methods Enzymol.* 1998;290:26-50.

Goldberger, R. F., Epstein, C. J., and Anfinsen, C. B. *J. Biol. Chem.* 238, 628-635 (1963).

Gregg CT, Chojnacki AK, Weiss S. Radial glial cells as neuronal precursors: the next generation? *J Neurosci Res.* 2002 Sep 15;69(6):708-13.

Gross E, Kastner DB, Kaiser CA, Fass D. Structure of Ero1p, source of disulfide bonds for oxidative protein folding in the cell. *Cell*. 2004 May 28;117(5):601-10.

Gunther R, Srinivasan M, Haugejorden S, Green M, Ehbrecht IM, Kuntzel H. Functional replacement of the *Saccharomyces cerevisiae* Trg1/Pdi1 protein by members of the mammalian protein disulfide isomerase family. *J Biol Chem*. 1993 Apr 15;268(11):7728-32.

H.

Hammes A, Guo JK, Lutsch G, Leheste JR, Landrock D, Ziegler U, Gubler MC, Schedl A. Two splice variants of the Wilms' tumor 1 gene have distinct functions during sex determination and nephron formation. *Cell*. 2001 Aug 10;106(3):319-29.

Hampton, R.Y. ER-associated degradation in protein quality control and cellular regulation. *Current Opinion in Cell Biology*. 14:476–482 (2002).

Harding, H. P. Calton, M. Urano, F. Novoa, I and Ron, D. Transcriptional and translational control in the mammalian unfolded protein response. *Annu. Rev. Cell Dev. Biol*. 18:575–99 (2002).

Hawkins HC, Blackburn EC, Freedman RB. Comparison of the activities of protein disulphide-isomerase and thioredoxin in catalysing disulphide isomerization in a protein substrate. *Biochem J*. 1991 Apr 15;275 (Pt 2):349-53.

Hayano T, Kikuchi M. Molecular cloning of the cDNA encoding a novel protein disulfide isomerase-related protein (PDIR). *FEBS Lett*. 1995 Sep 25;372(2-3):210-4.

Hebert DN, Foellmer B, Helenius A. Calnexin and calreticulin promote folding, delay oligomerization and suppress degradation of influenza hemagglutinin in microsomes. *EMBO J.* 1996 Jun 17;15(12):2961-8.

Helmann JD. OxyR: a molecular code for redox sensing? *Sci STKE.* 2002 Nov 5;2002(157):PE46.

Hendrick JP, Hartl FU. Molecular chaperone functions of heat-shock proteins. *Annu Rev Biochem.* 1993;62:349-84.

High S, Lecomte FJ, Russell SJ, Abell BM, Oliver JD. Glycoprotein folding in the endoplasmic reticulum: a tale of three chaperones? *FEBS Lett.* 2000 Jun 30;476(1-2):38-41.

Higo T, Hattori M, Nakamura T, Natsume T, Michikawa T, Mikoshiba K. Subtype-specific and ER lumenal environment-dependent regulation of inositol 1,4,5-trisphosphate receptor type 1 by ERp44. *Cell.* 2005 Jan 14; 120(1):85-98.

Hiniker A, Bardwell JC. Disulfide bond isomerization in prokaryotes. *Biochemistry.* 2003 Feb 11;42(5):1179-85.

Hogg PJ. Disulfide bonds as switches for protein function. *Trends Biochem Sci.* 2003 Apr;28(4):210-4.

Holmgren A. Thioredoxin. *Annu Rev Biochem.* 1985;54:237-71.

Holmgren A. Thioredoxin and glutaredoxin systems. *J Biol Chem.* 1989 Aug 25;264(24):13963-6.

Holmgren A. Thioredoxin structure and mechanism: conformational changes on oxidation of the active-site sulfhydryls to a disulfide. *Structure*. 1995 Mar 15;3(3):239-43.

Hong CC, Hashimoto C. An unusual mosaic protein with a protease domain, encoded by the nudel gene, is involved in defining embryonic dorsoventral polarity in *Drosophila*. *Cell*. 1995 Sep 8;82(5):785-94.

Hoshijima K, Metherall JE, Grunwald DJ. A protein disulfide isomerase expressed in the embryonic midline is required for left/right asymmetries. *Genes Dev*. 2002 Oct 1;16(19):2518-29.

Hosoda A, Kimata Y, Tsuru A, Kohno K. JPDI, a novel endoplasmic reticulum-resident protein containing both a BiP-interacting J-domain and thioredoxin-like motifs. *J Biol Chem*. 2003 Jan 24; 278(4):2669-76.

Hubbard SC and Ivatt RJ. Synthesis and processing of asparagine-linked oligosaccharides. *Annu. Rev. Biochem.* 50 (1981) 555-583.

Huber-Wunderlich M, Glockshuber R. A single dipeptide sequence modulates the redox properties of a whole enzyme family. *Fold Des*. 1998;3(3):161-71.

Hwang C, Sinskey AJ, Lodish HF. Oxidized redox state of glutathione in the endoplasmic reticulum. *Science*. 1992 Sep 11;257(5076):1496-502.

J.

Jakob U, Muse W, Eser M, Bardwell JC. Chaperone activity with a redox switch. *Cell*. 1999 Feb 5;96(3):341-52.

Jordan A, Reichard P. Ribonucleotide reductases. *Annu Rev Biochem.* 1998; 67: 71-98.

Johnson AE, van Waes MA. The translocon: a dynamic gateway at the ER membrane. *Annu Rev Cell Dev Biol.* 1999; 15: 799-842. Review.

K.

Kassenbrock CK, Garcia PD, Walter P, Kelly RB. Heavy-chain binding protein recognizes aberrant polypeptides translocated in vitro. *Nature.* 1988 May 5;333(6168):90-3.

Katti SK, LeMaster DM, Eklund H. Crystal structure of thioredoxin from *Escherichia coli* at 1.68 Å resolution. *J Mol Biol.* 1990 Mar 5; 212(1):167-84.

Katzen F, Beckwith J. Transmembrane electron transfer by the membrane protein DsbD occurs via a disulfide bond cascade. *Cell.* 2000 Nov 22;103(5):769-79.

Kaufman RJ. Stress signaling from the lumen of the endoplasmic reticulum: coordination of gene transcriptional and translational controls. *Genes Dev.* 13(1999) 1211-1233.

Kemmink J, Darby NJ, Dijkstra K, Nilges M, Creighton TE. Structure determination of the Nterminal thioredoxin-like domain of protein disulfide isomerase using multidimensional heteronuclear ¹³C/¹⁵N NMR spectroscopy. *Biochemistry.* 1996 Jun 18; 35(24):7684-91.

Kemmink J, Darby NJ, Dijkstra K, Scheek RM, Creighton TE. Nuclear magnetic resonance characterization of the N-terminal thioredoxin-like domain of protein disulfide isomerase. *Protein Sci.* 1995 Dec;4(12):2587-93.

Kemmink J, Dijkstra K, Mariani M, Scheek RM, Penka E, Nilges M, Darby NJ. The structure in solution of the b domain of protein disulfide isomerase. *J Biomol NMR.* 1999 Apr;13(4):357-68.

Kikuchi M, Doi E, Tsujimoto I, Horibe T, Tsujimoto Y. Functional analysis of human P5, a protein disulfide isomerase homologue. *J Biochem (Tokyo).* 2002 Sep;132(3):451-5.

Kim J, Mayfield SP. Protein disulfide isomerase as a regulator of chloroplast translational activation. *Science.* 1997 Dec 12; 278(5345):1954-7.

Kim PS, Arvan P. Endocrinopathies in the family of endoplasmic reticulum (ER) storage diseases: disorders of protein trafficking and the role of ER molecular chaperones. *Endocr Rev.* 1998 Apr;19(2):173-202.

Kivirikko KI, Myllyharju J. Prolyl 4-hydroxylases and their protein disulfide isomerase subunit. *Matrix Biol.* 16(7):357-68 (1998).

Klappa P, Freedman RB, Langenbuch M, Lan MS, Robinson GK, Ruddock LW. The pancreas-specific protein disulphide-isomerase PDIp interacts with a hydroxyaryl group in ligands. *Biochem J.* 2001 Mar 15;354(Pt 3):553-9.

Klappa P, Ruddock LW, Darby NJ, Freedman RB. The b' domain provides the principal peptide-binding site of protein disulfide isomerase but all domains contribute to binding of misfolded proteins. *EMBO J.* 1998 Feb 16; 17(4):927-35.

Klappa P, Stromer T, Zimmermann R, Ruddock LW, Freedman RB. A pancreas-specific glycosylated protein disulphide-isomerase binds to misfolded proteins and peptides with an interaction inhibited by oestrogens. *Eur J Biochem.* 1998 May 15;254(1):63-9.

Knoblach B, Keller BO, Groenendyk J, Aldred S, Zheng J, Lemire BD, Li L, Michalak M. ERp19 and ERp46, new members of the thioredoxin family of endoplasmic reticulum proteins. *Mol Cell Proteomics.* 2003. (in press).

Koivunen P, Pirneskoski A, Karvonen P, Ljung J, Helaakoski T, Notbohm H, Kivirikko KI. The acidic C-terminal domain of protein disulfide isomerase is not critical for the enzyme subunit function or for the chaperone or disulfide isomerase activities of the polypeptide. *EMBO J.* 1999 Jan 4; 18(1):65-74.

Kondrashov FA, Koonin EV. Evolution of alternative splicing: deletions, insertions and origin of functional parts of proteins from intron sequences. *Trends Genet.* 2003 Mar;19(3):115-9.

Konsolaki M, Schupbach T. windbeutel, a gene required for dorsoventral patterning in *Drosophila*, encodes a protein that has homologies to vertebrate proteins of the endoplasmic reticulum. *Genes Dev.* 1;12(1):120-31 (1998).

Kornfeld R, Kornfeld S. Assembly of asparagine-linked oligosaccharides. *Annu. Rev. Biochem.* 50 (1985) 631-664.

Kostova, Z. Wolf, D. H. For whom the bell tolls: protein quality control of the endoplasmic reticulum and the ubiquitin-proteasome connection. *Embo J.* 22 (10): 2309-17 (2003).

Kramer B, Ferrari DM, Klappa P, Pohlmann N, Soling HD. Functional roles and efficiencies of the thioredoxin boxes of calcium-binding proteins 1 and 2 in protein folding. *Biochem J.* 2001 Jul 1;357(Pt 1):83-95.

Kriventseva EV, Koch I, Apweiler R, Vingron M, Bork P, Gelfand MS, Sunyaev S. Increase of functional diversity by alternative splicing. *Trends Genet.* 2003 Mar;19(3):124-8.

Kroning H, Kahne T, Ittenson A, Franke A, Ansorge S. Thiol-proteindisulfide-oxidoreductase (proteindisulfide isomerase): a new plasma membrane constituent of mature human B lymphocytes. *Scand J Immunol.* 1994 Apr;39(4):346-50.

Kuznetsov G, Bush KT, Zhang PL, Nigam SK. Perturbations in maturation of secretory proteins and their association with endoplasmic reticulum chaperones in a cell culture model for epithelial ischemia. *Proc Natl Acad Sci U S A.* 1996 Aug 6;93(16):8584-9.

L.

Lahav J, Gofer-Dadosh N, Luboshitz J, Hess O, Shaklai M. Protein disulfide isomerase mediates integrin-dependent adhesion. *FEBS Lett.* 2000 Jun 16;475(2):89-92.

Lamberg A, Jauhiainen M, Metso J, Ehnholm C, Shoulders C, Scott J, Pihlajaniemi T, Kivirikko KI. The role of protein disulphide isomerase in the microsomal triacylglycerol transfer protein does not reside in its isomerase activity. *Biochem J.* 1996 Apr 15; 315 (Pt 2):533-6.

Langenbach KJ, Sottile J. Identification of protein-disulfide isomerase activity in fibronectin. *J Biol Chem.* 1999 Mar 12;274(11):7032-8.

LeMosy EK, Tan YQ, Hashimoto C. Activation of a protease cascade involved in patterning the *Drosophila* embryo. *Proc Natl Acad Sci U S A*. 2001 Apr 24;98(9):5055-60.

Liepinsh E, Baryshev M, Sharipo A, Ingelman-Sundberg M, Otting G, Mkrtchian S. Thioredoxin fold as homodimerization module in the putative chaperone ERp29: NMR structures of the domains and experimental model of the 51 kDa dimer. *Structure (Camb)*. 2001 Jun;9(6):457-71.

Liour SS, Yu RK. Differentiation of radial glia-like cells from embryonic stem cells. *Glia*. 2003 Apr 15;42(2):109-17.

Li Y, Musacchio M, Finkelstein R. A homologue of the calcium-binding disulfide isomerase CaBP1 is expressed in the developing CNS of *Drosophila melanogaster*. *Dev Genet*. 1998;23(2):104-10.

Lumb RA, Bulleid NJ. Is protein disulfide isomerase a redox-dependent molecular chaperone? *EMBO J*. 2002 Dec 16;21(24):6763-70.

M.

Ma Q, Guo C, Barnewitz K, Sheldrick GM, Soling HD, Uson I, Ferrari DM. Crystal structure and functional analysis of *drosophila* wind - a protein-disulfide isomerase-related protein. *J Biol Chem*. 2003 (in press)

MacLennan DH, Abu-Abed M, Kang C. Structure-function relationships in Ca(2+) cycling proteins. *J Mol Cell Cardiol*. 2002 Aug;34(8):897-918.

MacLennan DH, Wong PT. Isolation of a calcium-sequestering protein from sarcoplasmic reticulum. *Proc Natl Acad Sci U S A*. 1971 Jun;68(6):1231-5.

Martin JL. Thioredoxin--a fold for all reasons. *Structure*. 1995 Mar 15;3(3):245-50.

Martin JL, Bardwell JC, Kuriyan J. Crystal structure of the DsbA protein required for disulphide bond formation in vivo. *Nature*. 1993 Sep 30;365(6445):464-8.

Matthias LJ, Hogg PJ. Redox Control on the Cell Surface: Implications for HIV-1 Entry. *Antioxid Redox Signal*. 2003 Feb;5(1):133-8.

Matthias LJ, Yam PT, Jiang XM, Vandegraaff N, Li P, Pountourios P, Donoghue N, Hogg PJ. Disulfide exchange in domain 2 of CD4 is required for entry of HIV-1. *Nat Immunol*. 2002 Aug;3(8):727-32.

McCarthy AA, Haebel PW, Torronen A, Rybin V, Baker EN, Metcalf P. Crystal structure of the protein disulfide bond isomerase, DsbC, from *Escherichia coli*. *Nat Struct Biol*. 2000 Mar;7(3):196-9.

McCracken AA, Brodsky JL. Evolving questions and paradigm shifts in endoplasmic-reticulum-associated degradation (ERAD). *Bioessays*. 2003 Sep;25(9):868-77. Review.

Merry CL, Wilson VA. Role of heparan sulfate-2-O-sulfotransferase in the mouse. *Biochim Biophys Acta*. 2002 Dec 19;1573(3):319-27.

Mezghrani A, Fassio A, Benham A, Simmen T, Braakman I, Sitia R. Manipulation of oxidative protein folding and PDI redox state in mammalian cells. *EMBO J*. 2001 Nov 15;20(22):6288-96.

Missiakas D, Georgopoulos C, Raina S. Identification and characterization of the *Escherichia coli* gene *dsbB*, whose product is involved in the formation of disulfide bonds in vivo. *Proc Natl Acad Sci U S A*. 1993 Aug 1; 90(15):7084-8.

Misson JP, Edwards MA, Yamamoto M, Caviness VS Jr. Mitotic cycling of radial glial cells of the fetal murine cerebral wall: a combined autoradiographic and immunohistochemical study. *Brain Res.* 1988 Feb 1;466(2):183-90.

Misson JP, Edwards MA, Yamamoto M, Caviness VS Jr. Identification of radial glial cells within the developing murine central nervous system: studies based upon a new immunohistochemical marker. *Brain Res Dev Brain Res.* 1988 Nov 1;44(1):95-108. *Brain Res Dev Brain Res.* 1988 Nov 1;44(1):95-108.

Mkrtchian S, Baryshev M, Matvijenko O, Sharipo A, Sandalova T, Schneider G, Ingelman-Sundberg M, Mkrtchiana S. Oligomerization properties of ERp29, an endoplasmic reticulum stress protein. *FEBS Lett.* 1998 Jul 24; 431(3):322-6.

Molinari M, Helenius A. Glycoproteins form mixed disulphides with oxidoreductases during folding in living cells. *Nature.* 1999 Nov 4; 402(6757):90-3

Monnat J, Hacker U, Geissler H, Rauchenberger R, Neuhaus EM, Maniak M, Soldati T. Dictyostelium discoideum protein disulfide isomerase, an endoplasmic reticulum resident enzyme lacking a KDEL-type retrieval signal. *FEBS Lett.* 1997 Dec 1;418(3):357-62.

Monnat J, Neuhaus EM, Pop MS, Ferrari DM, Kramer B, Soldati T. Identification of a novel saturable endoplasmic reticulum localization mechanism mediated by the C-terminus of a Dictyostelium protein disulfide isomerase. *Mol Biol Cell.* 2000 Oct;11(10):3469-84.

Molinari M, Calanca V, Galli C, Lucca P, Paganetti P. Role of EDEM in the release of misfolded glycoproteins from the calnexin cycle. *Science.* 2003 Feb 28;299(5611):1397-400.

N.

Nakatsukasa K, Nishikawa S, Hosokawa N, Nagata K, Endo T. Mnl1p, an alpha-mannosidase-like protein in yeast *Saccharomyces cerevisiae*, is required for endoplasmic reticulum-associated degradation of glycoproteins. *J Biol Chem*. 2001 Mar 23;276(12):8635-8. Epub 2001 Jan 31

Neil J. Bulleid. Protein disulphide isomerase. *Curr Biol*. 2003 May 13;13(10):R380.

Neuman-Silberberg FS, Schupbach T. The *Drosophila* dorsoventral patterning gene *gurken* produces a dorsally localized RNA and encodes a TGF alpha-like protein. *Cell*. 1993 Oct 8;75(1):165-74.

Nicchitta CV, Blobel G. Luminal proteins of the mammalian endoplasmic reticulum are required to complete protein translocation. *Cell*. 1993 Jun 4;73(5):989-98.

Nigam SK, Goldberg AL, Ho S, Rohde MF, Bush KT, Sherman MYu. A set of endoplasmic reticulum proteins possessing properties of molecular chaperones includes Ca(2+)-binding proteins and members of the thioredoxin superfamily. *J Biol Chem*. 1994 Jan 21;269(3):1744-9.

Nilson LA, Schupbach T. Localized requirements for *windbeutel* and *pipe* reveal a dorsoventral prepatter within the follicular epithelium of the *Drosophila* ovary. *Cell*. 1998 Apr 17;93(2):253-62.

Noiva, R. Protein disulfide isomerase: the multifunctional redox chaperone of the endoplasmic reticulum. *Semin Cell Dev Biol*. 10, 481-93 (1999).

Nordstrand K, slund F, Holmgren A, Otting G, Berndt KD. NMR structure of *Escherichia coli* glutaredoxin 3-glutathione mixed disulfide complex: implications for the enzymatic mechanism. J Mol Biol. 1999 Feb 19;286(2):541-52.

O.

Oda Y, Hosokawa N, Wada I, Nagata K. EDEM as an acceptor of terminally misfolded glycoproteins released from calnexin. Science. 2003 Feb 28;299(5611):1394-7.

Oliver JD, Roderick HL, Llewellyn DH, High S. ERp57 functions as a subunit of specific complexes formed with the ER lectins calreticulin and calnexin. Mol Biol Cell. 1999 Aug;10(8):2573-82.

Oliver JD, van der Wal FJ, Bulleid NJ, High S. Interaction of the thiol-dependent reductase ERp57 with nascent glycoproteins. Science. 1997 Jan 3;275(5296):86-8.

O'Neill S, Robinson A, Deering A, Ryan M, Fitzgerald DJ, Moran N. The platelet integrin alpha IIb beta 3 has an endogenous thiol isomerase activity. J Biol Chem. 2000 Nov 24;275(47):36984-90.

Orrenius S, Zhivotosky B, Nicotera P. Regulation of cell death: the calcium-apoptosis link. Nat. Rev. Mol. Cell Biol. 4 (2003)552-565.

P.

Parnavelas JG, Nadarajah B. Radial glial cells. are they really glia? Neuron. 2001 Sep 27;31(6):881-4.

Paschen W, Gissel C, Linden T, Doutheil J. ERp72 expression activated by transient cerebral ischemia or disturbance of neuronal endoplasmic reticulum calcium stores. *Metab Brain Dis.* 1998 Mar;13(1):55-68.

Pihlajaniemi T, Helaakoski T, Tasanen K, Myllyla R, Huhtala ML, Koivu J, Kivirikko KI. Molecular cloning of the beta-subunit of human prolyl 4-hydroxylase. This subunit and protein disulphide isomerase are products of the same gene. *EMBO J.* 1987 Mar;6(3):643-9.

Pirneskoski A, Ruddock LW, Klappa P, Freedman RB, Kivirikko KI, Koivunen P. Domains b' and a' of protein disulfide isomerase fulfill the minimum requirement for function as a subunit of prolyl 4-hydroxylase. The N-terminal domains a and b enhances this function and can be substituted in part by those of ERp57. *J Biol Chem.* 2001 Apr 6;276(14):11287-93.

Puig A, Gilbert HF. Protein disulfide isomerase exhibits chaperone and anti-chaperone activity in the oxidative refolding of lysozyme. *J Biol Chem.* 1994 Mar 11;269(10):7764-71.

Q.

Qin J, Clore GM, Kennedy WM, Huth JR, Gronenborn AM. Solution structure of human thioredoxin in a mixed disulfide intermediate complex with its target peptide from the transcription factor NF kappa B. *Structure.* 1995 Mar 15;3(3):289-97.

R.

Ren B, Tibbelin G, de Pascale D, Rossi M, Bartolucci S, Ladenstein R. A protein disulfide oxidoreductase from the archaeon *Pyrococcus furiosus* contains two thioredoxin fold units. *Nat Struct Biol.* 1998 Jul;5(7):602-11.

Rietsch A, Belin D, Martin N, Beckwith J. An in vivo pathway for disulfide bond isomerization in *Escherichia coli*. *Proc Natl Acad Sci U S A*. 1996 Nov 12; 93(23):13048-53.

Ruoppolo M, Orru S, Talamo F, Ljung J, Pirneskoski A, Kivirikko KI, Marino G, Koivunen P. Mutations in domain a' of protein disulfide isomerase affect the folding pathway of bovine pancreatic ribonuclease A. *Protein Sci*. 2003 May;12(5):939-52.

Rupp K, Birnbach U, Lundstrom J, Van PN, Soling HD. Effects of CaBP2, the rat analog of ERp72, and of CaBP1 on the refolding of denatured reduced proteins. Comparison with protein disulfide isomerase. *J Biol Chem*. 1994 Jan 28; 269(4):2501-7.

Ryser HJ, Levy EM, Mandel R, DiSciullo GJ. Inhibition of human immunodeficiency virus infection by agents that interfere with thiol-disulfide interchange upon virus-receptor interaction. *Proc Natl Acad Sci U S A*. 1994 May 10;91(10):4559-63.

S.

Safran M, Farwell AP, Leonard JL. Thyroid hormone-dependent redistribution of the 55-kilodalton monomer of protein disulfide isomerase in cultured glial cells. *Endocrinology*. 1992 Nov;131(5):2413-8.

Safran M, Leonard JL. Characterization of a N-bromoacetyl-L-thyroxine affinity-labeled 55-kilodalton protein as protein disulfide isomerase in cultured glial cells. *Endocrinology*. 1991 Oct;129(4):2011-6.

Sargsyan E, Baryshev M, Szekely L, Sharipo A, Mkrtchian S. Identification of ERp29, an endoplasmic reticulum lumenal protein, as a new member of the thyroglobulin folding complex. *J Biol Chem*. 2002 May 10;277(19):17009-15.

Sarnat HB. Histochemistry and immunocytochemistry of the developing ependyma and choroid plexus. *Microsc Res Tech*. 1998 Apr 1;41(1):14-28.

Selleck SB. Proteoglycans and pattern formation: sugar biochemistry meets developmental genetics. *Trends Genet*. 2000 May;16(5):206-12.

Sen J, Goltz JS, Konsolaki M, Schupbach T, Stein D. Windbeutel is required for function and correct subcellular localization of the *Drosophila* patterning protein Pipe. *Development*. 127(24):5541-50 (2000).

Sen J, Goltz JS, Stevens L, Stein D. Spatially restricted expression of pipe in the *Drosophila* egg chamber defines embryonic dorsal-ventral polarity. *Cell*. 1998 Nov 13;95(4):471-81.

Sergeev P, Streit A, Heller A, Steinmann-Zwicky M. The *Drosophila* dorsoventral determinant PIPE contains ten copies of a variable domain homologous to mammalian heparan sulfate 2-sulfotransferase. *Dev Dyn*. 2001 Feb;220(2):122-32.

Sevier CS, Cuozzo J, Vala A, Åslund F and Kaiser CA. A flavoprotein oxidase defines a new endoplasmic reticulum pathway for biosynthetic disulphide bond formation. *Nat Cell Biol*. 2001 Oct;3(10):874-82.

Sevier CS, Kaiser CA. Formation and transfer of disulphide bonds in living cells. *Nat Rev Mol Cell Biol*. 2002 Nov;3(11):836-47.

Shen X, Zhang K, Kaufman RJ. The unfolded protein response--a stress signaling pathway of the endoplasmic reticulum. *J Chem Neuroanat.* 2004 Sep;28(1-2):79-92. Review.

Shnyder SD, Hubbard MJ. ERp29 is a ubiquitous resident of the endoplasmic reticulum with a distinct role in secretory protein production. *J Histochem Cytochem.* 2002 Apr;50(4):557-66.

Sitja R, Braakman I. Quality control in the endoplasmic reticulum protein factory. *Nature.* 2003 Dec 18;426(6968):891-4. Review.

Song JL, Wang CC. Chaperone-like activity of protein disulfide-isomerase in the refolding of rhodanese. *Eur J Biochem.* 1995 Jul 15;231(2):312-6.

Speake T, Whitwell C, Kajita H, Majid A, Brown PD. Mechanisms of CSF secretion by the choroid plexus. *Microsc Res Tech.* 2001 Jan 1;52(1):49-59.

Sullivan DC, Huminiecki L, Moore JW, Boyle JJ, Poulosom R, Creamer D, Barker J, Bicknell R. EndoPDI, a novel protein disulphide isomerase-like protein that is preferentially expressed in endothelial cells acts as a stress survival factor. *J Biol Chem.* 2003 (in press).

T.

Tachikawa H, Funahashi W, Takeuchi Y, Nakanishi H, Nishihara R, Katoh S, Gao XD, Mizunaga T, Fujimoto D. Overproduction of Mpd2p suppresses the lethality of protein disulfide isomerase depletion in a CXXC sequence dependent manner. *Biochem Biophys Res Commun.* 1997 Oct 29; 239(3):710-4.

Tateishi Y, Hattori M, Nakayama T, Iwai M, Bannai H, Nakamura T, Michikawa T, Inoue T, Mikoshiba K. Cluster formation of inositol 1,4,5-trisphosphate receptor requires its transition to open state. *J Biol Chem*. 2005 Feb 25; 280(8):6816-22. Epub 2004 Dec 6.

Terada K, Manchikalapudi P, Noiva R, Jauregui HO, Stockert RJ, Schilsky ML. Secretion, surface localization, turnover, and steady state expression of protein disulfide isomerase in rat hepatocytes. *J Biol Chem*. 1995 Sep 1;270(35):204106.

Trombetta ES, Parodi AJ. Quality control and protein folding in the secretory pathway. *Annu Rev Cell Dev Biol*. 2003;19:649-76. Review.

Tsai B, Rapoport TA. Unfolded cholera toxin is transferred to the ER membrane and released from protein disulfide isomerase upon oxidation by Ero1. *J Cell Biol*. 2002 Oct 28;159(2):207-16.

Tsai B, Rodighiero C, Lencer WI, Rapoport TA. Protein disulfide isomerase acts as a redoxdependent chaperone to unfold cholera toxin. *Cell*. 2001 Mar 23;104(6):937-48.

Tsai B, Ye Y, Rapoport TA. Retro-translocation of proteins from the endoplasmic reticulum into the cytosol. *Nat Rev Mol Cell Biol*. 2002 Apr;3(4):246-55.

Tu BP, Ho-Schleyer SC, Travers KJ, Weissman JS. Biochemical basis of oxidative protein folding in the endoplasmic reticulum. *Science*. 2000 Nov 24;290(5496):1571-4.

Tu BP, Weissman JS. The FAD- and O₂-dependent reaction cycle of Ero1-mediated oxidative protein folding in the endoplasmic reticulum. *Mol Cell*. 2002 Nov;10(5):983-94.

Tu BP, Weissman JS. Oxidative protein folding in eukaryotes: mechanisms and consequences. *J Cell Biol.* 2004 Feb 2;164(3):341-6. Review.

V.

Van der Wal FJ, Oliver JD, High S. The transient association of ERp57 with N-glycosylated proteins is regulated by glucose trimming. *Eur J Biochem.* 1998 Aug 15;256(1):51-9.

Van Eeden F, St Johnston D. The polarisation of the anterior-posterior and dorsal-ventral axes during *Drosophila* oogenesis. *Curr Opin Genet Dev.* 1999 Aug;9(4):396-404.

van Endert PM. Genes regulating MHC class I processing of antigen. *Curr Opin Immunol.* 1999 Feb;11(1):82-8.

Van PN, Peter F, Soling HD. Four intracisternal calcium-binding glycoproteins from rat liver microsomes with high affinity for calcium. No indication for calsequestrin-like proteins in inositol 1,4,5-trisphosphate-sensitive calcium sequestering rat liver vesicles. *J Biol Chem.* 1989 Oct 15;264(29):17494-501.

Van PN, Rupp K, Lampen A, Soling HD. CaBP2 is a rat homolog of ERp72 with protein disulfide isomerase activity. *Eur J Biochem.* 1993 Apr 15;213(2):789-95.

Veijola J, Pihlajaniemi T, Kivirikko KI. Co-expression of the alpha subunit of human prolyl 4-hydroxylase with BiP polypeptide in insect cells leads to the formation of soluble and insoluble complexes. Soluble alpha-subunit-BiP complexes have no prolyl 4-hydroxylase activity. *Biochem J.* 1996 Apr 15;315 (Pt 2):613-8.

Volkmer J, Guth S, Nastainczyk W, Knippel P, Klappa P, Gnau V, Zimmermann R. Pancreas specific protein disulfide isomerase, PDIp, is in transient contact with secretory proteins during late stages of translocation. *FEBS Lett.* 1997 Apr 14;406(3):291-5.

W.

Wadsworth SC, Vincent WS 3rd, Bilodeau-Wentworth D. A *Drosophila* genomic sequence with homology to human epidermal growth factor receptor. *Nature.* 1985 Mar 14-20;314(6007):178-80.

Wang CC. Protein disulfide isomerase assists protein folding as both an isomerase and a chaperone. *Ann N Y Acad Sci.* 13;864:9-13 (1998).

Wang CC. Isomerase and chaperone activities of protein disulfide isomerase are both required for its function as a foldase. *Biochemistry (Mosc).* 63(4):407-12 (1998).

Wang CC, Tsou CL. Enzymes as chaperones and chaperones as enzymes. *FEBS Lett.* 3;425(3):382-4 (1998).

Wang S, Trumble WR, Liao H, Wesson CR, Dunker AK, Kang CH. Crystal structure of calsequestrin from rabbit skeletal muscle sarcoplasmic reticulum. *Nat Struct Biol.* 1998 Jun;5(6):476-83.

Wetterau JR, Combs KA, Spinner SN, Joiner BJ. Protein disulfide isomerase is a component of the microsomal triglyceride transfer protein complex. *J Biol Chem.* 1990 Jun 15;265(17):9801-7.

Willnow TE, Rohlmann A, Horton J, Otani H, Braun JR, Hammer RE, Herz J. RAP, a specialized chaperone, prevents ligand-induced ER retention and

degradation of LDL receptor-related endocytic receptors. *EMBO J.* 1996 Jun 3;15(11):2632-9.

Wickner S, Maurizi MR, Gottesman S. Posttranslational quality control: folding, refolding, and degrading proteins. *Science.* 1999 Dec 3;286(5446):1888-93. Review.

Woycechowsky KJ, Raines RT. The CXC motif: a functional mimic of protein disulfide isomerase. *Biochemistry.* 2003 May 13;42(18):5387-94.

X.

Xu C, Bailly-Maitre B, Reed JC. Endoplasmic reticulum stress: cell life and death decisions. *J Clin Invest.* 2005 Oct;115(10):2656-64. Review.

Y.

Yao Y, Zhou Y, Wang C. Both the isomerase and chaperone activities of protein disulfide isomerase are required for the reactivation of reduced and denatured acidic phospholipase A2. *EMBO J.* 1997 Feb 3;16(3):651-8.

Yokoi T, Nagayama S, Kajiwara R, Kawaguchi Y, Horiuchi R, Kamataki T. Identification of protein disulfide isomerase and calreticulin as autoimmune antigens in LEC strain of rats. *Biochim Biophys Acta.* 1993 Nov 28;1158(3):339-44.

Z.

Zapun A, Darby NJ, Tessier DC, Michalak M, Bergeron JJ, Thomas DY. Enhanced catalysis of ribonuclease B folding by the interaction of calnexin or calreticulin with ERp57. *J Biol Chem.* 1998 Mar 13;273(11):6009-12.

Zapun A, Missiakas D, Raina S, Creighton TE. Structural and functional characterization of DsbC, a protein involved in disulfide bond formation in *Escherichia coli*. *Biochemistry*. 1995 Apr 18;34(15):5075-89.

Zhang SC. Defining glial cells during CNS development. *Nat Rev Neurosci*. 2001 Nov;2(11):840-3.

Acknowledgments

I would like to thank Professor Robert Huber for giving me the opportunity to work in his laboratory in Martinsried, for providing excellent experimental facilities, for his support and consideration.

I would like to thank Dr. Markus Wahl for his special interest, and also to his previous and present group members Rasso Willkomm, Thomas Conrad, Simon Trowitzsch, Gert Weber, Mihaela Diaconu, Nina Müllers, Catharina Netter, Elke Penka, Ulrich Reidt and Sunbin Liu for the warm and friendly working atmosphere.